

PHYSICS DEPARTMENT
NORTH CAROLINA STATE UNIVERSITY
BOX 8202
RALEIGH, NC 27695-8202



REPORT ON
NASA GRANT 1562
Entitled

"Effects of High Energy Radiation on the Mechanical
Properties of Epoxy/Graphite Fiber Reinforced Composites."

(NASA-CR-176487) EFFECTS OF HIGH ENERGY
RADIATION ON THE MECHANICAL PROPERTIES OF
EPOXY-GRAPHITE FIBER REINFORCED COMPOSITES
Interim Report, 1 Jan. - 31 Dec. 1985 (North
Carolina State Univ.) 263 p HC A12/MF A01

N86-17476

Unclas
G3/24 05341

covering the period
January 1, 1985-December 31, 1985

R.E.Fornes
R.D.Gilbert
J.D.Memory
Co-Principal Investigators





North Carolina State University
School of Physical and Mathematical Sciences

Department of Physics

Box 8202, Raleigh, NC 27695-8202

January 13, 1986

Dr. Edward Long
Technical Officer - NASA Grant 1562
M-S 399
NASA Langley Research Center
Hampton, VA 23665

Dear Dr. Long:

Enclosed are three copies of the interim report of NASA Grant 1562 entitled "Effects of High Energy Radiation on the Mechanical Properties of Epoxy/Graphite Fiber Reinforced Composites" concerning the period January 1, 1985 - December 31, 1985. The report consists of a copy of the Ph.D. manuscript of K.S. Seo and a literature review written by J.S. Park, both of whom were supported by the Grant, and a summary listing of presentations made on the subject grant. We feel that the work of Seo is the most definitive to date on the MY720/DDS system regarding ESR and surface energy characterization of irradiated specimens, and the mechanical model presented by Park will permit distinguishing radiation effects in bulk from those at the fiber matrix interface. The next report, to be submitted after the no cost extension work is completed, will contain a final summary of the work done on this grant. Two copies of this report have been sent to the NASA Scientific and Technical Information Center (NASA - STIC).

We appreciate the support of this work.

Sincerely,

A handwritten signature in dark ink, appearing to read "R.E. Fornes".

R.E. Fornes

A handwritten signature in dark ink, appearing to read "R.D. Gilbert".

R.D. Gilbert
Co-Principal Investigators

REF/gaw

cc: NASA - STIC
W.K. Walsh
L.B. Sims
J.D. Memory

Enclosures

Report on NASA Grant 1562

Summary of presentations on work done on NASA Grant 1562 during the report period covering the period from January 1, 1985 - December 31, 1985. The underlined indicates the presenter.

PRESENTATIONS

1. K.S. Seo, R.D. Gilbert, R.E. Fornes and J.D. Memory, "ESR Studies of Graphite Fiber/Epoxy Composites Irradiated with Ionizing Radiation, Bull. Amer. Phys. Soc. 30: 477 (1985).
2. J.S. Park, R.D. Gilbert, J.D. Memory and R.E. Fornes, "Effect of Ionizing Radiation on the Interlaminar Shear Strength (ILSS) of Graphite Fiber/Epoxy Composites, Bull. Amer. Phys. Soc. 30: 490 (1985).
3. T. Wilson, J.D. Memory, R.E. Fornes and R.D. Gilbert, "Effect of 0.5 MeV Electron Radiation on Dynamic Mechanical Properties of TGDDM/DDS Epoxy Resin and T300/5208 and T300 15209 Composites, Bull. Amer. Phys. Soc. 30: 434 (1985).
4. Surface Properties of Irradiation Epoxy Resin/Graphite Fiber Composites, K.S. Seo, J.D. Memory, R.E. Fornes and R.D. Gilbert. ACS National Meeting, Miami Beach, Florida April 28 - May 3, 1985.
5. Seminar Presented by R.D. Gilbert on "High Energy Radiation Effects on High Technology Composites" at Peking University, Peoples Republic of China, May, 1985.
6. Seminars presented by R.E. Fornes on "Effects of H₂O and High Energy Radiation on Properties of Epoxy/Graphite Fiber Composites".
A: At IBM in San Jose, CA (May, 1985) and B: At the Physics Department, N.C. State University, Raleigh, N.C. (Sept. 1985).
7. Seminar presented by R.E. Fornes on "ESR Studies of the Effects of High Energy Radiation on Epoxy/Graphite Fiber Composites" at JPL, Pasadena, CA in December 1985.

ELECTRON SPIN RESONANCE INVESTIGATIONS AND
SURFACE CHARACTERIZATION OF TGDDM-DDS EPOXY AND
T-300 GRAPHITE FIBER EXPOSED TO IONIZING RADIATION

by

KAB SIK SEO

A thesis submitted to the Graduate Faculty of
North Carolina State University at Raleigh
in partial fulfilment of the
requirements for the Degree of
Doctor of Philosophy


FIBER AND POLYMER SCIENCE


RALEIGH

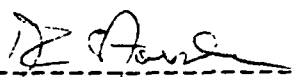
1 9 8 5

APPROVED BY:

-----

-----

-----
Co-Chairman of Advisory
Committee

-----
Co-Chairman of Advisory
Committee

ABSTRACT

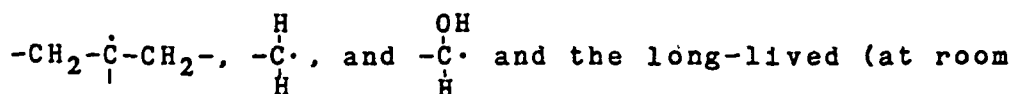
SEO, KAB SIK. Electron Spin Resonance Investigations and Surface Characterization of TGDDM-DDS Epoxy and T-300 Graphite Fiber Exposed to Ionizing Radiation (Under the direction of Drs. R. E. FORNES and R. D. GILBERT)

In an effort to elucidate the changes in molecular structural and mechanical properties of epoxy/graphite fiber composites upon exposure to ionizing radiation in a simulated space environment, spectroscopic and surface properties of tetraglycidyl-4,4'-diamino diphenyl methane (TGDDM) cured with diamino diphenyl sulfone (DDS) and T-300 graphite fiber were investigated following exposure to ionizing radiation.

Cobalt-60 gamma-radiation and 1/2 MeV electrons were used as radiation sources. The system was studied using electron spin resonance (ESR) spectroscopy, infrared absorption spectroscopy, contact angle measurements, and electron spectroscopy for chemical analysis.

Two kinetically-distinguishable (fast-decaying and slow-decaying) radical species are produced in TGDDM-DDS epoxy upon irradiation and their decay behavior is strongly affected by the crosslinking density distribution in the cured epoxy. The fraction of fast-decaying radicals increases with increasing decay temperature while the decay rate constant of slow-decaying radicals does not depend on

the decay temperature. The fast-decaying species are most likely associated with alkyl type radicals such as



and the long-lived (at room temperature) species associated with oxygenated radicals such as alkoxy ($-\dot{\underset{|}{\text{C}}}\text{O}\cdot$) and peroxy ($-\dot{\underset{|}{\text{C}}}\text{OO}\cdot$) radicals trapped in highly crosslinked regions of the epoxy. At an elevated temperature, additional radical species probably acyl

radicals ($-\overset{\text{O}}{\underset{|}{\text{C}}}\cdot$), are produced giving a narrow component ($\Delta H_{pp} < 13 \text{ G}$) in the ESR spectrum. Unirradiated T-300 graphite fibers have a large concentration of free radicals (10^{19} - 10^{20} spins/g), thus overshadow any change in ESR spectra of irradiated composites.

The surface energy of epoxy increases monotonically with radiation dose up to 1,000 Mrad and leveled off. This increase in the surface energy is mainly due to the increased concentration of polar groups, mostly carbonyl groups as confirmed by IR absorption at 1720 cm^{-1} . The increase in the surface energy was accelerated by the presence of oxygen. The surface energy of graphite fiber changes slightly with radiation dose.

Both the interaction of free radicals at the graphite fiber/epoxy interface and the increase in the surface energy would be possible factors which increase the interfacial strength of the composite after irradiation.

BIOGRAPHY

Kab Sik Seo was born September 15, 1951 in Jeon Nam, Korea. He was graduated from Kwang Ju High School in 1969. He received a Bachelor of Science degree in Textile Engineering from Seoul National University in 1974.

From 1974 to 1978 he worked as a researcher at the Agency for Defense Development in Korea, he also completed his military service duty there and retired as a first-lieutenant of Korean army. He came to the United States of America in 1978 and worked for Gaynes Testing Laboratories Inc. in Chicago, Illinois until 1979. He began his graduate study in the Polymer Group of the Department of Metallurgy and Mining Engineering at University of Illinois at Urbana-Champaign in 1980 and received his Master of Science degree there in 1982. He continued his studies toward a Doctor of Philosophy degree in Fiber and Polymer Science Program at North Carolina State University. Upon completion of his doctorate he will begin a career at Tennessee Eastman Company in Kingsport, Tennessee.

He is married to the former Miss Hou Soon Im, and they have one daughter and one son.

ACKNOWLEDGEMENTS

The author wishes to express his sincere appreciation to Professors R. E. Fornes and R. D. Gilbert, Co-Chairmen of his Advisory Committee, for their guidance and encouragement during the course of this study. Appreciation is also extended to Professors J. D. Memory and M. K. DeArmond, members of his Advisory Committee, for their valuable suggestions and understanding.

Special gratitude is expressed to Professors V. T. Stannett and M. K. DeArmond for the ESR Spectrometers which they provided to the author during the course of this study. The help of Mr. Tom Vess, Dr. David Morris and Mr. Mike Kent in using the ESR spectrometer is greatly acknowledged. NASA provided financial support for this study.

Finally, the author express deep thanks to his wife Hou Soon, daughter Jenny and son Eric for their patience and sacrifice.

page

LIST OF TABLES.....vii

LIST OF FIGURES.....viii

1. INTRODUCTION.....1

2. LITERATURE REVIEW.....3

 2.1 Interaction of Radiation with Matter.....3

 2.1.1 Radiation Sources.....3

 2.1.2 Energy Transfer Mechanism of Radiation.....5

 2.1.2.1 Photons.....5

 2.1.2.2 High Energy Electrons.....9

 2.1.2.3 Protons, α - and β -Particles and Neutrons.....12

 2.1.3 Radiation Induced Chemical Changes in Polymers.....13

 2.1.3.1 Formation of Free Radicals.....13

 2.1.3.2 Stability of Free Radicals.....13

 2.1.3.3 Reaction of Free Radicals.....14

 2.1.3.4 Crosslinking and Degradation.....17

 2.1.3.5 Effect of Temperature on Rates of Crosslinking and Degradation18

 2.2 Radiation Induced Oxidation.....20

 2.2.1 General Mechanism of Photooxidation of Polymers.....20

 2.2.1.1 Initiation Reaction.....20

 2.2.1.2 Formation of Hydroperoxides.....20

 2.2.1.3 Decomposition of Hydroperoxides.....21

 2.2.1.4 Formation of Hydroxyl Groups.....22

 2.2.1.5 Formation of Carbonyl Groups.....25

 2.2.1.6 Termination Reaction.....25

 2.2.2 Radiation Induced Degradation of Epoxies.....25

 2.3 Electron Spin Resonance (ESR).....35

 2.3.1 Basic Principles of ESR.....35

 2.3.2 The g-factor.....38

 2.3.3 Line Shape.....39

 2.3.4 ESR Studies of Oxidation in Irradiated Polymers.....43

 2.3.5 Radical Decay in Semicrystalline Polymers....46

 2.3.6 Radical Decay in Irradiated Epoxies.....53

TABLE OF CONTENTS (continued)

page

2.4 Polymer Surface Energetics.....	55
2.4.1 Theory of Surface Energetics.....	55
2.4.2 Adhesion of Composites.....	62
2.4.3 Methods of Surface Characterization.....	63
2.4.3.1 Contact Angle Measurement.....	63
2.4.3.2 Infrared Absorption Spectroscopy.....	65
2.4.3.3 Electron Spectroscopy for Chemical Analysis (ESCA).....	67
2.4.3.4 Microscopy.....	68
3. EXPERIMENTAL PROCEDURES.....	69
3.1 Materials.....	69
3.1.1 Epoxy Resins.....	69
3.1.2 Graphite Fiber and T300/5208 Composites.....	69
3.2 Sample Preparation.....	70
3.2.1 Mixing of TGDDM/DDS.....	70
3.2.2 Preparation of Epoxy Films.....	71
3.2.3 Preparation of Samples for ESR Measurements..	71
3.2.3.1 Epoxy Resin Samples.....	71
3.2.3.2 Graphite Fiber Samples.....	73
3.2.3.3 Composite Samples.....	73
3.2.4 Preparation of a Standard Radical Sample.....	73
3.3 Irradiation Procedures.....	74
3.3.1 Gamma Irradiation.....	74
3.3.2 Electron Irradiation.....	75
3.4 ESR Measurements.....	76
3.5 IR Measurements.....	80
3.6 Contact Angle Measurements.....	80
3.6.1 Epoxy Films and Fracture-Surfaces of Composites.....	80
3.6.2 Graphite Fiber.....	82
3.7 ESCA Measurements.....	82
4. RESULTS AND DISCUSSION.....	85
4.1 Electron Spin Resonance Analysis.....	88
4.1.1 Irradiation Conditions in Space.....	88
4.1.2 Effect of Irradiation Conditions on ESR Line Shape of TGDDM-DDS Epoxy.....	90
4.1.3 Identification of Radicals in TGDDM-DDS Epoxy.....	95

TABLE OF CONTENTS (continued)

page

4.1.4 Radical Decay in Irradiated TGDDM-DDS Epoxy.....	104
4.1.5 Effect of Curing Conditions on Radical Decay.....	114
4.1.6 ESR Spectra of Graphite Fiber and Composites.....	120
4.2 Surface Analysis.....	123
4.2.1 Surface Energy Measurements.....	123
4.2.2 ESCA Analysis of Irradiated Surfaces.....	136
4.2.3 IR Spectroscopy.....	137
5. CONCLUSIONS.....	151
6. RECOMMENDATIONS.....	155
7. REFERENCES.....	156
8. APPENDICES.....	164

LIST OF TABLES

	page
2.1 List of various epoxy resins and hardeners [29, 31].....	30
2.2 Initial rates of carbonyl and amide growths (absorbance units $\text{cm}^{-1}\text{h}^{-1}$) and electron density of the nitrogen atom in DGEBA epoxy.....	34
2.3 Major radical species in TGDDM/DDS epoxy system [46].	45
3.1 Surface tension properties of test liquids at 20°C...	81
4.1 Contact angle (degree) of 1/2 MeV electron-irradiated epoxy (TGDDM-DDS) measured with various liquids.....	124
4.2 Work of adhesion W_a of Liquid/Epoxy interface versus radiation dose (1/2 MeV electrons).....	125
4.3 Surface energy of irradiated epoxy (TGDDM-DDS) versus radiation dose (1/2 MeV electrons).....	128
4.4 Contact angles (degree) of 1/2 MeV electron-irradiated graphite fiber (T-300) measured with various liquids.....	130
4.5 Work of adhesion W_a of graphite fiber versus radiation dose (1/2 MeV electrons).....	131
4.6 Surface energy of irradiated graphite fiber (T-300) versus radiation dose (1/2 MeV electrons)...	132
4.7 Relative atomic concentration of oxygen and carbon on TGDDM-DDS epoxy and T300/5208 composite as determined by ESCA.....	138
4.8 Contact angles (degree) of water on shear-fracture surface of T300/5208 uniaxial composites irradiated with 1/2 MeV electrons in aluminium foil bags.....	139
A. Radical concentration, ESR line shapes and g-factors of TGDDM-DDS epoxy and T-300 graphite fiber.....	164

LIST OF FIGURES

2.1	Modified digram for the most important process involving electronically excited states and preionization states [6a].....	4
2.2	Schematic representation of processes leading to charge separation and excited-state formation in liquid and solid states [8].....	10
2.3	Possible radiation processes in DGEBA-EDA epoxy [22].....	27
2.4	Formation of carbonyl groups from secondary hydroxyl groups in cured epoxy in the presence of oxygen [29].....	31
2.5	Energy level scheme for the simplest system showing ESR absorption. W_a and W_b represent the energies of the $M_s = +1/2$ and the $M_s = -1/2$ states, respectively [36].....	37
2.6	Characteristics of the Lorentzian line shape and the Gaussian line shape [36].....	40
2.7	Decay curves of free radicals in various polyethylene irradiated at liquid nitrogen temperature [50].....	47
2.8	A drop of liquid (L) resting on the surface of solid (S) [78].....	56
2.9	A sessile drop on an inclined plane (gradient = $\tan \phi$) showing the advancing θ_a and receding θ_r angles [98].....	64
3.1	A schematic diagram of the assembled mold for the epoxy film preparation.....	72
3.2	Procedure for the aluminium bag preparation for electron irradiation [10].....	77
3.3	A schematic representation of Wilhelmy technique used for contact angle measurement of fibers.....	83
4.1	A schematic representation of the epoxy/graphite fiber interface.....	87

LIST OF FIGURES (continued)

- 4.2 ESR spectra of TGDDM-DDS epoxy irradiated at room temperature in air with a dose of 100 Mrad of γ -radiation. (a) as-irradiated and (b) after 27 days exposure to air at room temperature. Samples were cured at 150°C (1hr) and then at 177°C (5 hrs). The spectra were measured at -196°C.....91
- 4.3 ESR spectra of TGDDM-DDS epoxy γ -irradiated in liquid nitrogen with a dose of 100 Mrad. (a) as-irradiated and (b) after 200 minutes exposure to air at room temperature. Spectra were taken at -196°C. Samples were cured at 150°C (1 hr) and then at 177°C (5 hrs).....92
- 4.4 ESR spectra of TGDDM-DDS epoxy and 1/2 MeV electron-irradiated at room temperature with various doses and immediately stored in liquid nitrogen. Spectra were measured at -196°C. Samples are cured at 150°C (1 hr) and then 177°C (5 hrs).....94
- 4.5 ESR spectra of TGDDM-DDS epoxy γ -irradiated with a dose of 800 Mrad at room temperature (300°K): (1) in air, (2) in vacuum-sealed tube, and (3) spectrum-1 after exposure to air at 300°K for 90 days.....96
- 4.6 ESR spectra of TGDDM-DDS epoxy irradiated with a 100 Mrad of γ -radiation at room temperature under a continuous vacuum condition. The spectrum was measured at room temperature. Samples were stored in liquid nitrogen until ESR measurement.....97
- 4.7. Possible chain scission reactions of TGDDM-DDS epoxy under radiation.....99
- 4.8. ESR spectra of TGDDM-DDS epoxy cured at 137°C (2 hrs) and then 160°C (5 hrs), and irradiated with a 5 Mrad dose of γ -radiation in liquid nitrogen (77°K): (a) as-irradiated (b) after 5 minute exposure to air at room temperature and (c) after 200 minute exposure.....100

LIST OF FIGURES (continued)

4.9	The difference spectrum between spectrum-a and spectrum-b in Figure 4.8.....	102
4.10	Isothermal decay of radicals in the irradiated TGDDM-DDS epoxy.....	105
4.11	First-order plot of the isothermal decay curves in Figure 4.10.....	107
4.12	Second-order plot of the isothermal decay curves in Figure 4.10.....	108
4.13	ESR spectra of TGDDM-DDS cured at 150°C (1 hr) and then 177°C (5 hrs) and γ -irradiated with a dose of 5 Mrad at -196°C. (a) as-irradiated, (b) after 5 minutes at -150°C, and (c) difference spectrum between (a) and (b).....	109
4.14	ESR line shape of TGDDM-DDS epoxy cured at various temperatures, and irradiated with a dose of 5 Mrad of γ -radiation. ESR spectra were measured at -196°C.....	110
4.15	ESR line shape vs. curing time of TGDDM-DDS epoxy irradiated with 5 Mrad and 30 Mrad at -196°C. Spectra were measured at -196°C.....	111
4.16	Radical decay in air at room temperature (23°C) of TGDDM-DDS epoxy samples cured at various temperatures.....	115
4.17	Radical decay, in air at room temperature (23°C), of TGDDM-DDS epoxy cured with different curing times.....	116
4.18	A schematic representation of cured TGDDM-DDS epoxy network.....	118
4.19	Radical decay in air at room temperature of TGDDM-DDS epoxy γ -irradiated with various radiation doses.....	119
4.20	ESR Spectra of (1) graphite fiber (~1 mg) (2) T300/5208 composites (~40 mg) irradiated with a 9,000 Mrad dose of 1/2 MeV electrons at room temperature in air, and (3) TGDDM-DDS (~170 mg) epoxy γ -irradiated with 5 Mrad and exposed to air for several months.....	121

LIST OF FIGURES (continued)

4.21	Plot of $W_a/2\alpha_L$ against β_L/α_L of TGDDM-DDS epoxy. Samples were irradiated with 1/2 MeV electrons at room temperature.....	126
4.22	Surface energy changes of TGDDM-DDS epoxy with radiation dose.....	129
4.23	Plot of $W_a/2\alpha_L$ against β_L/α_L of T-300 graphite fiber. Samples were irradiated with 1/2 MeV electrons at room temperature.....	133
4.24	Surface energy changes of T-300 graphite fiber with radiation dose.....	134
4.25	Contact angle changes (with H_2O) with radiation dose of TGDDM-DDS epoxy irradiated with 1/2 MeV electrons: \square in air, Δ in nitrogen-filled bag, and \circ in vacuum.....	135
4.26	IR spectra of TGDDM-DDS epoxy: (1) as-cured and (2) irradiated with a 1,000 dose of 1/2 MeV electrons in air.....	140
4.27	Growth of carbonyl peak at 1720 cm^{-1} upon irradiation. Samples were irradiated with 1/2 MeV electrons in air at room temperature.....	141
4.28	IR spectrum of the as-mixed TGDDM-DDS.....	143
4.29	IR spectra of pure TGDDM and heat-treated TGDDM at 150°C for 1 hr and 177°C for 5 hrs in air.....	144
4.30	IR spectra of pure DDS and heat-treated DDS at 150°C for 1 hr and 177°C for 5 hrs in air.....	145
4.31	IR spectra of DDM: (1) pure and (2) heat-treated at 150°C for 1 hr and 177°C for 5 hrs in air.....	149
A.	Power saturation behavior of long-lived radicals in TGDDM-DDS epoxy irradiated with a dose of 5 Mrad of γ -radiation. ESR measurements were made at room temperature.....	166

1. INTRODUCTION

High performance fiber/polymer composite materials are widely used today in aerospace technology because of their high strength/weight ratio and dimensional stability. However, materials used in long-term geosynchronous orbit operations will be exposed to a substantial amount of ionizing radiation including gamma-radiation, electrons and protons. In some cases, a 20 - 30 year space operation will result in radiation dose levels up to 10,000 Mrad [1-2].

In order to predict the change in mechanical properties of fiber/polymer composites under the ionizing radiation, it is necessary to observe responses of both the fiber and the matrix to ionizing radiation. The direct observation of physical and chemical changes at the fiber/matrix interface is often difficult. Nevertheless, great efforts have been made to understand the interaction between two phases at the interface of composites and many mechanisms have been proposed for the radiation-induced degradation or oxidation of epoxies, particularly those based on the diglycidyl ether of bisphenol A (DGEBA) or, less frequently, based on the tetraglycidyl diamino diphenyl methane (TGDDM) cured with diamino diphenyl sulfone (DDS) which is widely used today for high performance composites. However, no mechanisms or theories have fully explained the radiation-induced chemical changes in epoxies, in fibers, or at the interface of composites to-date.

The main objective of this study is to examine molecular-structural changes in the TGDDM-DDS epoxy system upon exposure to high energy radiation and the resultant surface property changes in both epoxy and graphite fiber to elucidate the changes in interfacial strength of graphite fiber/epoxy composites exposed to the ionizing radiation.

2. LITERATURE REVIEW

2.1. Interaction of Radiation with Matter

2.1.1 Radiation Sources

Radiation sources can generally be classified into two groups: charged particles and uncharged particles. Electrons, protons and alpha-particles belong to the former group, while ultraviolet (uv) light, visible light, x-ray, gamma-ray and neutrons belong to the latter group.

If the energy of the particles is much greater than the binding energy of any orbital electron to the nucleus, the radiation is called 'ionizing radiation' or 'high energy radiation' since the particles can ionize the matter directly or indirectly depending on the nature of the interaction. Charged particles directly ionize the molecules of the irradiated medium while uncharged particles do not directly ionize the matter but are capable of transferring their energy to electrons which are themselves ejected from the irradiated molecule and create secondary ionizing tracks [3a].

The process in which chemical reactions are induced by the ionizing radiation is often called 'radiolysis' in contrast to 'photolysis' which refers to the process in which the reaction is induced by low energy photons such as ultraviolet light or visible light. The lowest ionizing level for most elements and organic compounds is about 15 eV

but many excitation levels may lie close to 5 eV [4a]. Therefore, a photon of uv-light with a wavelength of 2500 Å⁰, which has an energy of 4.96 eV, does not ionize the matter directly but is able to induce chemical reactions through electronically excited species [5a]. In many chemical compounds including polymers, however, the products of photolysis are at least quantitatively similar to those of radiolysis [6a]. A comparison between the photolysis (photo process) and radiolysis (radiation process) is illustrated schematically in Figure 2.1,

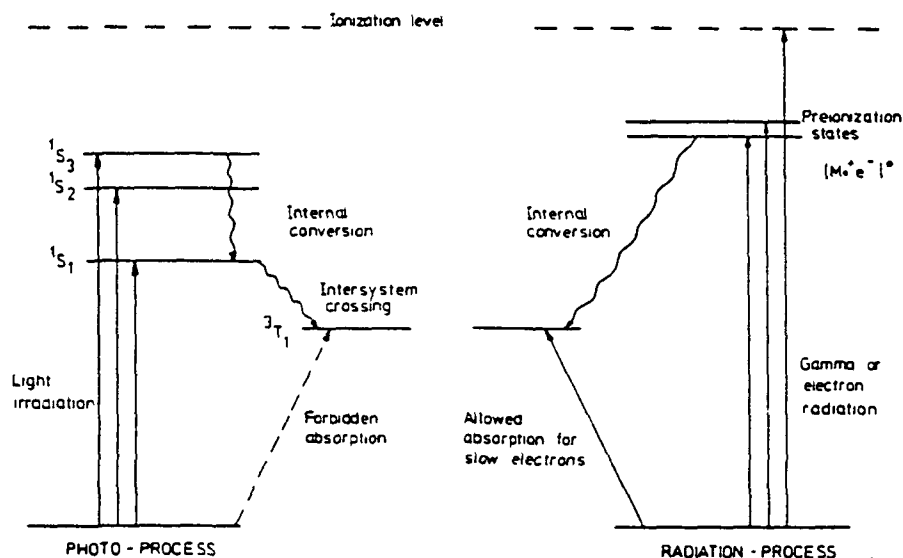


Figure 2.1. Modified diagram for the most important processes involving electronically excited states and preionization states [6a].

where S denotes the excited singlet state and T is the lowest triplet state.

2.1.2 Energy Transfer Mechanism of Radiation

2.1.2.1 Photons

Depending on the intensity of the photon energy and the nature of the irradiated medium, electromagnetic photons such as x-ray, gamma-ray and uv-light may lose their energy via [4a]:

- 1) collisions with the orbital electrons (Compton effect)
- 2) photoelectric absorption
- 3) reactions with the nucleus
- 4) electron/positron pair production

The reduction in intensity of the electromagnetic radiation (dI_1) on passing through a small thickness (dl) of the medium is given by:

$$dI_1 = - I_1 \mu dl \quad (2.1)$$

where I_1 is the intensity of the incident radiation before transmitting the thickness dl and μ is 'total linear absorption coefficient' or 'total linear attenuation coefficient.' The intensity of the transmitted radiation I through a thickness l is obtained by integrating equation (2.1) [4a, 5a, 7a]:

$$I = I_0 \exp(-\mu l) \quad (2.2)$$

where I_0 is the intensity of the incident radiation.

PHOTOELECTRIC ABSORPTION: When the incident photon has an energy greater than the K-binding energy of the absorbing element, photoelectric absorption occurs mainly in the K-shell with L-shell contributing approximately 20 % and the outer shells contributing even less. The vacancy resulting from ejection of an electron in an inner shell is filled by an electron from an outer shell with emission of characteristic x-radiation or low energy Auger electrons [7a]. In the photoelectric interaction the entire energy of a photon is assumed to transfer to a single atomic electron. Thus, the electron ejected from the atom has an energy E_e which is equal to the difference between the incident photon energy $h\nu_0$ and the binding energy of the electron in the atom E_b :

$$E_e = h\nu_0 - E_b \quad (2.3)$$

The angles of the ejected electrons to the direction of the incident photon are mainly 90° . The ionization of molecules of the absorbing medium by the low energy photons occurs primarily through the ejected photoelectrons [5a]. At energies below 60 KeV, the photoelectric effect is the major process in the case of water [4a]. As the photon energy increases, the distribution of the angles of the ejected electrons shifts increasingly toward the forward direction and the photoelectric effect becomes less important. The chance of photoelectric absorption also depends on the

nature of the medium. For example, the photon energy in which 5 % is dissipated by photoelectric absorption is 0.15 MeV for aluminum, 0.4 MeV for copper, 1.2 MeV for tin, and 4.7 MeV for lead. Therefore, except for heavier elements, the photoelectric effect of Co-60 gamma-radiation with 1.17 MeV and 1.33 MeV, is not significant [7b].

COMPTON EFFECT: The loss of the photon energy by Compton scattering arises from a collision between a photon and an electron as in a billiard ball collision. By this interaction the photon is accelerated with a reduced energy and the electron is scattered. The energy and momentum of the original photon are shared between the scattered photon and the recoil electron. Since both energy and momentum are conserved, the energy of the scattered photon can be expressed as following equation:

$$h\nu = \frac{h\nu_0}{1 + (h\nu_0/mc^2)(1 - \cos \theta)} \quad (2.4)$$

where $h\nu$ and $h\nu_0$ are energies of scattered photon and the incident photon, respectively, θ is the scattering angle of recoil photon, and mc^2 the rest energy of electron.

The energy of a recoil electron E_e is equal to the energy difference between the incident and scattered photons [5b]:

$$E_e = h\nu_0 - h\nu \quad (2.5)$$

E_e may have values ranging from 0 to a fraction of the incident energy, $2h\nu_0 / (mc^2 + 2h\nu_0)$, depending on the scattering angle of the photon [4a]. When the energy of the incident photon is large compared to the electron binding energy, the binding energy of electron is generally ignored and the electron in an atom can be considered as a free electron. For example, at an energy range of 60 KeV to 25 MeV, Compton scattering is predominant for water in which the binding energy of electrons is the order of 500 eV [4a, 5b, 7b]. Either the photoelectric absorption or Compton scattering may produce one or more fast electrons which cause major radiation-induced changes in organic materials producing subsequent ionization or excitation of the absorbing molecules [4a].

PHOTO NUCLEAR REACTION: Nuclear reactions produce radioactive species that can also cause continuing radiochemical changes in the irradiated samples. The energy required for nuclear reactions depends on the particular nucleus involved but is usually well above 8 MeV for higher atomic number (Z) materials and in the region of 10 to 20 MeV for lower-Z materials. For example, natural lead and C-12 undergo a (γ, n) reaction with a threshold energy of 7.9 MeV and 18.7 MeV, respectively [4a, 5b].

PAIR PRODUCTION: Pair production of an electron and a positron can occur when a photon with an energy exceeding

1.02 MeV, which is two times the rest energy of electron ($2mc^2$), is completely absorbed in the field of an atomic nucleus or, less frequently, an electron [4a, 5a]. The positron is slowed down and eventually combines with an electron with simultaneous emission of two 0.51 MeV gamma-rays in opposite directions (annihilation radiation) [5a]. Since polymers usually contain atoms of low atomic numbers, pair production is of little importance in the radiation chemistry of polymers.

2.1.2.2 High Energy Electrons

Accelerated electrons used in radiation work lose most of their energy by reacting with orbital electrons. Consequently the primary electron is deviated and the bound electron may either be given sufficient energy to leave its parent atom completely (ionization) or move to an orbital of higher energy (excitation) [4a].

The observed chemical effects of fast electrons may therefore be due to positive ions, free electrons, and excited molecules produced by the primary reactions, or due to ions and radicals produced subsequently by the products of the primary reaction. Figure 2.2 summarizes the various radiation processes which may occur in both liquid and solid,

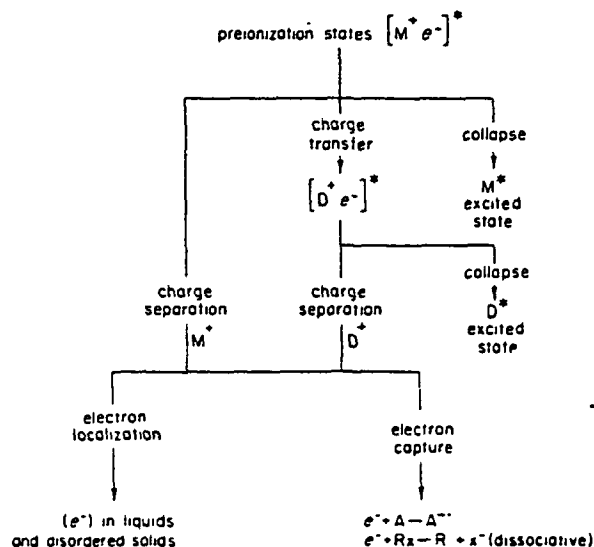


Figure 2.2. Schematic representation of processes leading to charge separation and excited state formation in liquid and solid states [8].

where the asterisk denotes an excited state, M^* an excited molecule, A and R molecules which present in the medium, and D a suitable molecule of low ionization potential [8].

Although generalities can be stated, theory can not predict the specific molecular processes which follow excitation, ionization and electron attachment. Even when information about these elementary steps is available from gas phase experiments, it is questionable to assume that these findings can be applied directly to liquid and solid systems [8].

Owing to the considerable difference in the masses involved, very little energy is transmitted to the nuclei when fast electrons are absorbed by the medium. Thus, only electrons of high energy are capable of causing chemical changes by direct displacement of the atomic nucleus or by subsequent ionization or excitation caused by the motion of the ejected nucleus through the specimen. The number of such close collisions is, in any case, small and the main effect of electron-nucleus interaction is scattering of the incident electrons. An electron may suffer a number of such close collisions and be reversed in direction (back scattering). The deflection of an electron depends on the square of the nuclear charge, Z^2 , and thus the energy loss due to the back scattering is low for most polymeric materials which contain light atoms [4a].

Scattering of the primary electrons causes the liberation of electrons (δ -ray) from the parent atom which causes small side tracks, spurs or clusters of ions and excited molecules. In principle, any type of ionizing radiation can cause such tracks or spurs resulting in non-uniform ionization of the medium [5b]. The ionization density distribution or effective dosage across the sample varies with the depth such that a maximum value is reached near the sample surface and subsequently drops to a small value [4a, 9-10]. A uniform field of ionization is generally achieved either by using a thin specimen or by irradiating both side of the sample. A useful parameter for

the distribution of ionization or penetration of the particles is 'linear energy transfer (LET)' defined as the average energy loss per unit path of the radiation. The LET decreases as radiation energy increases and is practically constant above 1 MeV [5a], but increase again as the velocity of the incident particles reaches the velocity of light [4a].

2.1.2.3 Protons, α - and β -particles and Neutrons

The manner in which high energy protons and other charged particles react with matter is similar to that of high energy electrons [5b]. However, the penetration depth of these particles are much smaller than that of electrons of the same energy due to their larger mass and slower velocities. Therefore, they may be used for treatment of surfaces and thin foils, or for initiating reactions in gases [4a].

Being uncharged, fast neutrons do not interact with the orbital electrons but lose their energy primarily by collisions with atomic nuclei. Since in many polymers hydrogen constitutes the largest number of atoms present, the main effect of fast neutrons is production of protons within the specimen. These protons have a very short penetration depth but are responsible for intense local ionization and excitation [4a].

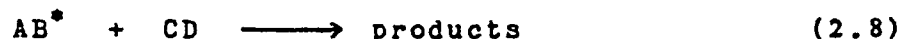
2.1.3 Radiation-Induced Chemical Changes in Polymers

2.1.3.1 Formation of Free Radicals

Free electrons, ions, and excited molecules are primarily produced in the irradiated medium by ionizing radiation (see Figure 2.2). The dissociation of the excited molecules as in equation (2.6) is believed to be largely responsible for the formation of free radicals [3b].



The excited molecules may also be converted into other products through a dissociation reaction, or by reacting with other molecules:



2.1.3.2 Stability of Free Radicals

Free radicals are characteristically unstable and quite reactive due to the presence of an unpaired electron in each radical. The unpaired electron may be paired with another unpaired electron in the other radical, or may undergo an electron transfer reaction with another molecule to produce a new and more stable radical.

The stability or, in the opposite sense, the reactivity of free radicals primarily depends on their chemical structure [5c]. If a radical has a structure

providing delocalization of the unpaired electron, the stability of free radical will increase. For example, aromatic free radicals in which the unpaired electrons resonate with the π -electrons in the phenyl ring are more stable than aliphatic free radicals [6b]. For the same reason unsaturated substituents adjacent to the carbon atom carrying the unpaired electron, e.g. as in allyl radicals, stabilize the radical [5c].

Another important factor of the chemical structure influencing radical stability is steric hindrance. As the steric hindrance effect increases the stability of the radical increases. For example, phenolic antioxidants convert highly reactive radicals such as the alkyl radical ($R\cdot$), the alkoxy radical ($RO\cdot$) and the peroxy radical ($ROO\cdot$) into less reactive aromatic radicals ($Ar\cdot$) or phenoxy radicals ($ArO\cdot$). The relative stability of the less reactive aromatic or phenoxy radicals increases as the steric hindrance in the ortho- or para-position increases [6b]. The fact that radical stability increases with the number of substituents (e.g. halogens) attached to the carbon atom carrying the unpaired electron is also attributed to the steric hindrance effect [5c].

2.1.3.3 Reaction of Free Radicals

Typical free radical reactions are kinetic chain reactions which involve three principal steps: initiation, propagation and termination [6a].

INITIATION: In this process free radicals are formed by homolytic cleavage of a bond through many ways as previously discussed [5c, 6a,c]:

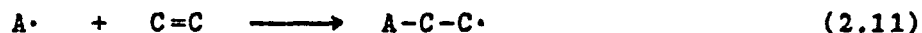


PROPAGATION: Free radicals may undergo following four types of propagation reactions.

Atomic Transfer Reaction: An atom such as hydrogen or halogen is transferred to the radical resulting in a new radical [6a, 5c, 7c]:



Addition Reaction: The free radical is added to a double bond leading to a new radical:



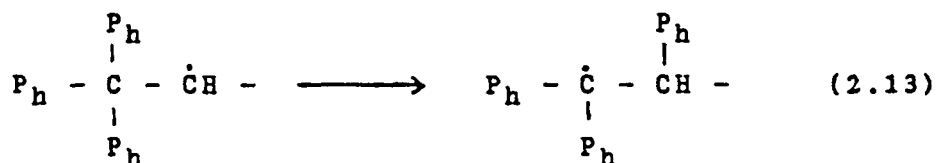
Fragmentation Reaction: A typical example of this reaction is known as 'β-scission' since the unpaired electron splits a bond in β-position producing a free radical and a molecule with a double bond:



The break-down of an alkyl radical which has sufficient activation energy belongs to this reaction [7c].

Rearrangement Reaction: The unpaired electron in a free

radical may change its position in a molecule by migration of a group leading to a more stable radical, for example :



where P_h represents a phenyl group. Groups that migrate include phenyl, halogen, hydrogen and methyl groups [7c].

TERMINATION: Termination reactions occur in all systems where free radicals are present. There are two types of termination reactions, combination and disproportionation [6a]:

Combination:



This reaction is generally favored since it has little or no activation energy but rather energy is liberated by an amount equal to the bond dissociation energy. The simple combination generally results in dimerization, branching or crosslinking [5c].

Disproportionation:



This reaction is less common than the simple combination and is rare with aromatic radicals [5c].

2.1.3.4 Crosslinking and Degradation

Crosslinking and degradation upon irradiation are important chemical processes which change the physicochemical structure and properties of polymers [11a]. Charlesby [12] and Lawton et al. [13] observed earlier that polymers may crosslink or degrade upon irradiation depending on their chemical nature. Under radiation, tertiary C-C bonds ($\geq\text{C}-\text{R}$) break more readily than secondary bonds ($>\text{CH}-\text{R}$), and secondary bonds more readily than primary bonds ($-\text{CH}_2-\text{R}$) since their dissociation energies are in the following order: primary $>$ secondary $>$ tertiary [5d]. For the same reason, polymers having $-\text{CH}_2-\overset{\text{R}}{\underset{|}{\text{CH}}}-$ groups tend to crosslink upon irradiation while polymers having $-\text{CH}_2-\overset{\text{R}}{\underset{\text{R}}{\underset{|}{\text{C}}}}-$ groups degrade [14]. There are such exceptions for this generality as, for example, polyvinyl alcohol undergoes degradation upon irradiation [15].

In general, both crosslinking and chain-scission can take place simultaneously upon irradiation. The final properties of polymers are therefore controlled by the net result of these two competing processes. As crosslinking density of an unmodified amorphous polymer system increases, the polymer usually becomes stiffer, stronger, tougher and less soluble in solvent and the glass transition temperature increases. However, excessive crosslinking may deteriorate

the mechanical property and lead to embrittlement of the polymer depending on the method of crosslinking and location of the crosslinks (crystalline regions or amorphous regions) [16]. Polymers that degrade upon irradiation show a decrease in intrinsic viscosity [4b] and in mechanical integrity such as modulus or strength [17-18]

2.1.3.5 Effect of Temperature on Rates of Crosslinking and Degradation

In general, rates of crosslinking and degradation of polymers increase as the irradiation temperature increases [11b]. Chapiro [3c] has described the temperature dependence of the crosslinking rate of polyethylene according to the Arrhenius equation. Since the temperature dependence is, however, very much related to the chemical structure and physical state of the polymer it can not be generalized in a simple equation. Jenkins [19] has reported that the rate of crosslinking of a rubber mixture (based on polydimethyl siloxane) did not follow the Arrhenius equation.

Two factors which must be taken into account during investigation of the irradiation temperature effect on degradation and crosslinking of polymers are: (1) mobility of radicals and (2) diffusivity of gaseous products generated by irradiation, which may undergo a recombination reaction with the radicals. For most polymers the irradiation temperature dependence of crosslinking and

degradation rates changes dramatically near the glass transition temperature (T_g) or melting temperature (T_m). Due to lack of mobility of polymer radicals at temperatures below T_g , crosslinking is retarded and a high concentration of stabilized radicals accumulate. If the irradiation temperature rises above T_g , the crosslinking rate increases sharply and conditions may occur favoring the crosslinking of polymers which preferentially undergo degradation at temperatures below T_g . In some cases, such a sharp change in temperature dependence can take place below T_g . For example, the degradation rate of polymethyl methacrylate changes sharply at -20°C and thereafter the degradation rate remains unchanged even at the glass transition temperature ($T_g \approx 100^\circ\text{C}$) [11b].

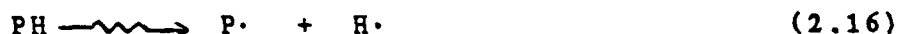
The gaseous products, e.g. hydrogen, generated by irradiation may accumulate in the sample at lower temperature and thus the probability of reverse recombination between polymer radicals and the gaseous products increases resulting in a decrease in crosslinking rate. As temperature rises, the diffusivity of the gaseous products becomes higher so that the gases escape more easily out of the sample. Consequently, the chance of reverse recombination of the radicals with the gases becomes lower but the chance of combination reactions between radicals becomes higher resulting in more crosslinks in the sample [11b].

2.2 Radiation-Induced Oxidation

2.2.1 General Mechanism of Photooxidation of Polymers

2.2.1.1 Initiation Reaction

For rapid oxidation of polymers (PH) formation of polymer radicals (P•) is necessary:



This reaction can be initiated by physical means such as thermal energy, uv-radiation, ionizing radiation, ultrasonic or mechanical forces, or this reaction can be induced chemically with initiators [20a].

2.2.1.2 Formation of Hydroperoxides

Polymer radicals (P•) can easily react with oxygen which is biradical in nature and produce peroxy radicals (POO•):



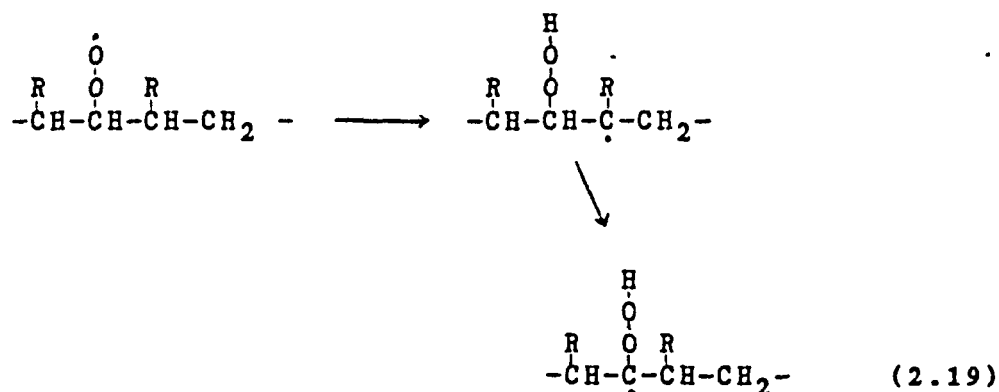
The peroxy radical attacks and abstracts a hydrogen atom from other molecules to form a hydroperoxide:



The peroxy radicals are strongly resonance stabilized and are relatively selective electrophilic species such that they abstract tertiary bonded hydrogens in preference to

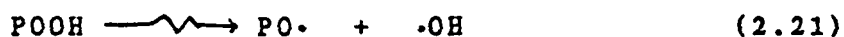
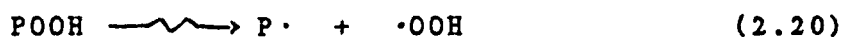
secondary bonded or primary bonded ones [20a]. Reactions (2.17) and (2.18), taken together, constitute a chain reaction of the type responsible for 'auto oxidation' (self-oxidation under mild condition) [5c].

Formation of hydroperoxide groups by intramolecular transfer of hydrogen atom is also possible, for example [20a]:



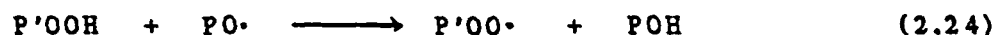
2.2.1.3 Decomposition of Hydroperoxides

A polymer peroxide may decompose under irradiation in three ways:



Of these three reactions, reaction (2.21) probably predominates since the bond energy of RO-OH (42 Kcal/Mole) is less than those of R-OOH (70 Kcal/Mole) and ROO-H (90 Kcal/mole). Reaction (2.22) rarely occurs under low energy

radiation such as uv-light with a wave length above 300 nm. Free radicals produced from reaction (2.21) can decompose the peroxide to produce peroxy radicals [20a]:



2.2.1.4 Formation of Hydroxyl Groups

Hydroxyl groups are formed in the reaction between alkoxy radicals ($\text{PO}\cdot$) and other polymer molecules (PH):

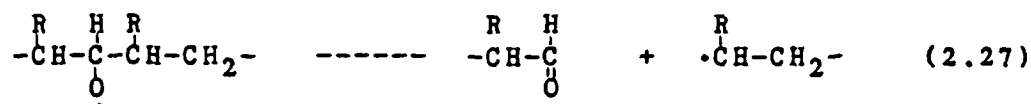
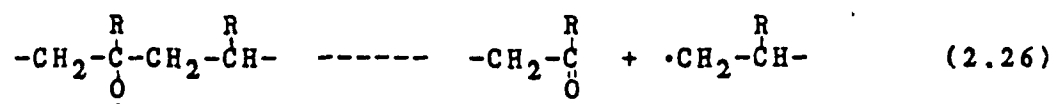


The -OH groups may be formed either along the polymer chain or on its end groups but the latter is rare. The typical IR absorption band of the hydroxyl group is in the range of $3400 - 3600 \text{ cm}^{-1}$ [20a].

2.2.1.5 Formation of Carbonyl Groups

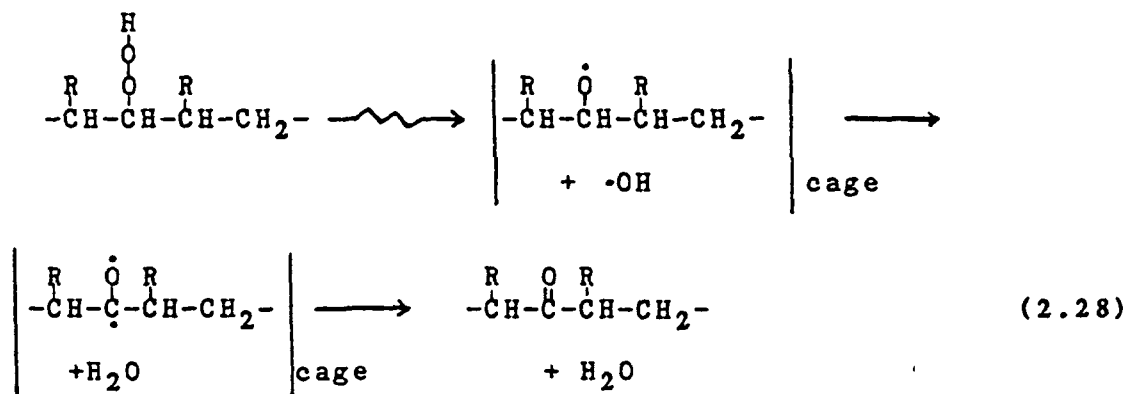
Carbonyl groups can be formed in different ways:

1) β -scission of alkoxy radicals yields either ketone or aldehyde groups:

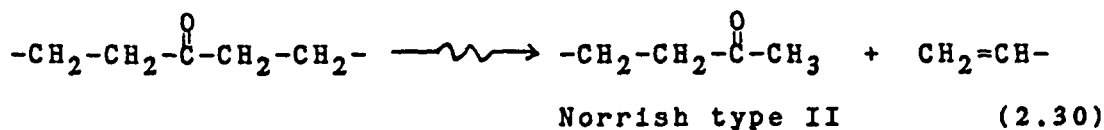
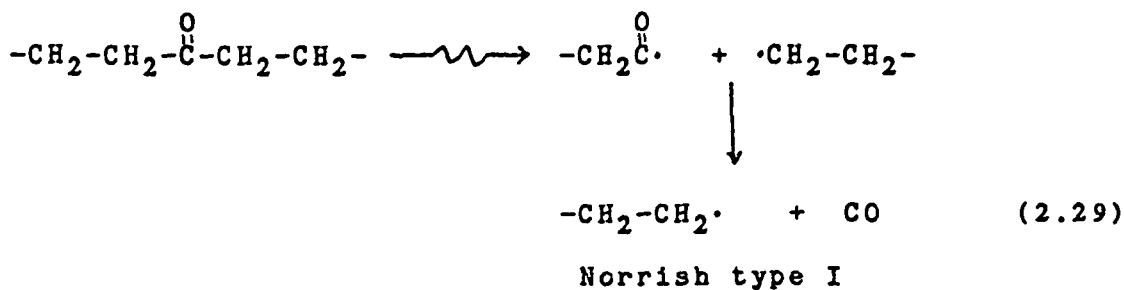


This process plays a very important role in the main-chain scission of polymers and in the formation of alkyl radicals at the end of the polymer chains [20a]. Recently, Li and Guillet [21] claimed that the β -scission of the macroalkoxy radical would only be a minor process in comparison to hydrogen abstraction since the rate constant of β -scission for alkoxy radicals in small molecules or in macromolecular systems is usually of the order of $40 \text{ M}^{-1}\text{s}^{-1}$ whereas that of bimolecular hydrogen abstraction lies in the range of $10^5 - 10^6 \text{ M}^{-1}\text{s}^{-1}$.

2) The highly reactive hydroxyl radicals (HO^\bullet) under certain conditions (e.g. cage effect) may abstract labile atoms, e.g. tertiary bonded hydrogens, and form an intermediate biradical which consequently gives a carbonyl group:

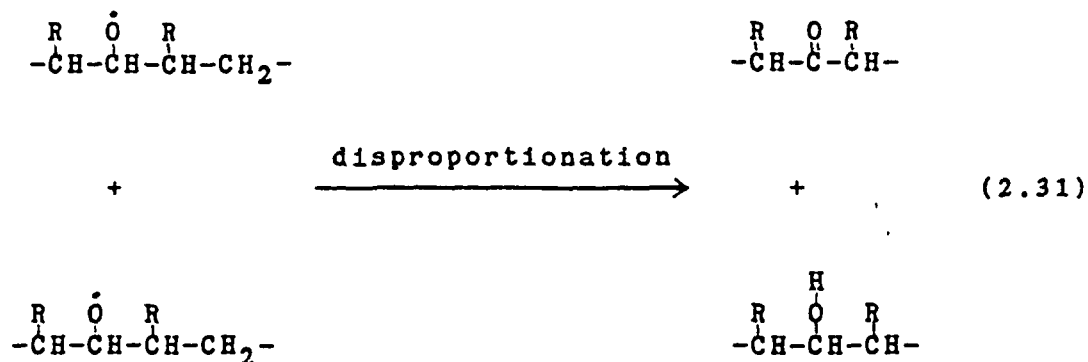


Upon further irradiation, the ketones could undergo decomposition via Norrish type I and type II reactions, for example:



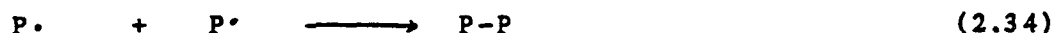
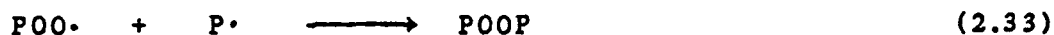
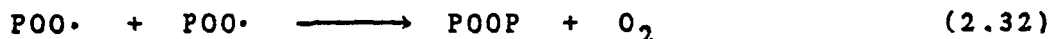
Both reactions cause chain scission and at ordinary temperature around 300°K type II reaction is predominant. Type I reaction is strongly temperature-dependent and as the temperature increases it accounts for a higher fraction of the total reaction [20b].

3) Reaction between two alkoxy radicals can simultaneously produce a carbonyl group and a hydroxyl group [20a]:



2.2.1.6 Termination Reaction

Reaction of free radicals with each other by combination produces inactive products:



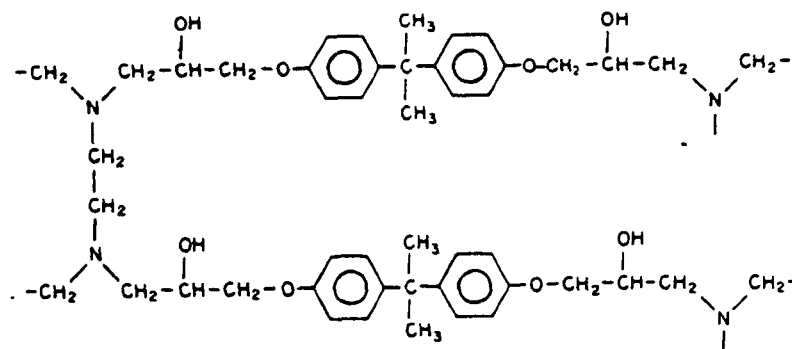
When there is a sufficient amount of oxygen in the system the termination reaction almost exclusively follows equation (2.32). At lower oxygen content, reactions (2.33) and (2.34) take place to some extent. The competition between hydrogen abstraction reaction (2.18) leading to the formation of hydroperoxides and the reaction (2.32) resulting in peroxide crosslinks depends on the temperature and the nature of the irradiated polymers [20a].

2.2.2 Radiation Induced Degradation of Epoxies

Several studies have been reported on radiation induced degradation of polymers. A broad review of those papers has been made by Ranby and Rabek [6]. Although some studies of the degradation of epoxies under various irradiation conditions have also been reported, the degradation mechanisms proposed in the literature are still controversial.

Ranby and Rabek [20b] have listed all possible radiation processes of the phenoxy polymer diglycidyl ether of bisphenol A (DGEBA) without indicating which reactions

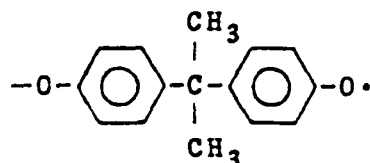
would be predominant ones among the processes. Burnay [22] suggested six possible degradation reactions (see Figure 2.3) in an epoxy system, based on DGEBA cured with ethylene diamine (EDA), exposed to 1/2 MeV electrons on the basis of UV and IR absorption results.



DGEBA-EDA epoxy network

Among the six possible radiation processes, he concluded, reaction (I) and reaction (II) would be the dominant ones (see Figure 2.3).

Hikita et al. [23] have proposed that the photodegradation process of DGEBA resin, exposed to radiation from an ultra-low pressure mercury arc (254 nm), occurs by formation of phenoxy radicals (as confirmed by the sharp ESR peak with $g = 2.0042$):



Phenoxy Radical of DGEBA

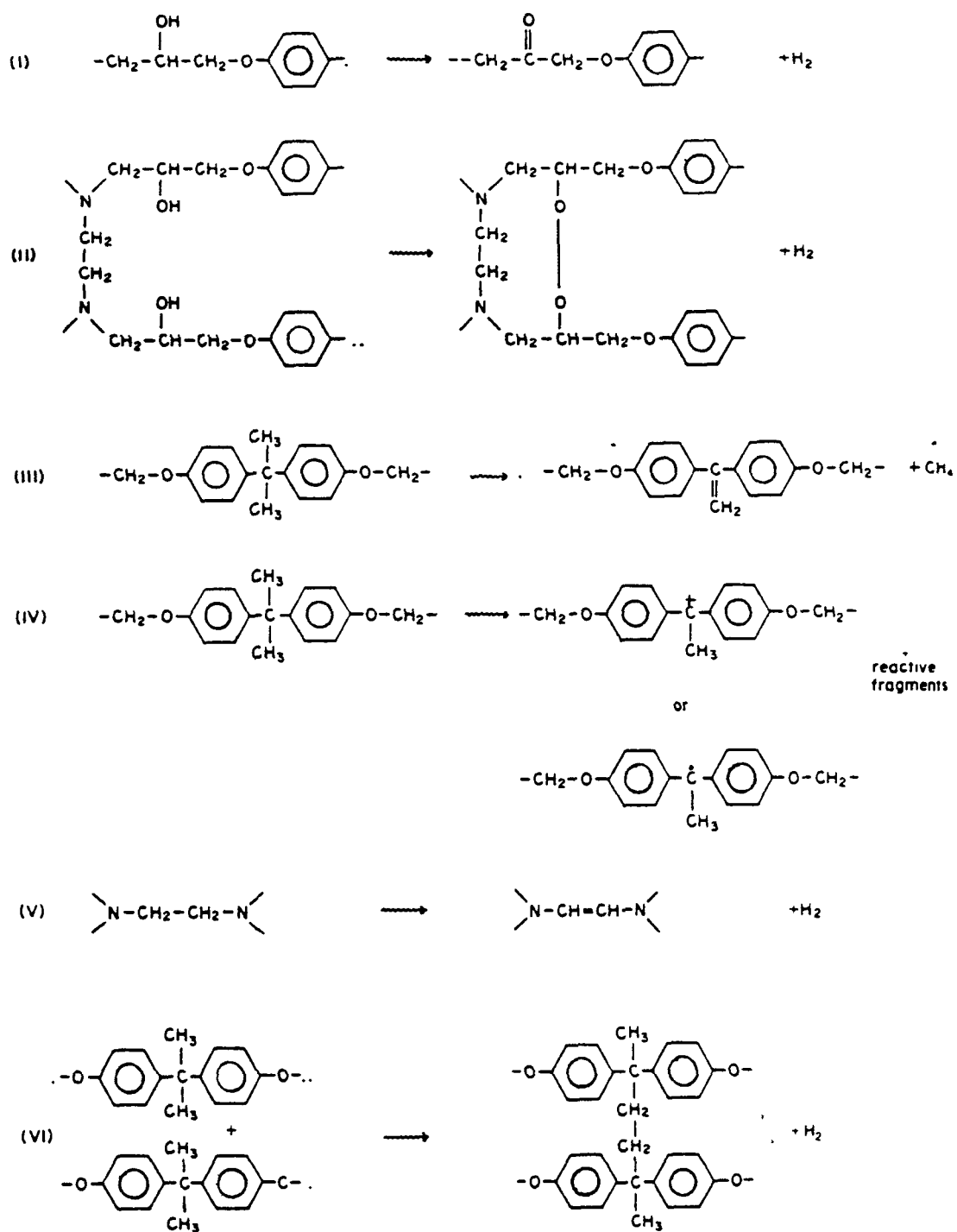
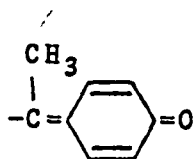
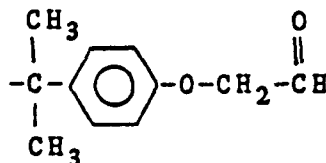


Figure 2.3 Possible radiation processes in DGEBA-EDA epoxy [22].

then quinonoid and aldehyde compounds appears gradually with various low molecular weight products such as CO , CO_2 , CH_4 and C_6H_6 escaping:



Quinonoid



Aldehyde

They attributed the increase in the 1675 cm^{-1} IR absorption peak, which is normal for α,β -unsaturated ketone, to the formation of a quinonoid, and the decrease in the 1259 cm^{-1} peak to the decrease of C-O linkage of phenol.

It is not easy to examine non-oxidative degradation since there is always the possibility that the original sample contains dissolved oxygen which is not completely removed. This dissolved oxygen would lead to some oxidative degradation, especially at the initial stage of irradiation [11a, 24]. In the presence of air, polymers can be thermally oxidized producing hydroperoxide groups and carbonyl groups as in ketones or aldehydes [21]. The hydroperoxide and carbonyl groups are considered to be very important species causing photodegradation since they act as an effective sensitizer in photooxidation [21, 25].

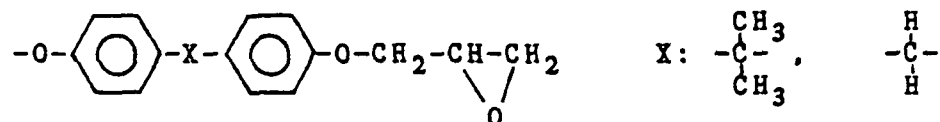
Tsuji et al. [26-28] have proposed a different point of view on the role of oxygen in photodegradation. They found that at all wavelengths of uv-light that they

investigated the radical yield in an oxygen atmosphere was greater than that in a nitrogen atmosphere. They attributed the greater radical yield in the oxygen atmosphere to greater absorption of uv-light by the charge-transfer complexes which are composed of oxygen molecules and polymers and act as UV-absorbers. The energy absorbed by the complexes is transferred to other parts of the polymer to produce free radicals, or the complexes themselves make free radicals through the excited states. The behavior of cured epoxy under radiation depends strongly on the chemical structure of the epoxy resin and the hardener. Recently, Bellenger et al. [29-31] attempted to examine the influence of the structure of epoxy resin and the hardener on photooxidation of the cured epoxy system under uv-light (300 nm - 450 nm). The epoxy systems they examined are listed in Table 2.1. They attributed the IR absorption peaks at 1735 cm^{-1} and at 1670 cm^{-1} , which are observed in both aromatic and non-aromatic amine cured epoxy systems, to carbonyl groups and amide groups, respectively. They claimed that a majority of the carbonyl groups are derived from the secondary hydroxyl groups in the cured epoxy, and that there could be many ways to reach the final carbonyl groups (see Figure 2.4) [29].

The growth rate of amide groups determined from absorbance changes in the 1670 cm^{-1} IR peak per unit thickness of sample (cm) as a function of exposure time (hour) to uv-light was closely related to the number of α -

Table 2.1 List of various epoxy resins and hardeners [29, 31]

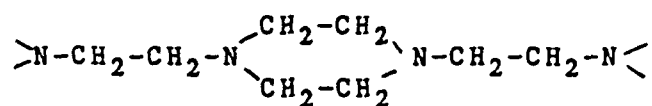
Resins



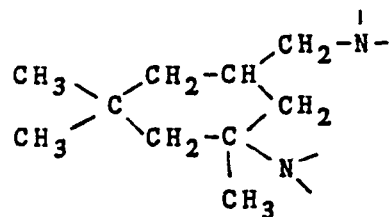
Hardeners (aromatic)



Hardeners (non-aromatic)



Aminoethyl piperazine (AEP)



Isoporone diamine (IPD)

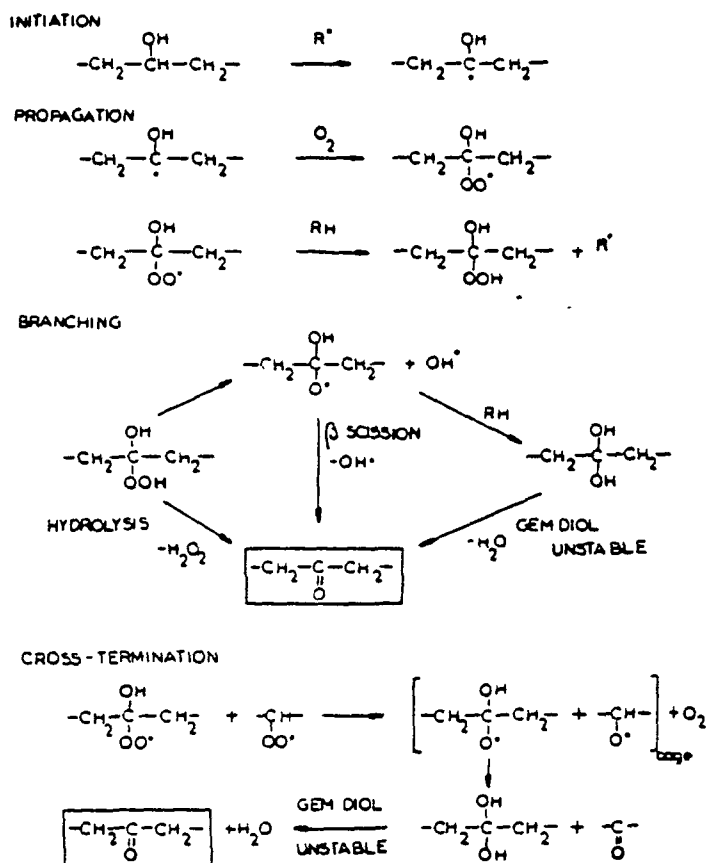
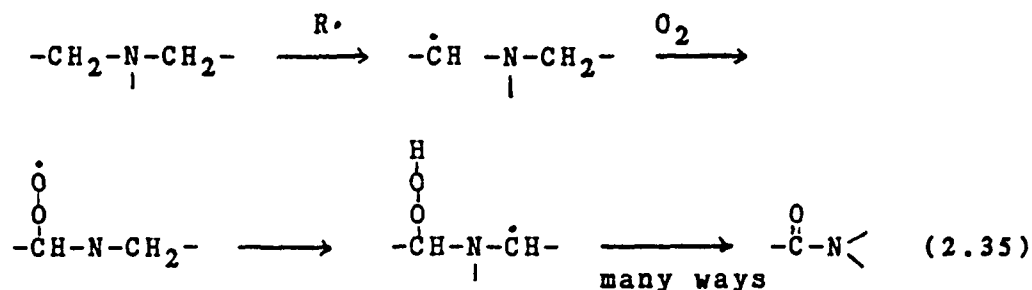
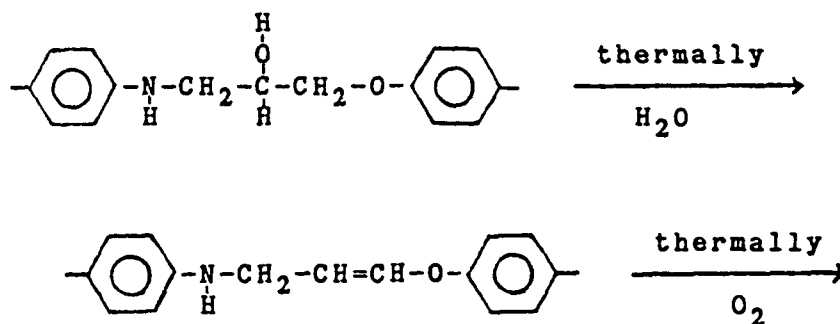


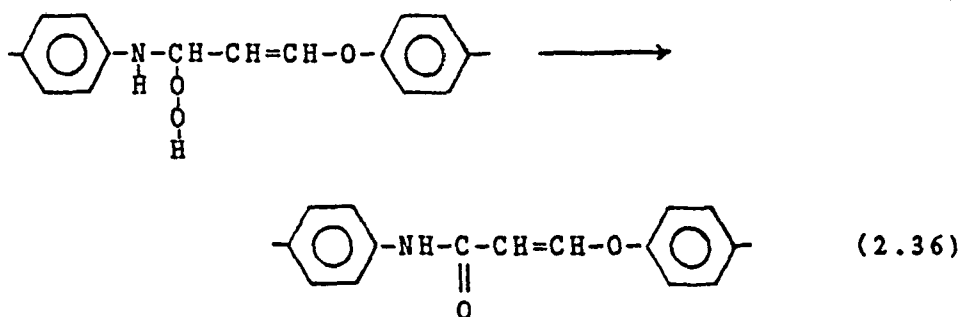
Figure 2.4 Formation of carbonyl groups from secondary hydroxyl groups in cured epoxy in the presence of oxygen [29].

methylene groups [α -CH₂] in the non-aromatic amine hardeners such that the square root of the growth rate of amides was proportional to the number of α -CH₂. Thus the order of growth rates of amides in the cured epoxies with non-aromatic hardeners was: AEP (12 α -CH₂) > DETA (9 α -CH₂) > IPD(5 α -CH₂). From these observations they suggested a mechanism for amide formation including an intramolecular propagation and a catalytic effect of the tertiary amine structure [29, 31]:



A similar oxidation reaction of the secondary amine structure in a thermally-treated DGEBA cured with P,P'-diamino diphenyl methane (DDM) was postulated by Keenan et al. [24]:





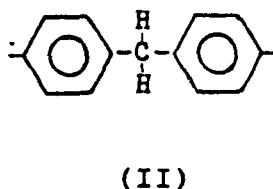
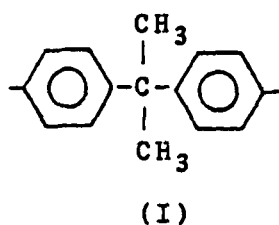
George et al.[32] have also observed an increase in the IR absorption peak at 1665 cm^{-1} upon exposure to uv-light. Contrary to Bellenger et al., they attributed the 1665 cm^{-1} peak to aromatic carbonyl groups produced by extended oxidation of the methylene bridge. The peak at 1735 cm^{-1} was, on the other hand, attributed to aliphatic carbonyl groups produced by oxidation of methylene groups near aliphatic ether linkages in the cured novolac. The aromatic carbonyl group formation by thermal oxidation of the methylene bridge of polybenzyl was proposed by Conley early in 1965 [33]. Bellenger et al. [31] found that the epoxy system had different rates of carbonyl or amide formation depending on the bridge between phenyl rings such that initial rates of amide and carbonyl group formation increased with the electron density at the nitrogen atom of the amine hardener (see Table 2.2). The electron density was calculated from a theory based on quantum mechanics as suggested by Eichler et al. [34]. Bellenger et al. [31] interpreted the decrease of the growth rates of carbonyl and amide groups with the electron density of the adjacent nitrogen in terms of the inductive effect of the bridge Z

(see Table 2.1) on hydrogen abstraction from the α -methylene, the secondary alcohol, or the methylene next to ether linkage of DGEBA resulting in the formation of amide or carbonyl groups.

Table 2.2. Initial rates of carbonyl and amide growths (absorbance units $\text{cm}^{-1}\text{h}^{-1}$) and electron density of the nitrogen atom in DGEBA epoxy [31]

	Electron density	Growth Rates ($\text{cm}^{-1}\text{h}^{-1}$)	
		Carbonyls	Amides
DGEBA-DDE	1.882	0.30	0.26
DGEBA-DDM	1.859	0.25	0.13
DGEBA-DDS	1.683	0.13	0.00

Bellenger et al. [31] also claimed that the initial growth rates of carbonyl and amide groups were noticeably decreased as the isopropylidene unit (I) of the epoxy was replaced by a methylene unit (II):



This result is contradictory to George et al.'s [32] observation that the epoxy novolac (DEN 438), where two phenyl rings are connected by a methylene, had an oxidation rate eight times that of DGEBA (Epon 828) upon exposure to uv-light (300 - 350 nm).

2.3 Electron Spin Resonance (ESR)

2.3.1 Basic Principles of ESR

The magnetic moment $\vec{\mu}$ of an electron is given by the equation:

$$\vec{\mu} = -g\beta\vec{M}_S \quad (2.37)$$

where $\hbar\vec{M}_S$ (\hbar is Planck's constant divided by 2π) is the spin angular momentum vector of electron, g is a dimensionless constant called 'Lande g-factor,' 'electron spin g-factor' or simply called 'g-factor' and β is the Bohr magneton equal to $e\hbar/2mc$ (m = mass of electron, e = charge of electron, c = velocity of light). \vec{M}_S and g are the quantities associated with electron spins and whose different values distinguish one electron from another so far as magnetic resonance is concerned [35].

The allowed values of \vec{M}_S along an arbitrary direction range from $-S$ to $+S$ in unit increments where S denotes the spin quantum number. The case of $S = 1/2$, in which the free radicals are in the singlet state, occurs most frequently and is usually of most interest in organic materials. For magnetic ions, especially those of the transition metals and rare earth metals, states with $S > 1/2$ are very common [36].

The energy of the magnetic dipole, W , in a magnetic field is given as:

$$W = -\vec{\mu} \cdot \vec{H} = -\mu H \cos(\vec{\mu}, \vec{H}) \quad (2.38)$$

where $\vec{\mu}$ is the magnetic dipole moment as defined in equation

(2.37), \vec{H} is the applied magnetic field and $(\vec{\mu}, \vec{H})$ represents the angle between $\vec{\mu}$ and \vec{H} .

By inserting equation (2.37) into equation (2.38) the energy of the magnetic dipole in the direction of \vec{H} , W_z , can be obtained:

$$W_z = g\beta M_z H_z \quad (2.39)$$

where the subscript z denotes the direction of \vec{H} . When $S = 1/2$ as for the electron \vec{M}_s has two possible projections, $+1/2$ and $-1/2$, along the direction of \vec{H} . It has a value of $+1/2$ when the dipole is antiparallel to the direction of \vec{H} and a value of $-1/2$ when the dipole is parallel to the direction of \vec{H} . Therefore, two possible values of W_z are $+1/2 (g\beta H)$ and $-1/2 (g\beta H)$. These two values are sometimes referred to as 'Zeeman energies.' The energy difference $g\beta H$ between the Zeeman levels increases linearly with the magnetic field intensity (see Figure 2.5) and is the basis of the electron spin resonance experiments. Transition between these two energy levels can be induced, if a electromagnetic field of an appropriate frequency (ν) matches the energy-level separation, $g\beta H$:

$$h\nu = g\beta H_r \quad (2.40)$$

where H_r is the magnetic field at which the resonance condition is satisfied.

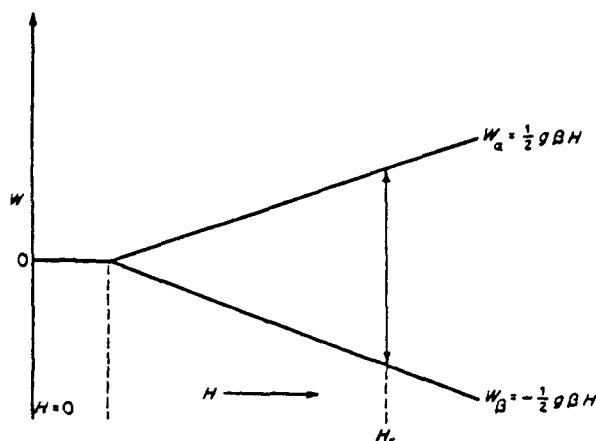


Figure 2.5 Energy-level scheme for the simplest system showing ESR absorption. W_a and W_B represent the energies of the $M_S = +1/2$ and $M_S = -1/2$ states, respectively [36].

The ESR signal intensity is directly proportional to the population difference of parallel (N_B) and antiparallel (N_a) spin states in thermal equilibrium. The ratio of the two populations is given by the Boltzmann equation:

$$\frac{N_B}{N_a} = \exp (g\beta H/kT) \quad (2.41)$$

where k is the Boltzmann constant. In thermal equilibrium N_B is slightly greater than N_a which give rise to a small temperature-dependent paramagnetism. At ordinary temperatures (i.e., $g\beta H \ll kT$) the ratio is approximately $(1 + g\beta H/kT)$ and the population difference $\Delta n = N_B - N_a =$

$N_0(g\beta H/kT)/2$, where N_0 is the total number of unpaired electrons, $N_0 = N_\beta + N_\alpha$. Therefore, the ESR intensity is inversely proportional to the absolute temperature. The probability of a transition between the two energy levels is proportional to the square of the irradiation field amplitude (in the microwave region for most experiments) [35]. With increasing microwave energy, the ESR signal intensity increases to a maximum. With a further increase of the microwave power the signal intensity decreases because the spins can not relax fast enough and the line shape becomes distorted as the Boltzmann equilibrium distribution is disturbed. This condition is described as 'saturation' [6, 35].

2.3.2 The g-factor

The g-factor can be evaluated directly from the resonance equation (2.40) which can be rewritten as:

$$g = \frac{h\nu}{H_r\beta} \quad (2.42)$$

In general, the g-value of an unknown sample is determined from the following equation [6]:

$$g_u = g_s - \frac{\Delta H}{H_u} g_s \quad (2.43)$$

where ΔH is the magnetic field difference between centers of

spectra of the standard and unknown samples measured at the same microwave frequency. H_u is the magnetic field at the center of spectrum of the unknown sample. Subscripts u and s represent the unknown and standard samples, respectively.

The g-value depends on the type of radical and its electronic environment. For instance, the g-value of the peroxy radical is higher than that of the alkoxy radical. For a free electron the g-value is 2.00232. Most free radicals or transitional metal ions do have g-values of about 2, but there are also systems which show marked deviation from this value [36].

A sample may have different g-values depending on its orientation in the magnetic field when the radical has anisotropic magnetic properties. This anisotropy causes asymmetry of ESR absorption lines and gives important information about the radical structure [6, 36]. However, determination of the g-value of randomly oriented radicals as in an amorphous solid or semicrystalline polymer powder provides less information of the radical structure and electron distribution around the radical since the anisotropies are averaged spatially [6].

2.3.3 Line Shape

There are two common ESR line shapes: the Lorentzian line shape and the Gaussian line shape (see Figure 2.6). General expressions for these lines are as follows [36]:

ORIGINAL PAGE IS
OF POOR QUALITY

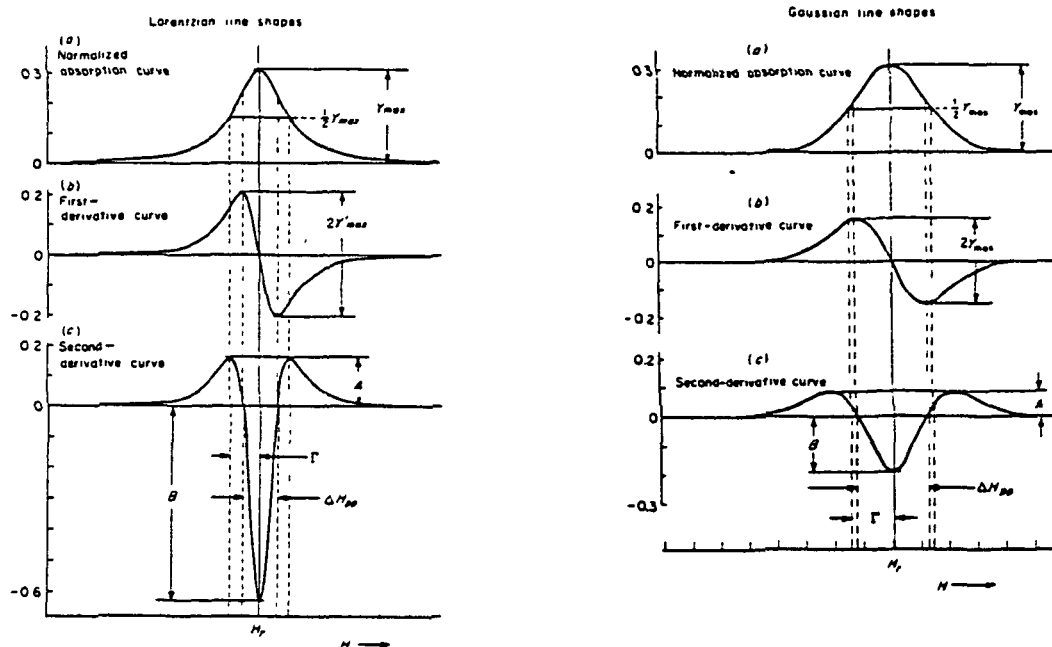


Figure 2.6 Characteristics of the Lorentzian line shape and the Gaussian line shape [36].

$$\text{Lorentzian: } Y = \frac{a}{1 + bX^2}$$

$$\text{Gaussian: } Y = a \exp (-bX^2)$$

where a and b are constants related to relaxation time of the electron spins, and X indicates the direction of field intensity. The Lorentzian line shape has relatively longer shoulders and is usually observed in liquid solution with low concentration. On the other hand, Gaussian line shapes are often obtained in crystalline solids or in samples which contain many paramagnetic components (referred to as 'spin packets') Many spectra are however a combination of both line shapes [6, 36].

The ESR line width is influenced not only by the environment of the external magnetic field but also by the interaction of electron spins, for example, with the crystal lattice (spin-lattice) or with other spins (spin-spin) within the sample. The total line width ΔH is inversely proportional to the total relaxation time T_2 :

$$\Delta H \propto \frac{1}{T_2} = \frac{1}{2T_1} + \frac{1}{T_2'} \quad (2.44)$$

where T_1 is the spin-lattice relaxation time and T_2' the

spin-spin relaxation time. For many systems, especially for stable radicals, T_1 is much greater than T_2' ($T_1 \gg T_2'$) so that for all practical purposes $T_2 \approx T_2'$ [36].

McConnel [37] has reported that line widths of symmetrical ion radicals such as negative ions of benzene, triphenylene and coronene are larger compared with those of negative ions that are less symmetrical but otherwise similar. This result was attributed to the fact that the rate of spin-lattice relaxation ($1/T_1$) in the symmetrical ion radical is significantly higher than in less symmetrical one due to larger spin-orbit interaction in the symmetrical ion radical.

Line-broadening also occurs when the unpaired electrons in various free radicals are subjected to slightly different effective magnetic fields. Some causes of the inhomogeneous broadening are listed below:

- 1) An inhomogeneous magnetic field
- 2) Anisotropic g-factor and hyperfine interaction
- 3) Unresolved hyperfine structure. For instance, when the number of hyperfine components is so great, no structure is observed but an envelope of a multitude of lines is detected.

If delocalization of the unpaired electron in the radical occurs, then any hyperfine splitting will be small and only a single broad line composed of many narrow hyperfine structures will be observed [38-40]. Onishi et al.

[40-42] have observed that many polymers such as polyethylene, polypropylene, polyvinyl chloride, rubber, polymethyl methacrylate and polyvinyl alcohol give a singlet spectrum when they are highly irradiated (1,000 Mrad) or heated after irradiation, and that the line width of the singlet decreases with radiation dose (delocalization narrowing). They suggested that as irradiation doses increase the number of unsaturated double bonds (n) in the polyenyl radicals, $-\text{CH}_2-\dot{\text{C}}\text{H}-(\text{CH}=\text{CH})_n-\text{CH}_2-$, becomes larger, i.e., delocalization of the unpaired electron increases, so that the spectrum becomes a singlet.

2.3.4 ESR Studies of Oxidation in Irradiated Polymers

The oxidation of polymeric materials exposed to either ionizing radiation or uv-radiation has been investigated by infrared spectroscopy more extensively than by the ESR technique [41]. Nevertheless, several authors [22, 28, 41-45] have reported effects of oxygen on the ESR spectra of irradiated polymers.

The ESR spectra of oxygenated radicals in most polymers are often asymmetric singlet lines. Onishi et al. [41-42] reported that it was possible to differentiate the spectrum of oxygenated radicals from that of parent ones by using a power-saturation method. The ESR spectra of the oxygenated radicals could be obtained without power-saturation line broadening at a microwave power of one to two orders of magnitude higher than for the parent radicals because the

oxygenated radicals have much shorter spin-lattice relaxation times than the parent radicals. However, this different saturation behavior was not observed in polymers that form hydrogen bonds such as polyvinyl alcohol and polyethylene glycol. From the power-saturation results they proposed that most of the parent radicals (alkyl, enyl or short polyenyl) react quickly with oxygen producing peroxy radicals which, in general, decay very fast. They observed a stable singlet spectrum after the irradiated sample had been exposed to air for a prolonged time and attributed the singlet to the polyenyl radicals.

Contrary to Onishi et al. [40], many authors have attributed the stable singlet spectra to oxygenated radicals such as peroxy radicals ($-\overset{|}{\underset{|}{\text{C}}}\text{OO}\cdot$) in polyethylene [43] or nylon [44], acyl radicals ($-\overset{\text{O}}{\underset{|}{\text{C}}}\cdot$) in polyethylene [28], alkoxy radicals ($-\overset{|}{\underset{|}{\text{C}}}\text{O}\cdot$) in TGDDM/DDS epoxy system [46], or phenoxy radicals ($-\text{C}_6\text{H}_5\text{-O}\cdot$) in DGEBA epoxy [22].

Relatively fewer ESR studies have been reported on the radiation-induced oxidation of epoxies. Jain [45] has observed a narrow singlet spectrum with a peak-to-peak width (ΔH_{pp}) varying between 10 and 12 gauss (G) in a pyrolyzed Bondar (epoxy-modified polyesteramide). Later, Overall [47] observed a symmetric narrow singlet line ($\Delta H_{pp} = 10$ G) and attributed it to semiquinone or phenoxy type radicals. Overall excluded aliphatic or alkyl radicals as the origin

of the narrow singlet claiming that the aliphatic or alkyl radicals would have much greater line width than the observed 10 G due to hyperfine splitting of protons. He also ruled out peroxy or alkoxy radicals which should have an asymmetric ESR line shape. An unusually broad singlet ($\Delta H_{pp} = 100$ G) for DGEBA epoxy was reported by Burnay [22] but no identification of radicals was made for this spectrum. Schaffer [48] has observed a broad spectrum ($\Delta H_{pp} = 24$ G) in electron- or gamma-irradiated tetraglycidyl - 4,4' diamino diphenyl methane (TGDDM) cured with 4,4' diamino diphenyl sulphone (DDS). Gupta et al. [46,49] have proposed that the ESR spectrum of irradiated TGDDM/DDS epoxy at liquid nitrogen temperature (77 °K) could be a combination of a broad singlet ($\Delta H = 30$ G), a narrow singlet ($\Delta H = 16.6$ G) and other doublet or triplet (see Table 2.3).

Table 2.3. Major radical species in TGDDM/DDS epoxy system [46]

Radical	Spectrum	Proton hyperfine constant(A) and Line width (H)
$-\text{CH}_2-\dot{\text{C}}-\text{CH}_2-$	Quintet	A: 19.2 G
$-\dot{\text{C}}=\text{O}$	Narrow Singlet	H: 16.6 G
$-\dot{\text{C}}-\text{O}\cdot$	Broad Singlet	H: 30 G
$\text{HO}-\dot{\text{C}}-\text{H}$	Broad Doublet	A: 15 G H: 30 G
$\text{H}-\dot{\text{C}}-\text{H}$	Broad Triplet	A: 13.5 G H: 30 G

They assigned the broad singlet to alkoxy type radicals ($-\dot{\text{C}}-\text{O}\cdot$), the narrow one to acyl type radicals ($-\dot{\text{C}}=\text{O}$), and the doublet and triplet to alkyl type radicals (see Table 2.3). They claimed that the computer simulated spectrum combining those spectra agreed well with the observed spectrum.

2.3.5 Radical Decay in Semicrystalline Polymers

In determining the decay kinetics of free radicals, (1) the stability of the radicals associated with their chemical structure and (2) the molecular mobility of the matrix polymers where the free radicals are trapped must be taken into account. It is often found that the decay kinetics of radicals for one polymer fails to fit other polymers. In some cases, different decay mechanisms are suggested for the same polymer. This is probably due to the fact that chemically different radical species are produced depending on polymer types and irradiation conditions and the mobility of the radicals varies depending on the physical state of the matrix polymer where they are trapped.

Several studies have been reported on the relationship between the molecular motion and radical decay kinetics. Nara et al. [50] interpreted the decay reaction of free radicals trapped in gamma-irradiated polyethylene in connection with the molecular motion of the matrix polymer. They observed three temperature regions, 120°K (T_a), 200°K (T_l) and 250°K (T_b), where the radicals decay rapidly but with different rates (see Figure 2.7).

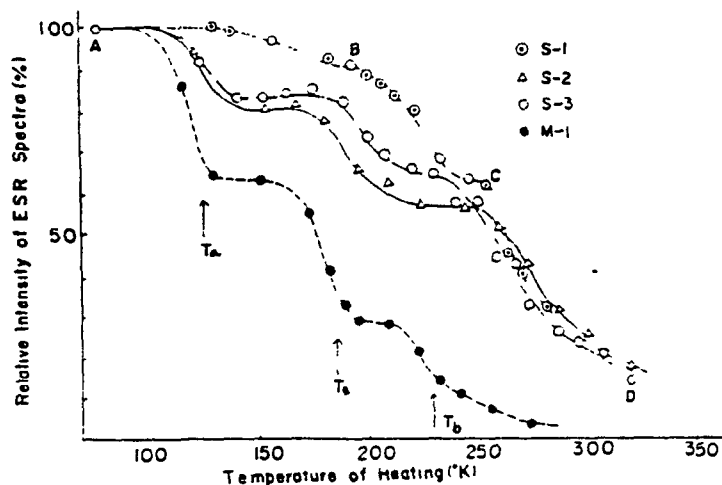


Figure 2.7. Decay curves of free radicals in various polyethylene irradiated at liquid nitrogen temperature [50].

Comparing the rate constants of the radical decay reactions (based on the second-order) and the time constants of the molecular motion in different regions of the matrix polymers, Nara et al. [50] have concluded that the decay reactions at T_a and T_b are closely related to the molecular motion in the amorphous regions of the polymer, i.e., T_a corresponds to δ -dispersion and T_b corresponds to β -dispersion of polyethylene. The decay at T_1 was attributed to the molecular motion (γ -dispersion) associated with local

mode relaxation at lamellar surfaces. They observed a similar decay behavior for a polypropylene [51] but it had only two fast decay regions at 170°K and 260°K which were considered to be associated with γ -dispersion and β -dispersion, respectively.

The three decay regions of radicals in irradiated polyethylene were also observed by Fujimura et al. [52]. Contrary to Nara and coworkers [50], they proposed that the first decay region (120°K) should be associated with radical pairs rather than the radicals trapped in amorphous regions undergoing δ -dispersion which is not generally observed in the polyethylene. Fujimura et al. also claimed that the third decay region (250°K) could not correspond to β -dispersion associated with noncrystalline regions but could correspond to α -dispersion associated with decay of radicals in crystalline regions because the ESR spectrum showed a clear anisotropy which is a characteristic of radicals trapped in crystalline regions. They provided two reasons why the temperature of the third decay region (250°K) is lower than α -relaxation temperature of polyethylene which is 350°K. First, the existence of hydrogen molecules produced by irradiation can accelerate the radical migration. Second, the formation of crystalline defects by the presence of radicals provides more molecular mobility than the regular crystalline regions.

Waterman and Dole [53] reported that alkyl radicals (in polyethylene) which persist at room temperature after an electron irradiation at liquid nitrogen temperature convert to ally radicals reacting with trans-vinylene or vinyl double bonds. The decay of alkyl radicals through the conversion process followed a first-order reaction and markedly catalyzed by molecular hydrogen [53]. Fujimura et al. [54-55] have also proposed that the alkyl radicals in gamma-irradiated polyethylene may transform into more stable allyl radicals reacting with double bonds which, for example, are produced by pre-irradiation. When such transformation of the radicals is involved during the radical decay process the overall decay kinetics becomes more complicated.

Dole and coworkers [56-58] later proposed two simultaneous first-order reactions with different rate constants associated with two reaction zones (crystalline and amorphous regions) for the decay of alkyl radicals in the irradiated polyethylene. This is contradictory to Shimada and Kashiwabara's suggestion [59] that the decay of alkyl radicals in the polyethylene follows two second-order kinetics rather than the first-order kinetics. Dole et al. [56] have also suggested that the recombination of allyl radicals in the irradiated polyethylene, on the other hand, followed two simultaneous second-order reactions with

- -

different reaction rates. They derived a theoretical equation for the two simultaneous non-diffusion controlled second-order reactions:

$$\frac{t}{(1/C - 1/C_0)} = \frac{1 + C_0 X_f X_s (k_f + k_s)t}{X_f^2 k_f + X_s^2 k_s + C_0 X_f X_s k_f k_s t} \quad (2.45)$$

where C_0 is the initial radical concentration, C the total radical concentration at time t , X_f and X_s are fractions of free radicals in fast and slow decay regions, and k_f and k_s are their reaction constants, respectively. By assuming $k_s \ll k_f$, equation (2.45) can be reduced to:

$$Q = \frac{t}{(1/C - 1/C_0)} = \frac{1}{X_f^2 k_f} + C_0 \frac{X_s}{X_f} t \quad (2.46)$$

From the slope and intercept of the plot of Q vs. t , X_f , k_f and X_s can be evaluated. If the rate of each reaction zone is diffusion-controlled, equation (2.45) can be modified by including a diffusion constant and other constants related to the radius of the reaction cage (ca. 10^{-8} cm). The Q -function is very sensitive to the initial concentration C_0 [57]. Therefore, a careful measurement of C_0 is a critical factor to test the equation.

Wuenche et al. [60] developed a scheme of interpretation of the radical decay behavior of irradiated polyethylene having three discrete decay zones. They

considered a continuous, but not constant, distribution of activation energy over the temperature range observed, and derived an equation:

$$\frac{C(t,T)}{C_0} = 1 - K\phi(F^*) (T - T_{\min}) \quad (2.47)$$

where $C(t,T)$ is the radical concentration after a constant storing time t at temperature $T(^{\circ}\text{K})$, $\phi(F^*)$ is the distribution function of activation energy F^* at each temperature, T_{\min} is the temperature at which the radical decay starts, and K is a constant given by:

$$K = R \ln(\nu t)$$

here ν is a jumping frequency factor. If the concentration of radicals is measured as a function of temperature, the free energy distribution function $\phi(F^*)$ is easily obtained by differentiating equation (2.47) with respect to $(T - T_{\min})$. The plot of $\phi(F(T))$ against T showed three distinct zones, 125°K , 150°K and $200-250^{\circ}\text{K}$ which they attributed to decay of radical pairs, alkyl radicals in the amorphous region and radicals which migrate out of the crystalline region to the crystalline surface, respectively.

If oxygen is present in the sample during irradiation, the radical decay reaction can be accelerated since the oxygen may cause oxidative chain-scission which enhances the mobility of the chain [54-55]. It is well known that peroxy radicals are produced when air or oxygen is introduced to

the system during or after irradiation. However, the decay kinetics of the peroxy radicals is still under controversy. For example, Eda et al. [61] proposed a first-order reaction with two reaction rates associated with the crystalline and amorphous region of polypropylene but Mayo [62] suggested, on the other hand, a second-order decay reaction for the peroxy radicals in polypropylene.

Recently, Hori et al [43] proposed another model for the decay of peroxy radicals and the nature of the two different decay rates in polypropylene. They considered that the ESR spectra observed after introducing air to the irradiated sample originated from two chemically identical radical species both trapped in crystalline regions but having different mobilities. They attributed the mobility difference of the peroxy radicals in crystalline regions to the local factors such as defects in the crystalline region. They claimed that the overall reaction could not be explained by either first-order or second-order kinetics but could be explained by a diffusion-controlled reaction mechanism expressed as:

$$f(t) = (1 - X_0) / (1 + At^{1/2} + Bt) \quad (2.48)$$

where X_0 is a constant representing the fraction of immobile radicals which are assumed not to contribute to the decay kinetics, $f(t)$ is thus a decay curve for mobile radicals as a function of time, and A and B are constants given by:

$$A = 8 \pi r_0^2 C_0 (\pi D)^{1/2}$$

$$B = 8 \pi r_0 D C_0$$

where r_0 is the capture radius, C_0 is the initial radical concentration of mobile peroxy radicals and D is the diffusion constant of the radical.

Rate constants and activation energies of decay reactions of radicals in the gamma-irradiated polymers can also be evaluated from a series of isothermal decay curves by using Guggenheim method and the Arrhenius equation [63]. This scheme is useful for simple first- or second-order reactions in an homogeneous phase but is not easy to apply to an inhomogeneous phase which has two or more reaction rates.

2.3.6 Radical Decay in Irradiated Epoxies

Very little information has been published on the radical decay of irradiated epoxies. Schaffer [48] and Kent [64] suggested two types of radical species in TGDDM/DDS epoxy system irradiated with gamma-radiation or high energy electrons. Both authors found radical species with two characteristic decay rates at room temperature, one decays relatively fast and the other decays relatively slowly. They interpreted the decay reaction of the TGDDM/DDS epoxy in terms of two simultaneous second-order reactions with different rate constants following Dole's Q-function although the Q-function did not fit the decay reaction of

long-lived radicals. They attributed the two decay rates to the two-phase nature arising from an inhomogeneous distribution of crosslink density in the epoxy, i.e., the fast-decaying radicals are associated with low crosslinked regions while the slow-decaying radicals are associated with highly crosslinked regions in the cured epoxy.

The two phase nature of cured epoxies has usually been observed by electron microscopy [65-70] and magnetic resonance spectroscopy [71-73]. The microscopic observations indicate that cured epoxies have a composite network structure in which a dispersed phase associated with highly crosslinked regions, known as 'nodules' or 'microgels,' etc., are embedded in a less crosslinked matrix phase. Possible reasons for the inhomogeneous phase formation are as follows [74]:

- 1) Steric and diffusional restrictions of the reactants during cure
- 2) Presence of impurities that act as catalysts
- 3) Reactivities of the epoxide and curing agent
- 4) Isomerization of epoxide groups
- 5) Non-homogeneous mixing of the reactants
- 6) Cyclic polymerization of growing chains.

Brown and coworkers [71-73, 75-76] have investigated extensively the two phase nature of epoxies using NMR or ESR spectroscopy with spin-probes and spin-labels. They proposed that the observed mobile and immobile components of the nitroxide spin-label or spin-probe are associated with

low cross-linked regions and highly crosslinked regions of the cured epoxy, respectively. They also considered that the free volume which is mostly present in low crosslinked regions might be responsible for the mobile component.

Tsay et al. [117] claimed that there is no need to invoke the existence of such microstructure heterogeneity or different aggregation states for the observed double population of spin-probe and spin-label motions, but the rapid motion of the nitroxide component, for example in poly methyl methacrylate below the glass transition temperature, is associated with the presence of excess free volume in the solid polymers.

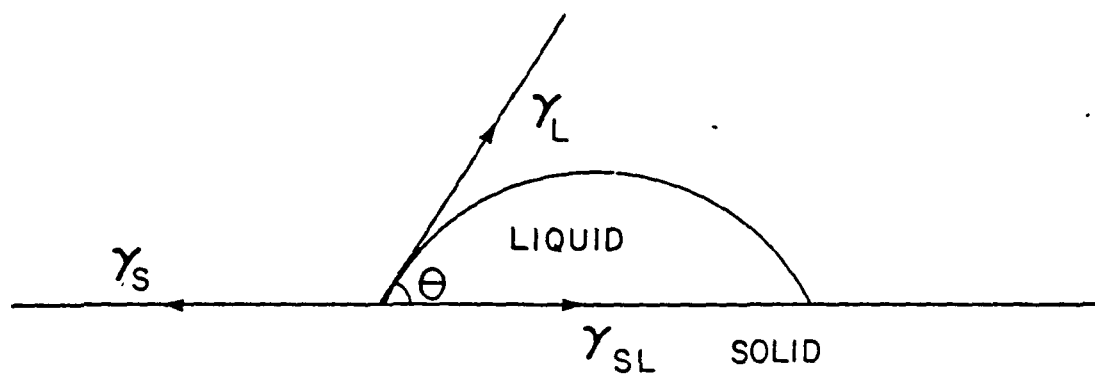
2.4 Polymer Surface Energetics

2.4.1 Theory of Surface Energetics

Over 150 years ago Thomas Young realized that the contact angle provides a relationship between the adhesion of the liquid to the solid and its cohesion to itself as expressed in the following equation [77]:

$$\gamma_S = \gamma_{SL} + \gamma_L \cos \theta \quad (2.49)$$

Equation (2.49) is often called Young's equation [74] and describes the situation of a liquid placed on the surface of a solid under balanced forces as illustrated in Figure 2.8 [78]. θ is the contact angle as defined in the figure, γ_S , γ_L



$$\gamma_S = \gamma_{SL} + \gamma_L \cos \theta$$

Figure 2.8 A drop of liquid (L) resting on the surface of solid (S) [78].

and γ_{SL} are the free energies per square centimeter (surface tensions) of the solid, liquid and solid/liquid interface, respectively.

The surface energy is defined by:

$$\gamma = \left(\frac{\partial A}{\partial a} \right)_{T,V,N} \quad (2.50)$$

where the quantity A is the Helmholtz free energy, a is the area of interface and N is the number of moles of the liquid at the interface [78].

The work of adhesion W_a , the work required to separate the liquid from the solid, is given by the Dupre equation (2.51):

$$W_a = \gamma_S + \gamma_L - \gamma_{SL} \quad (2.51)$$

Combination of Young's equation (2.49) and Dupre equation (2.51) leads to the Dupre-Young equation which describes the relation between the work of adhesion and the contact angle of a liquid on a solid:

$$W_a = \gamma_L (1 + \cos \theta) \quad (2.52)$$

Thus, W_a is simply obtained from measurable quantities θ and γ_L through equation (2.52).

The work of adhesion W_a is the practical value for the situation when the solid surface is covered with a film of liquid vapors. The surface tension of the vapor-covered

surface, γ_S , is lower than that for the vapor-free surface γ_S^0 by an amount π , the surface pressure of the adsorbed film, i.e.,

$$\gamma_S = \gamma_S^0 - \pi \quad (2.53)$$

π can be obtained experimentally by use of the integrated form of the Gibbs adsorption equation:

$$\pi = RT \int_0^{P^0} \Gamma d(\ln P) \quad (2.54)$$

where P^0 is the saturated vapor pressure of the liquid and Γ the amount of vapor adsorbed at the pressure P . Similarly, equation (2.49) can be rewritten for the vapor-free surface as:

$$\gamma_S - \pi = \gamma_{SL} + \gamma_L \cos \theta \quad (2.55)$$

Then, the work of adhesion to the vapor-free surface of a solid, W_a^0 , can be expressed as:

$$W_a^0 = W_a + \pi \quad (2.56)$$

The work of adhesion, W_a , for the film-covered surface is practically much more important than the work of adhesion, W_a^0 , for the film-free surface since the former is the only work that can be directly measured [77], and π in equation (2.56) is often neglected [79].

The surface energy of the solid or liquid can be considered as sum of several components of different

contributions and generally represented as [80-84]:

$$\gamma = \gamma^d + \gamma^p + \delta \quad (2.57)$$

where d and p represents the disperse and polar contributions, respectively, and the excess term δ includes many other components such as hydrogen bonding [80, 82], acid/base [83], or electrostatic contributions, etc. [84]. The hydrogen bonding contribution may be considered as a part of polar components and the excess term δ can reasonably be neglected for systems associated with non-polar, polar and hydrogen bonding liquids [81].

The interfacial tension for interacting faces, γ_{SL} may be defined by the following equations neglecting the excess term [80-81].

$$\gamma_{SL} = (\alpha_S - \alpha_L)^2 + (\beta_S - \beta_L)^2 \quad (2.58)$$

$$\text{or } \gamma_{SL} = \gamma_S + \gamma_L - 2(\alpha_S\alpha_L + \beta_S\beta_L) \quad (2.59)$$

where

$$\alpha_S = (\gamma_S)^{1/2}$$

$$\beta_S = (\gamma_S)^{1/2}$$

$$\alpha_L = (\gamma_L)^{1/2}$$

$$\beta_L = (\gamma_L)^{1/2}$$

The excess term can simply be added to equation (2.58) when its contribution is significant. By combining equation

(2.51) and equation (2.59), the work of adhesion W_a can be rewritten as:

$$W_a = 2 (\alpha_S \alpha_L + \beta_S \beta_L) \quad (2.60)$$

$$\text{or} \quad \frac{W_a}{2\alpha_L} = \alpha_S = \beta_S (\beta_L / \alpha_L) \quad (2.61)$$

W_a is easily calculated from equation (2.52) from measured values of θ and γ_L . α_L and β_L may be obtained experimentally. Therefore, the dispersion component (α_S) and polar component (β_S) of the surface energy of the substrate can be evaluated from the plot of $W_a/2\alpha_L$ vs. β_L/α_L for various liquids [85]. It is noteworthy that the dispersion components of various polymers are very close to each other and do not change significantly with surface treatments [82-83, 85].

If we consider the hydrogen bonding interaction separately from other polar interactions, an excess term can be added to equation (2.60) [82], i.e.,

$$W_a = 2 (\alpha_S \alpha_L + \beta_S \beta_L + \delta_S \delta_L) \quad (2.62)$$

where

$$\delta_S = (\gamma_S^h)^{1/2} \quad \text{and} \quad \delta_L = (\gamma_L^h)^{1/2}$$

The superscript h represents the hydrogen bonding component. Due to the additional term the graphical method as for

equation (2.61) can not be used to solve equation (2.62). However, a numerical method may be used instead. In the latter method, α_S and β_S must be evaluated first with liquids which have no hydrogen bonding interaction, i.e. $\delta_L = 0$, and then δ_S is evaluated with liquids having hydrogen bonding interaction by knowing α_S and β_S .

Equation (2.59) is based on the geometric-mean of polar and dispersion components. Wu [86] claimed, however, that better results may be obtained for polar/polar systems if the third term of equation (2.59) is replaced by the reciprocal-mean of each component, i.e.

$$\gamma_{SL} = \gamma_S + \gamma_L - 4 \left(\frac{\gamma_{SYL}^{d d}}{\gamma_S^d + \gamma_L^d} + \frac{\gamma_{SYL}^{p p}}{\gamma_S^p + \gamma_L^p} \right) \quad (2.63)$$

If the interfacial and surface tension data of the polar surface against a non-polar surface is known, then γ_S^d and γ_S^p can be evaluated [86].

The applicability of equations (2.58) through (2.63), which is derived for a liquid/solid interface, to the solid/solid interface has not been tested even though they are very practical expressions. If we assume that the chemical and physical changes (e.g. generated by irradiation) of two phases at the interface of a composite are, at least, qualitatively identical to changes at the

free surfaces of the individual components, then we may indirectly predict the change in the work of adhesion W_a of a solid/solid interface after irradiation from surface energy change data of free surfaces of the individual components after irradiation.

2.4.2 Adhesion in Composites

Adhesion in composites may be classified into three major groups [84, 87-88]:

- 1) Surface energetics
- 2) Chemical bonds or polymer chain interlocking across the interface
- 3) Mechanical interference such as frictional force or grabbing force generated by the matrix.

Many attempts have been made to determine which factors are primarily responsible for the observed differences in the bond strength of composites, but the basic question has not been answered clearly. Levine et al. [89] have reported a linear dependence of the tensile strength of the adhesion joint on the 'critical surface tension' of a substrate. The critical surface tension of a substrate is a hypothetical surface tension and is obtained by extrapolation (to $\cos \theta = 1$) of a linear plot of $\cos \theta$ vs. γ_L [90]. All liquids with a value of surface tension less than the critical surface tension of the substrate would spread while those with a larger value would have a finite contact angle [91].

Several authors [81, 92-95] have proposed that the intrinsic strength of an adhesive bond is probably controlled by the interactions associated with, e.g., surface energetics or covalent bond formation (molecular interlinking) of two phases at the interface. However, such close range atomic interactions across a clearly defined interface may not be the only cause of adhesive bond strength since the magnitude of adhesive energy in mechanical tests is always much greater than the work of adhesion W_a . The results of other factors such as inter-diffusion of bonding phases, electrostatic charges [87, 89, 96], and mechanical interference such as friction and grabbing forces arising from the difference in thermal expansion coefficients between the two components [88,97] are also taken into account for the origin of interfacial bond strength.

2.4.3 Methods of Surface Characterization

2.4.3.1 Contact Angle Measurement

FILMS: Equilibrium contact angles of polymer films are usually measured on profiles of sessile drops (see Figure 2.8) by using a microscope fitted with a goniometer eyepiece [77]. Advancing and receding angles are often measured for a sessile drop on an inclined plane as illustrated in Figure 2.9 [98]. The surface roughness and chemical heterogeneity of different surfaces can be compared by the difference between the advancing θ_a and the receding θ_r angles, which is referred to as 'wetting hysteresis.'

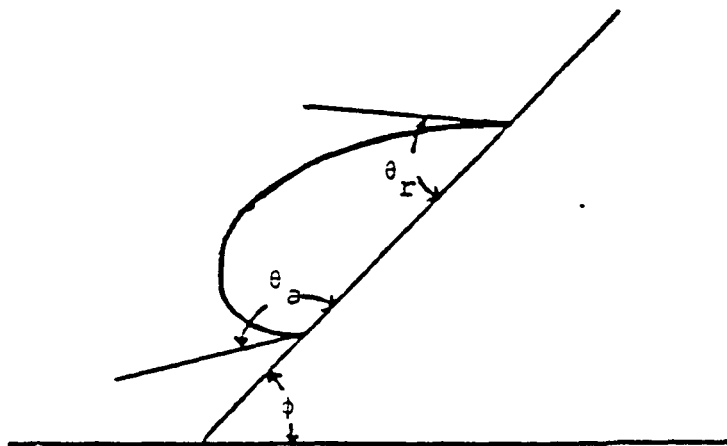


Figure 2.9 A sessile drop on an inclined plane (gradient = $\tan \phi$) showing the advancing θ_a and receding θ_r angles [98].

SINGLE FIBERS: The contact angle of a single fiber is indirectly measured by using the Wilhelmy technique (see Figure 3.2). A fiber is suspended vertically from one arm of a balance in a liquid. If the contact angle of the liquid on the solid is θ , the balance of forces is expressed as:

$$f = \pi D \gamma_L \cos \theta \quad (2.64)$$

where f is the contact force of a fiber in the liquid and D is the diameter of the fiber. The contact force f can be

evaluated from the weight difference, ΔM , of the fiber before and after the immersion into the liquid using the following relationship:

$$f = \Delta M \cdot g \quad (2.65)$$

where g is the gravity. ΔM is usually measured precisely in a μg range using a microbalance [85, 99-100]. From equations (2.64) and (2.65),

$$\cos \theta = \frac{\Delta M \cdot g}{\pi D \gamma_L} \quad (2.66)$$

There are many factors which affect the value of contact angle measured by this method. The sources of error are buoyancy, deviation of the fiber from the vertical line, variation of liquid surface tension (usually due to temperature) and variation of fiber diameter. However, all these factors should change the final result to a negligible extent ($<1\%$) under normal experimental conditions [99]. Observation of a liquid drop on the fiber by optical methods is also used, but its accuracy is generally low [99].

2.4.3.2 Infrared (IR) Absorption Spectroscopy

Transmission infrared absorption spectroscopy of thin films ($< 10\ \mu\text{m}$) is sensitive ($\sim 1\%$) but usually not selective for the detection of changes located in the surface layer of the sample. The infrared absorption spectroscopy based on attenuated total reflection (ATR) at a

film surface is most useful for surface analysis. The depth of penetration (D_p) of incident beam is determined by the following equation:

$$D_p = \frac{\lambda/n_1}{2\pi[\sin^2\theta_1 - (n_2/n_1)^2]^{1/2}} \quad (2.67)$$

where θ_1 = effective angle of incidence

λ = wavelength of radiation

n_2 = reflective index of sample

n_1 = reflective index of ATR crystal, e.g., ~2.4

for thallium-bromo-iodide (KRS-5) and ~4.0

for germanium.

D_p can be varied from 0.1 to about 4 μm with different ATR crystals. This method provides information, in principle, of the amount and location of modified groups at the polymer surface [101-103].

Recently, Garton [104] carried out crosslinking reactions of epoxies directly on the surface of a germanium ATR crystal and examined the influence of surface treatments of the germanium on the reaction kinetics of the epoxies. Although the similarity of the surface of germanium to that of the filler material such as graphite fiber or glass fiber is questionable, the methodology he used would be applicable for the investigation of chemical processes occurring at the interface of the composite material under high energy radiation.

2.4.3.3 Electron Spectroscopy For Chemical Analysis (ESCA)

ESCA involves the measurement of binding energies of electrons ejected from a molecule that absorbs an x-ray from a monoenergetic source. The relative binding energy can be determined on the basis of the following equation [105]:

$$E_k = h\nu - (E_b - \phi_{\text{spec}}) \quad (2.68)$$

where $h\nu$ is the photon energy, E_b the binding energy of the core electron, and ϕ_{spec} the work function of the spectrometer which remains constant. The absorbed binding energies and relative peak intensities give information about the distinctive nature of valence electrons and their relative concentration. A shift of the binding energy occurs depending on the chemical state of the electron and reflects the structural features of the polymer surfaces. The penetration depths of ESCA for polymers are of the order 1-3 nm, i.e., 3 -10 molecular layers [106]. Since ESCA uses a soft x-ray photon probe it is much less destructive than Auger electron spectroscopy which uses an electron probe which could damage the polymer samples during experiments [107].

Many ESCA studies of surface modification or surface oxidation of polymers as a result of irradiation have been reported [108-114]. Peeling and coworkers [109] examined the contact angle (H_2O) change on polyethylene terephthalate (PET) film exposed to uv-light. They interpreted the

decrease in contact angles with irradiation dose in terms of formation of oxidation products such as alcohol, phenol, carboxyl and carbonyl groups. They suggested that the formation of oxidation products may be confirmed by means of ESCA. Hammer and Drzal [110] found a good relationship between the oxygen concentration measured by ESCA and the ratio of polar and disperse components of surface energies for the case of graphite fibers. Waterson [115] have reported, on the basis of ESCA results, that there could be a reaction between epoxy groups with oxygen containing groups such as -OH or -COOH on the graphite fiber surface while the remaining parts of the molecules might be absorbed on the fiber surface with van der Waals forces.

2.4.3.4 Microscopy

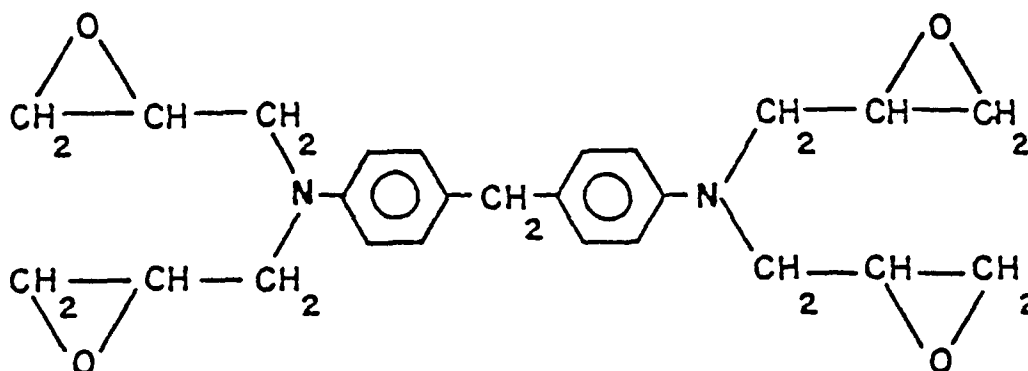
This may be used to study changes in surface geometry or morphology induced by irradiation. Optical microscopy has a limited resolution of about $1\text{ }\mu\text{m}$ but it gives information of coarse cracks, crevices, bubbles, etc.. Scanning electron microscopy (SEM) is one of the most versatile methods for surface studies giving the resolution of the order of 10-20 nm. Higher resolution (5-10 nm) could be achieved by the replica technique but sample preparation of this method is difficult and artifacts from the preparation may be involved on the micrographs [101].

3. EXPERIMENTAL PROCEDURES

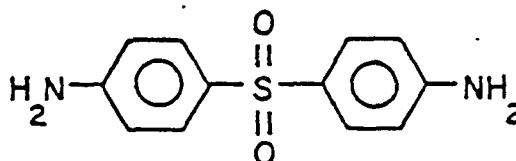
3.1 Materials

3.1.1 Epoxy Resins

The epoxy resin system used in this study was tetraglycidyl-4,4'-diaminodiphenyl methane (TGDDM: MY 720, CIBA-Geigy) cured with 4,4'-diaminodiphenyl sulfone (DDS: CIBA-Geigy). Both components were used as-received without further purification. The structure of the epoxy resin and the hardener are as follows:



Tetraglycidyl - 4,4'-diamino diphenyl methane (TGDDM)



4,4'-diamino diphenyl sulfone (DDS)

3.1.2 Graphite Fiber and T300/5208 Composites

The graphite fiber samples used in the present study

were unsized T-300 graphite fiber (Union Carbide) in a multifilament tow. The uniaxially oriented T300/5208 composite, a composite of T-300 graphite fiber and NARMCO-5208 epoxy based on TGDDM-DDS containing a minor amount of a bisphenol-A based resin (DGEBA) [119], was used for composite samples. All these materials were supplied by NASA Langley Research Center.

3.2 Sample Preparation

3.2.1 Mixing of TGDDM/DDS

Approximately 45 g of TGDDM was weighed out in a tared glass bottle and heated to 110-120°C in a silicone oil bath. The appropriate amount of DDS giving a 73/27 (TGDDM/DDS) weight ratio was calculated. The powdery DDS was gradually added to the liquid phase TGDDM and mixed by means of an overhead mechanical stirrer. The stirring was continued until no trace of undissolved DDS was observed. The mixture of TGDDM/DDS was then deaerated in a vacuum oven at 110°C. The system was frequently flushed with nitrogen and put under vacuum again to avoid over flow of the mixture. This procedure was repeated until most of air bubbles disappeared. The mixture was then maintained under vacuum until no bubble remained in the mixture. The deaerated mixture was subjected to the next procedure. The unused mixture was stored in a refrigerator until use.

3.2.2 Preparation of Epoxy Films

An appropriate amount of TGDDM/DDS mixture was placed inside a picture-frame-shaped spacer (aluminium or Mylar) inserted between two teflon sheets (1 mm thick). Stainless steel supports were placed outside the teflon sheets (see Figure 3.1). The assembled mold was then put on the lower platen of a Carver press preheated at 110°C. When the epoxy sample was completely melted a slight pressure was applied to the system to provide uniform spreading. The mold was then clamped and immediately transferred into the curing oven preset at 137°C. The temperature control of the oven was then set to 150°C. This procedure was necessary since a sudden exposure of the sample to 150°C often resulted in many bubbles in the cured films. The samples were cured at 150°C for 1 hr and then at 177°C for additional 5 hrs. Epoxy films with a thickness range of 1-10 mil were obtained depending on the thickness of the spacers placed between two teflon sheets.

3.2.3 Preparation of Samples for ESR Measurements

3.2.3.1 Epoxy Resin Samples

The deaerated TGDDM/DDS mixture in liquid state was sucked into teflon tubes (from Cole-Palmers) with a 2.4 mm inner-diameter and a length of 5-6 cm by using an aspirator and was solidified at room temperature. Both ends of the tubes were trimmed on a hot plate to remove any air gaps

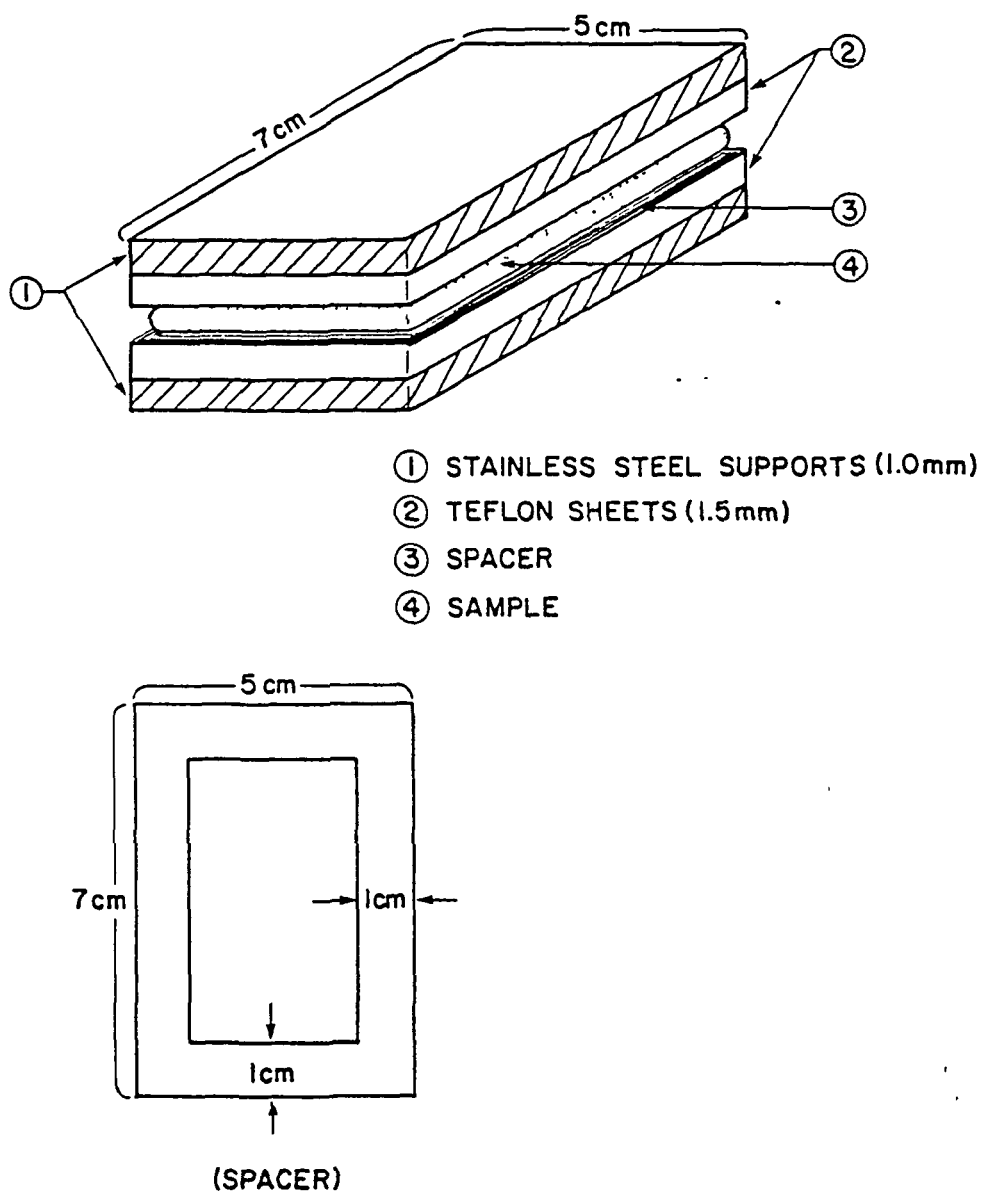


Figure 3.1 A schematic diagram of the assembled mold for the epoxy film preparation

and sealed with teflon tape. The tubes were then cured in a nitrogen-filled oven. The curing schedules were either:

schedule 1: 130°C for 2 hours and then 160°C
for 5 hours

or schedule 2: 150°C for 1 hour and then 177°C
for 5 hours

Other curing conditions were also used and are described elsewhere. The cured rods were cut into 3 cm lengths and the teflon tubes peeled off by a razor blade. The unused rods were placed in a refrigerator until use.

3.2.3.2 Graphite Fiber Samples

A bundle of graphite fibers was inserted into a teflon tube (2.4 mm inner diameter) taking care to maintain a parallel arrangement of fibers. The sample tubes were cut into lengths of approximately 3 cm and used for ESR measurements. The approximate weight of graphite fibers in each sample tube was 1-2 mg.

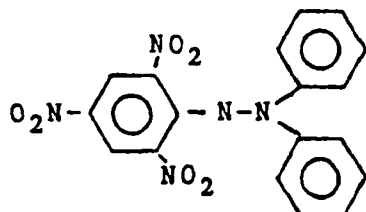
3.2.3.3 Composite Samples

Specimens of composite samples were prepared for ESR measurements from uniaxially oriented T300/5208 composites. Pieces of 3 cm long and approximately 50 mg weight were made by splitting the composite coupons in the fiber direction.

3.2.4 Preparation of Standard Radical Sample

The standard material for the calculation of radical concentration from the first derivative ESR spectrum was

2,2-diphenyl-1-picrylhydrazyl (DPPH) from Eastman Kodak Company:



2,2-diphenyl-1-picrylhydrazyl (DPPH)

The DPPH (~20 mg) was mixed at room temperature, first, with an Elmers brand epoxy resin (~10 g) in a glass bottle using an overhead mechanical stirrer. Then, the Elmers hardener (~10 g) was added to the system and the mixing was continued for about additional 20 minutes. The mixture was deaerated in a vacuum oven at room temperature as described 3.2.1 and sucked into teflon tubes (2.4 mm inner diameter) by using an aspirator. After being cured at room temperature for 24 hours, the tube was cut into a length of 3 cm and the teflon tube was peeled off with a razor blade. The resulting spin concentration of the DPPH samples was about the same order of magnitude of that of irradiated epoxy ($\sim 10^{18}$ spins/g).

3.3 Irradiation Procedures

3.3.1 Gamma Irradiation

Gamma irradiation was carried out in a Gamma Cell-220, manufactured by Atomic Energy of Canada, containing a

cobalt-60 source generating 1.33 and 1.17 MeV γ rays. The irradiation dose rate was in the range of 0.140 to 0.175 Mrad/hr. ESR samples were irradiated either in a Dewar bottle filled with liquid nitrogen (77°K) or at ambient temperature. The temperature increase in the sample due to heat dissipation under the gamma-radiation was negligible. Most of the irradiated samples were stored in liquid nitrogen until ESR measurements.

3.3.2 Electron Irradiation

The 1/2 MeV electron beam, which scanned an area of 48" by 6", was generated by an electron accelerator, manufactured by High Voltage Engineering Corporation, with 500 kilovolts and 8.3 milliamperes. The samples were hung vertically on a conveyor which carried them in front of the electron beam twice in each revolution so that the sample received half of the total dose on each side. The speed of the conveyor was adjusted such that a dose rate of 10 Mrad per revolution (about 1 Mrad/sec) was obtained. Due to the radiational heat under the electron beam, the sample temperature was much higher than the room temperature. No temperature measurement was made during irradiation. It has been reported that the temperature of graphite fiber(T300)/epoxy(TGDDM-DDS) composites reaches 49°C under electron beams at a dose rate of 10.8 Krad/sec [119]. All composite samples were pre-conditioned at 80°C under vacuum

for one week and vacuum-sealed in aluminum foil bags as originally designed by Naranong[10] (see Figure 3.2). Some epoxy films were also irradiated in this manner but others irradiated in Ziploc bags filled with air or nitrogen. Graphite fibers were spread as thin as possible on aluminum foil for uniform irradiation and irradiated in nitrogen-filled Ziploc bags.

3.4 ESR Measurements

ESR spectra were obtained at various temperatures using a JEOL X-band ESR spectrometer (JES-ME-1X) with a variable temperature adapter. The cavity temperatures below -150°C were obtained by blowing liquid nitrogen with nitrogen gas but temperatures above -150°C were obtained by a temperature controller which controls a heating element in a liquid nitrogen tank. The typical spectrometer settings were as follows:

Magnetic field: 3700 - 3750 + 100 Gauss

Modulation width: 0.5 x 10 Gauss

Microwave frequency: ~ 9.35 GHz

Microwave power: ~ 2.0 mW

Crystron current: ~ 1.0 mA

Response time: 0.1 - 0.3 second

Gain: x 1 - 1,000

Scan time: 5 - 10 minutes

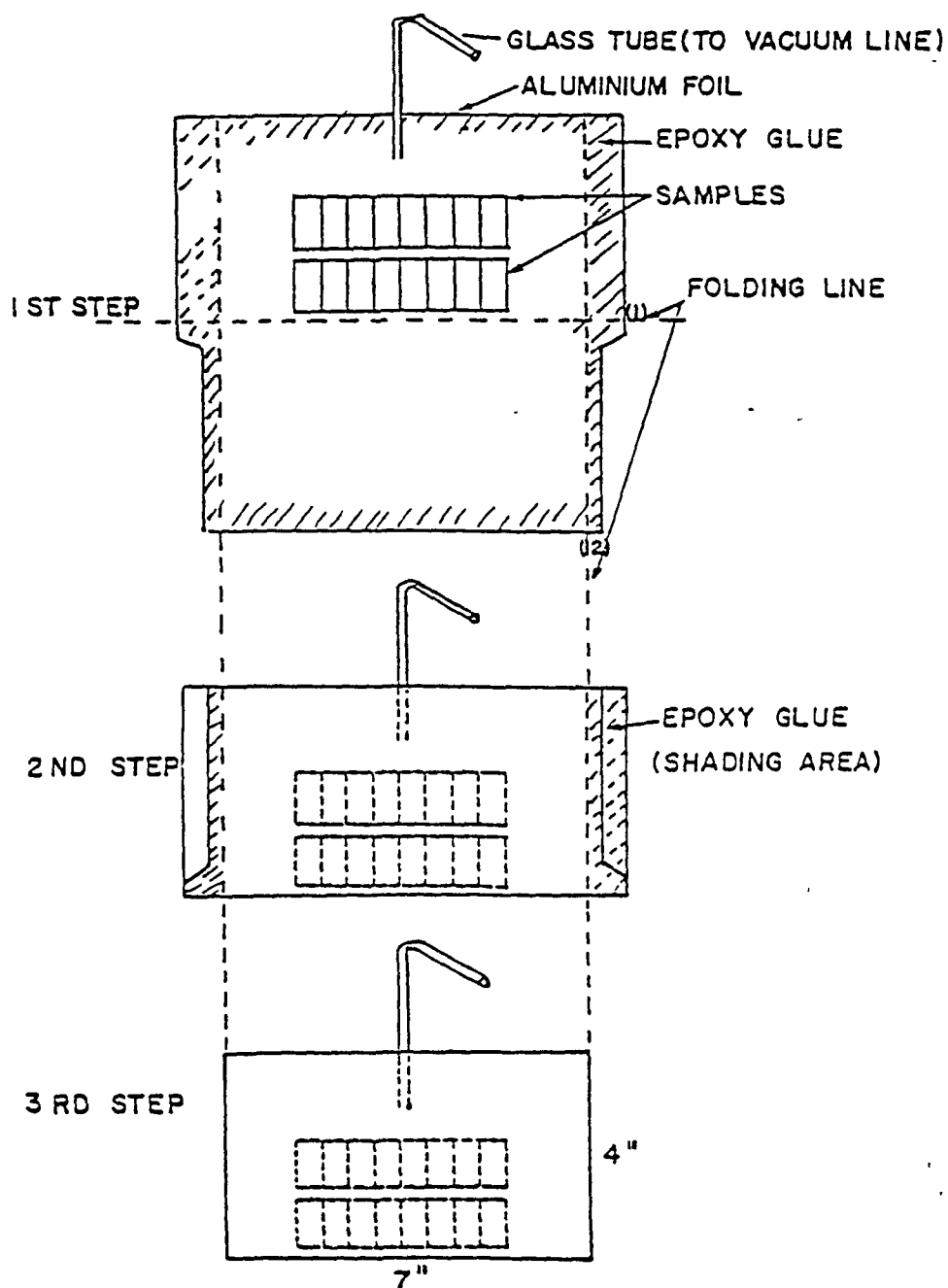


Figure 3.2 Procedure for the aluminium bag preparation for electron irradiation.

To determine the radical concentration, the first derivative ESR spectra were double integrated graphically using the following equation:

$$A = 1/2 h^2 \sum_{r=1}^n (2n - 2r + 1) Y_r$$

where h is the width of the intervals into which the spectrum was divided ($1/10''$ for epoxy, and $1/16''$ for DPPH), n is the number of the intervals at each side of the first derivative curve, Y_r is the intensity of the spectrum at the r^{th} interval, and A is the area of the absorption spectrum which is proportional to the radical concentration of the sample. The radical concentration of an unknown samples was calculated by comparing the area of ESR absorption spectra of the unknown and that of DPPH by using the following relationships:

$$C_u = \frac{A_u G_s W_s}{A_s G_u W_u} \times C_s$$

where subscripts u and s represent the unknown sample and the standard sample, respectively, A is the integrated area of the spectrum, G the gain factor, W the sample weight and C the radical concentration.

Approximate calculations of the relative intensity (A) of the ESR spectra were also made for some symmetric singlet

spectra from the following relationship and the results were compared with those of DPPH:

$$A \propto Y_{pp}(\Delta H_{pp})^2$$

where Y_{pp} is the peak to peak height and ΔH_{pp} is the peak to peak width [36].

The radical decay in air at room temperature (27°C) was monitored using the following procedures. The irradiated sample was transferred from the liquid nitrogen to a sample holder (NMR tube or teflon tube-ended wood stick) as quickly as possible and then the sample holder, with the sample inside it, was kept in liquid nitrogen until transferred into the cavity. The sample holder with the sample inside it was placed as quickly as possible into the ESR cavity (about -196°C) and the spectrum was measured. The sample holder was then removed from the cavity and allowed to warm to room temperature in air. After a measured period of time had elapsed, e.g. 5 minutes, the sample holder with the sample inside it was again immersed into the liquid nitrogen until the next measurement. This procedure was repeated until no significant change in the spectral intensity was recorded. The radical decay at other temperatures (22°C, -80°C, -120°C and -150°C) was monitored by holding the sample in the ESR cavity at each temperature. The intensities of all spectra were normalized in terms of the sample weight and the measuring temperature.

3.5 IR Measurements

The IR spectra of the uncured TGDDM-DDS mixture, TGDDM, DDS and DDM (4,4'-diamino diphenyl methane) were taken with thin layers cast from acetone solution on a KBr plate using a Perkins-Elmer 281B IR Spectrometer. Each sample on the KBr plate was dried in a vacuum oven at room temperature until no trace of acetone was detected in the IR spectrum. Both pure DDS and pure DDM were heated at 150°C in air for 1 hr and consecutively heated at 177°C for 5 hrs and the IR absorption spectrum of each was taken using the same method as for the untreated samples. The IR spectrum of the cured epoxy was obtained from thin films with about a 1 mil thickness. The IR spectra for the same epoxy film were taken after irradiation treatment with various doses.

3.6 Contact Angle Measurements

3.6.1 Epoxy Films and Fracture-Surfaces of Composites

Contact angle measurements of epoxy films were made using an NRL goniometer (Rame-Hart Inc.) and various liquids, Surface tension properties of which are listed in Table 3.1. Due to the roughness, no measurable sessile drop was formed on the shear-fracture surface, prepared by the interlaminar shear test [116, 118], of the T300/5208 uniaxial composite in the flat position. Instead, with a 10 degree inclined angle of the surface both advancing and

Table 3.1 Surface tension properties of test liquids at 20°C [85].

Test Liquids	α_L	β_L	γ_{LA}^d	γ_{LA}^p	γ_{LA}	β_L/α_L
Water	4.67	7.14	21.8	51.0	72.8	1.53
Formamide	5.68	5.10	32.3	26.0	58.3	0.89
Ethylene-glycol	5.41	4.35	29.3	19.0	48.3	0.80
Tricresyl-phosphate	6.26	1.3	39.2	1.7	40.9	0.21
1-Bromo-naphthalene	6.68	0.00	44.6	0.0	44.6	0.00
Hexadecane	5.25	0.00	27.6	0.0	27.6	0.00
Hexane	4.29	0.00	18.4	0.0	18.4	0.00

Note: α and β in $(\text{dyne/cm})^{1/2}$, γ in dyne/cm

receding angles were measured in both the fiber and lateral directions of the uniaxial composite. Samples were washed with ethanol and then with acetone prior to each measurement. The average of five to ten measurements was used for the contact angle determination.

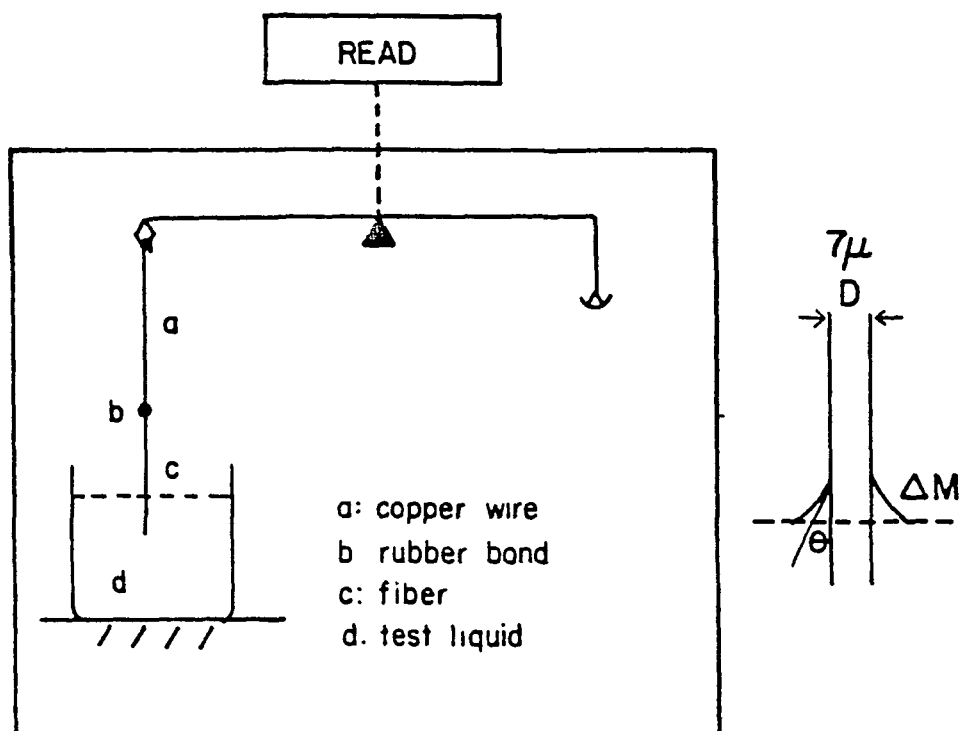
3.6.2 Graphite Fiber

The contact angle of the graphite fiber was measured by means of Wilhelmy technique using a Cahn micro balance (see Figure 3.3). The single fiber was bonded to a thin copper wire with rubber cement. Each fiber was washed with ethanol and then with acetone, and dried at room temperature before each measurement. Surface tensions of the test liquids for surface energy calculations were obtained from the literature [85].

3.7 ESCA Measurements

The oxygen contents at the epoxy surface and the fracture surface of the composite were measured by a X-ray photoelectron spectrometer from Physical Electronics located in the Chemistry Department at the University of North Carolina at Chapel-Hill. Prior to ESCA measurements, the sample surfaces were washed with acetone and ethanol. The sample was placed in the prevacuum chamber of the spectrometer and then in the vacuum chamber with a pressure of approximately 10^{-9} torr. After a general survey scan to

C-2



$$\Delta M \cdot g = \pi D \gamma_{LA} \cos \theta$$

$$\cos \theta = \frac{\Delta M \cdot g}{\pi D \gamma_{LA}}$$

Figure 3.3 A schematic representation of Wilhelmy technique used for contact angle measurement of fibers [10].

identify the elements present at the sample surface, a low energy survey scan was made to magnify the region below the binding energy of 280 eV so that the peak in this region were more distinguishable. A high resolution window was plotted for the peak of each element. The area under the high resolution peak was calculated by a computer interfaced with the spectrometer. Atomic ratios were obtained by dividing this area by the number of scans and the atomic sensitivity factor of the element. The atomic sensitivity factor was referenced to fluorine whose sensitivity was selected as one and all other elemental sensitivities were relative to this number.

4. RESULTS and DISCUSSION

To understand the long-term effect of high energy radiation on fiber/polymer composites, knowledge of responses of the component materials, that is, fiber and matrix polymer, to radiation is required. Wolf [116] and Park et al. [118] have shown that the flexural modulus and the interlaminar shear strength of T300/5208 epoxy/graphite fiber composites increase after exposure to 1/2 MeV electrons. To attempt to understand the reasons for these changes in mechanical properties, the effect of radiation have been examined using a variety of experimental techniques including Electron Spin Resonance (ESR), Electron Spectroscopy for Chemical Analysis (ESCA), Infrared Absorption (IR) Spectroscopy, and contact angle measurements.

The bond strength between the fiber and matrix is of prime concern for composite materials since the separation of the fiber and matrix polymer usually occurs under a shear stress [116, 118]. The adhesion between fiber and matrix is controlled by various factors such as (1) interlocking of polymer chains, (2) chemical bond formation, (3) polar-interaction, and 4) mechanical interference including frictional force or grabbing force of matrix polymer generated by differential thermal shrinkage between the matrix and the fiber during the curing process of composites [84, 87-88].

Figure 4.1 shows a schematic representation of an epoxy/graphite fiber interface with the several factors that may affect the interfacial strength of the epoxy/graphite fiber composite. There are well-contacted regions as well as voids with various sizes. There may exist tightly linked polymer chains, loosely linked chains, and even dangling chains. The black dots in the figure represent free radicals at the surface of graphite fiber and K represents the polar-polar interaction.

It is often difficult to observe changes in the physico-chemical properties directly at the fiber/epoxy interface. Therefore, some of the changes that occur at free surfaces as well as in bulk system of the epoxy and graphite fiber upon irradiation were examined in the present study. The results have been used to explain the effect of high energy radiation on the interface of epoxy/graphite fiber composites.

The first part of this investigation deals with types of free radicals produced in TGDDM-DDS epoxy and T-300 graphite fiber which have been irradiated with cobalt-60 gamma-radiation or 1/2 MeV electron beams at various dose levels, irradiation temperatures and irradiation environments (air, nitrogen and vacuum conditions). Electron spin resonance (ESR) line shapes and the decay behavior of radicals produced under various irradiation conditions were analyzed for this purpose. The radical

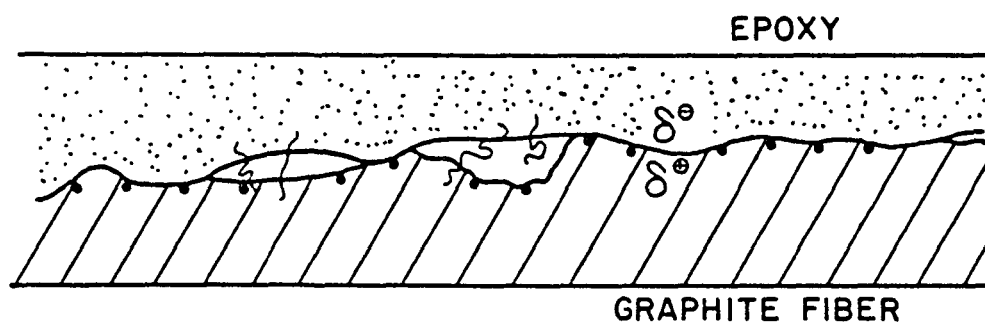


Figure 4.1 A schematic representation of the epoxy/graphite fiber interface.

decay behavior was also discussed in terms of the inhomogeneous network structure of the cured epoxy consisting of highly crosslinked regions and low crosslinked regions. The crosslinking density distribution in the epoxy may vary with curing temperature, curing time, or irradiation dose.

The second part of this investigation deals with how the surface properties of the component materials and the fiber/epoxy interface of composites are modified under the effect of high energy radiation. Contact angle measurements, infrared spectroscopy (IR) and electron spectroscopy for chemical analysis (ESCA) were used for this study. On the basis of the observed results, possible radiation processes in TGDDM-DDS epoxy will be proposed. The observed radiation processes and resultant surface energy changes will be discussed in relation to the interfacial strength changes of epoxy/graphite fiber composites reported in the literature.

4.1 Electron Spin Resonance Analysis

4.1.1 Irradiation Conditions in Space

The composite materials used for spacecraft in geosynchronous orbits are periodically eclipsed from the sun by the earth and may face different thermal conditions which may produce a significant thermal shock effect on them [119]. The equilibrium temperatures of spacecraft

components depend on the ratio of solar absorbance to thermal emittance for the spacecraft surface. While transients during eclipse conditions can lower the surface temperature to lower than -60°C , the heat capacity of the spacecraft and the internal sources of heat (primarily due to electronics) may result in internal temperature above up to 100°C [2].

The vacuum of space varies from $\sim 10^{-4}$ torr (at a 100 km altitude) to less than 10^{-10} torr (at altitudes greater than 1,000 km). The molecular mean path, heat transfer rates, and degassing rates at an altitude above 200 km are such that the bulk properties of the composite will remain essentially constant. Therefore, the vacuum from 10^{-6} to 10^{-7} torr which might be chosen in the laboratory is sufficiently small that reducing it even more would have no effect on results obtained during the irradiation exposure [2].

Although the energy transfer mechanisms of various types of ionizing radiation are different and are not unequivocally confirmed yet, the primary effect of energy absorption from either gamma radiation or high energy electrons is that energetic electrons are produced randomly throughout the material, and the majority of the radiation-chemical reactions are caused by these secondary electrons. The final products, e.g., free radicals, do not seem to be dependent on radiation sources. The main difference between

the effects of radiation sources is in the penetration power through the materials or the distribution of chemical events in the irradiated materials.

4.1.2 Effect of Irradiation Conditions on ESR Line Shape of TGDDM-DDS Epoxy

In this section, how the ESR line shape change at different irradiation conditions including the irradiation temperature and the irradiation environment will be discussed.

The ESR line shape of TGDDM-DDS epoxy irradiated with a dose of 100 Mrad (see Figure 4.2) in air at room temperature is different from that of the sample similarly irradiated with the same dose but in liquid nitrogen (see Figure 4.3). The former has an additional narrow component ($\Delta H_{pp} = 13$ G) and the overall line shape appears to be a composite spectrum of the narrow line and the broad line ($\Delta H_{pp} \sim 25$ G) which is observed for a low temperature (77°K) irradiated sample after a prolonged decay time (see Figure 4.3b). It is also notable that there are no long tails, which are usually observed for 77°K -irradiated samples, in the spectrum of the room temperature irradiated samples. The decay rate of the narrow component at room temperature is faster than the other component so that the overall spectrum became a slightly asymmetric broad line after 27 days of exposure to air at room temperature (see Figure 4.2b). This result indicates that under the higher irradiation

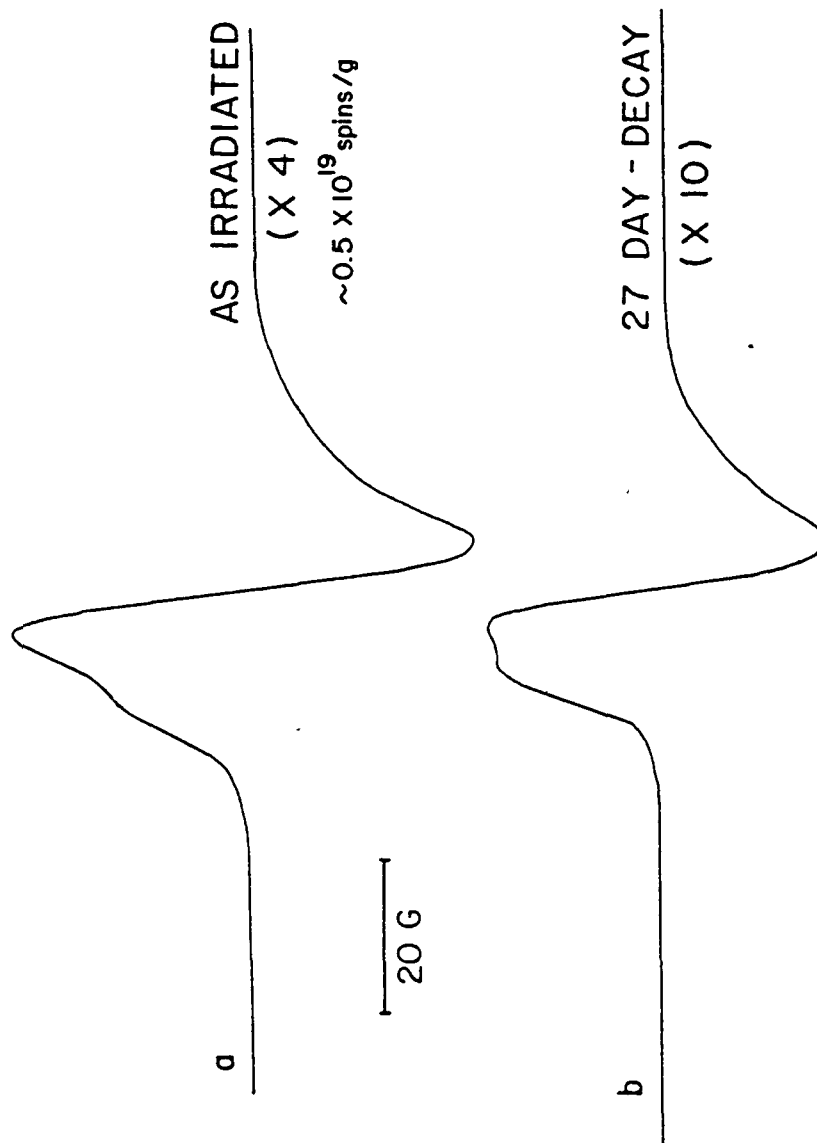


Figure 4.2 ESR spectra of TGDDM-DDS epoxy irradiated at room temperature in air with a dose of 100 Mrad of γ -radiation. (a) as-irradiated and (b) after 27 days exposure to air at room temperature. Samples were cured at 150°C (1hr) and then at 177°C (5 hrs). The spectra were measured at -196°C.

γ -IRRADIATION AT

77°K, 100 Mrad

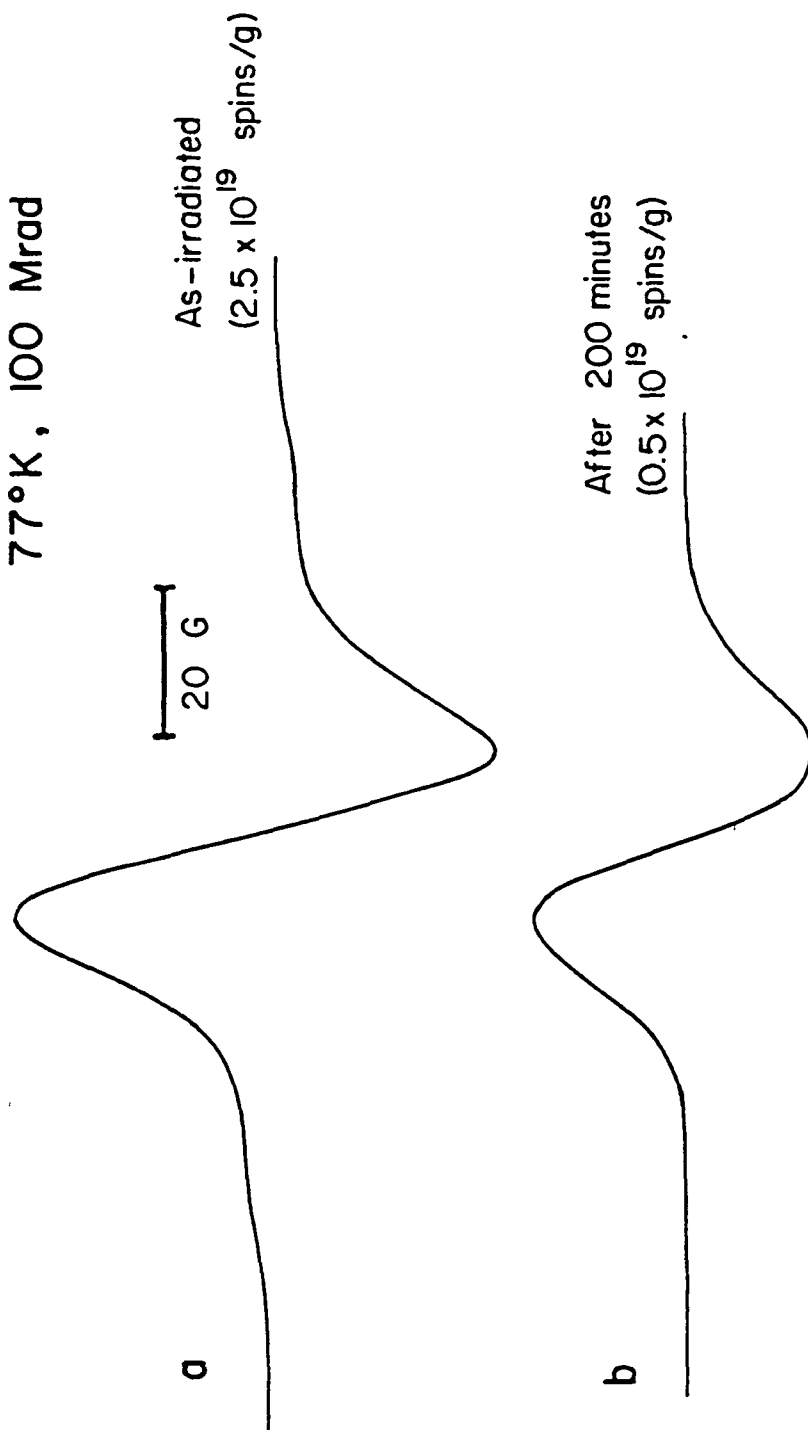


Figure 4.3 ESR spectra of TGDDM-DDS epoxy γ -irradiated in liquid nitrogen with a dose of 100 Mrad. (a) as-irradiated and (b) after 200 minutes exposure to air at room temperature. Spectra were taken at -196°C. Samples were cured at 150°C (1 hr) and then at 177°C (5 hrs).

temperature additional radical species with faster decay rates compared to the other broad component are produced in the TGDDM-DDS epoxy system. A similar narrow component is also observed in the electron irradiated (at room temperature) samples (see Figure 4.4) although the decay of radicals during exposure to electrons should be at a much higher rate than for the case of the samples irradiated with gamma-radiation at room temperature because the radiational heat generated by the electron beams causes the temperature to be significantly higher than the room temperature. For example, if there is no heat dissipation, then the temperature rise of the epoxy for each turn (10 Mrad/turn) is approximately 60°C (calculation based on specific heat of epoxy is $0.4 \text{ cal/g}^{\circ}\text{C}$). An epoxy/graphite fiber composites have been reported to reach 49°C at the dose rate of 10.8 Krad/sec of high energy electrons [119]. The heat generated in the epoxy/graphite fiber composite by exposure to gamma-radiation is easily dissipated and the temperature rise is negligible.

Exposure of samples in liquid nitrogen protects the sample from the external oxygen compared to exposure of samples in air at room temperature. Also, the samples have more thermal energy at room temperature (300°K) than at the liquid nitrogen temperature (77°K). In order to see whether the narrow ESR component for room temperature irradiated epoxy samples is due to the temperature effect or due to

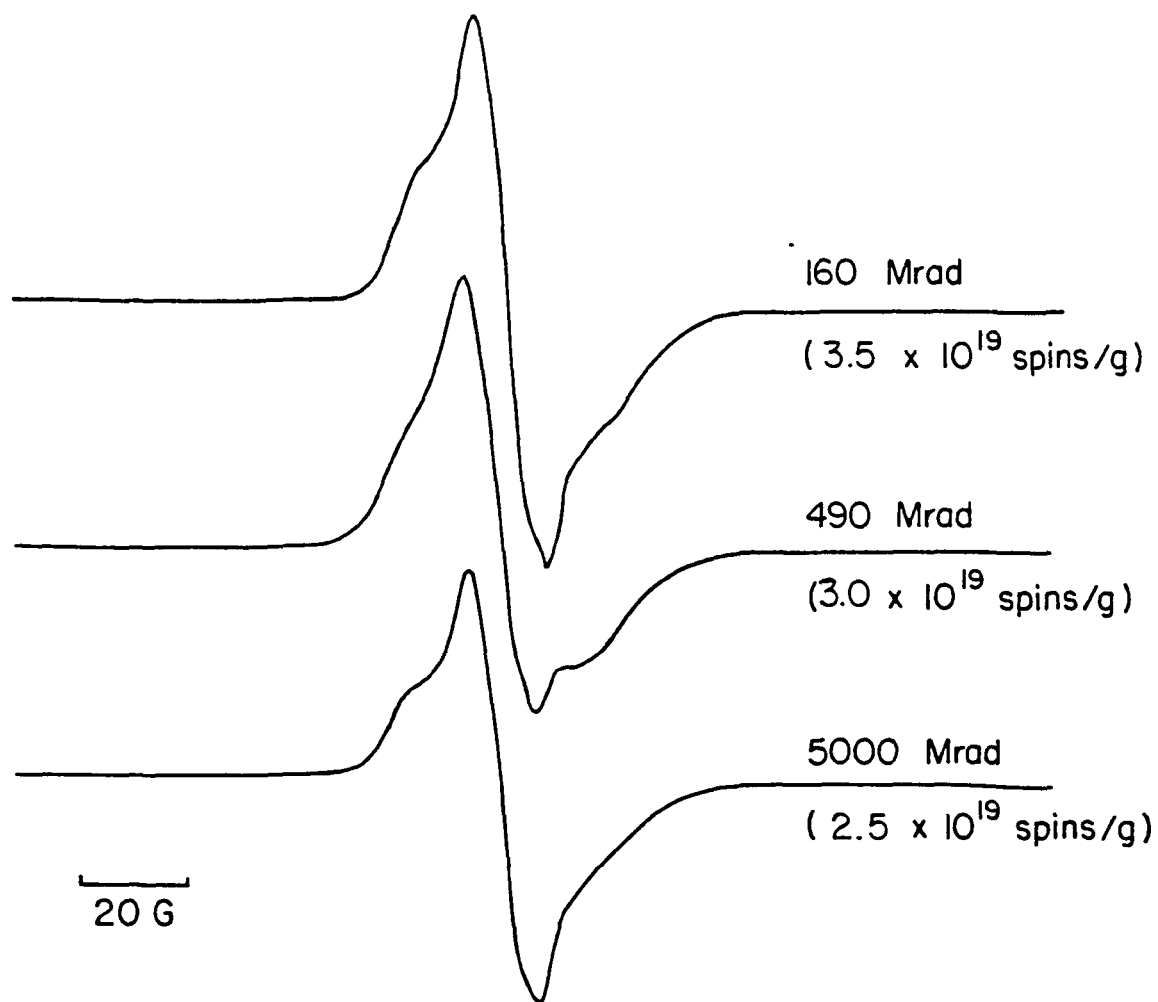


Figure 4.4 ESR spectra of TGDDM-DDS epoxy and 1/2 MeV electron-irradiated in air at room temperature with various doses and immediately stored in liquid nitrogen. Spectra were measured at -196°C . Samples are cured at 150°C (1 hr) and then 177°C (5 hrs).

oxygen effect, one sample was vacuum-sealed in a ESR tube and gamma-irradiated at room temperature with a dose of 800 Mrad. ESR measurements for vacuum-sealed samples were carried out after one end of the ESR tube had been annealed sufficiently so that no detectable signal from the tube occurred. As seen in Figure 4.5 the narrow component still appears with a small change in intensity compared to the sample irradiated in air. Another sample was gamma-irradiated with a dose of 100 Mrad under a continuous vacuum condition (with a rotary pump) at room temperature. The ESR line shape for this sample (see Figure 4.6) is basically the same as for any other room temperature irradiated samples. It cannot be confirmed at the present time whether the narrow ESR component is due to the dissolved oxygen which is not completely removed from the epoxy sample under the vacuum treatment, or due to higher thermal energy effect at the higher irradiation temperature.

4.1.3 Identification of Radicals in TGDDM-DDS Epoxy

Since irradiation both at an elevated temperature and in the presence of oxygen can facilitate polymer main-chain scission, the narrow ESR component of room-temperature irradiated samples may be attributed to mobile radicals such as acyl type radicals ($-\overset{\text{O}}{\underset{\cdot}{\text{C}}}$) which can be produced through Norrish type I reaction which is favorable at higher temperature, i.e., breakage of C-C bonds of carbonyl groups already produced during irradiation. A possible reaction

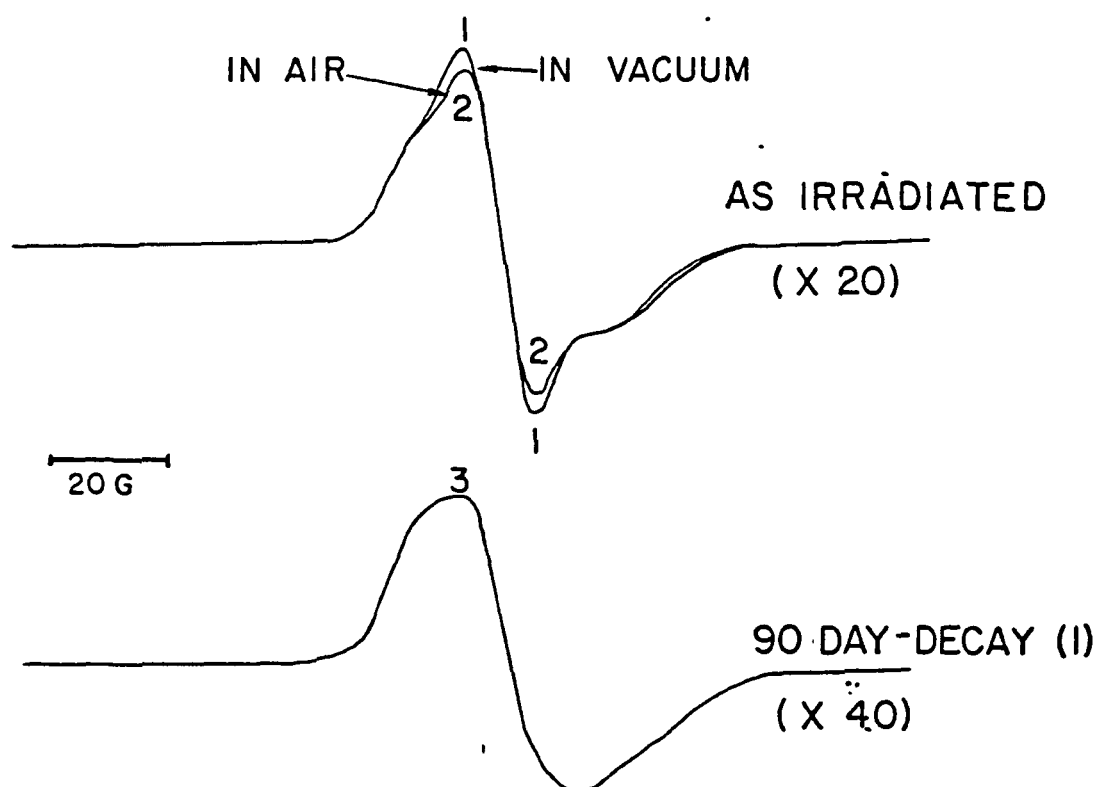


Figure 4.5 ESR spectra of TGDDM-DDS epoxy γ -irradiated with a dose of 800 Mrad at room temperature (300°K), (1) in air, (2) in vacuum-sealed tube, and (3) spectrum-1 after exposure to air at 300°K for 90 days.

CONTINUOUS VACUUM

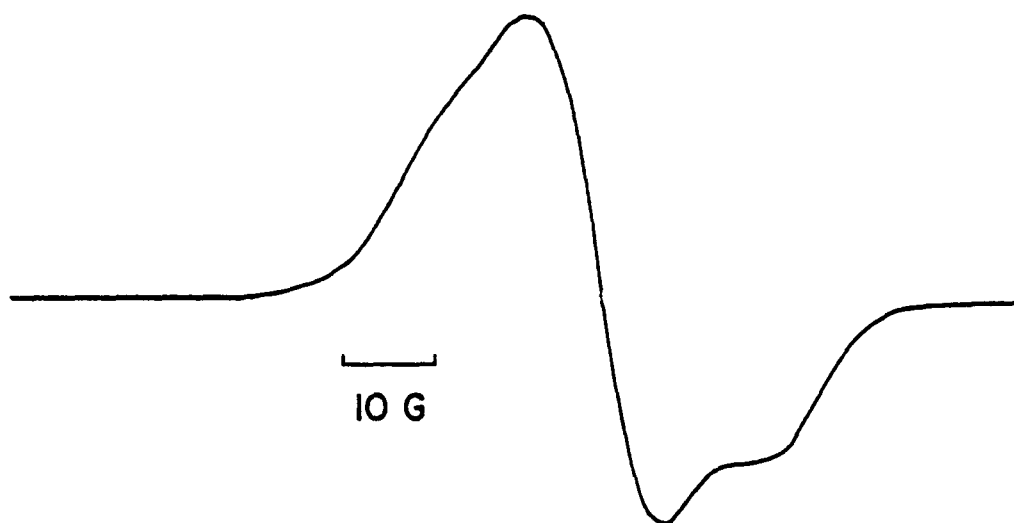


Figure 4.6 ESR spectra of TGDDM-DDS epoxy irradiated with a 100 Mrad of γ -radiation at room temperature under a continuous vacuum condition. The spectrum was measured at room temperature. Samples were stored in liquid nitrogen until ESR measurement.

scheme for the formation of acyl radicals and other possible chain-scission reactions are illustrated in Figure 4.7. The alkyl radicals produced through reactions (II), (III) and (V) in Figure 4.7 will decay rapidly during irradiation at room temperature and may not be observed at the time when the ESR spectrum is taken. However, the acyl radicals should be more stable than the alkyl radicals due to the resonance stabilized structure. The acyl radicals existing at the chain-ends are also relatively mobile compared to the oxygenated radicals along the main chains and, therefore, they may cause a narrower ESR component than other oxygenated radicals. The line width of 13 G of the narrow component is comparable to 16.6 G estimated for acyl radicals by Gupta et al. [46] (see Table 2.3).

An ESR spectrum of TGDDM-DDS epoxy cured at 137°C for 2 hours and postcured at 160°C for 5 hours (note that these temperatures are lower than for the previous samples), and irradiated with a 5 Mrad dose of gamma-radiation in liquid nitrogen (77°K) is shown in Figure 4.8a. It is very broad and has wide shoulders. The radical concentration measured for this spectrum was 3.8×10^{18} spins/g. When the irradiated sample is exposed to air at room temperature the long shoulders disappear within 5 minutes and the spectrum becomes a broad singlet with a peak-to-peak width (ΔH_{pp}) of 22-25 G (see Figure 4.8b). The apparent singlet line shape did not significantly change thereafter (see Figure 4.8c).

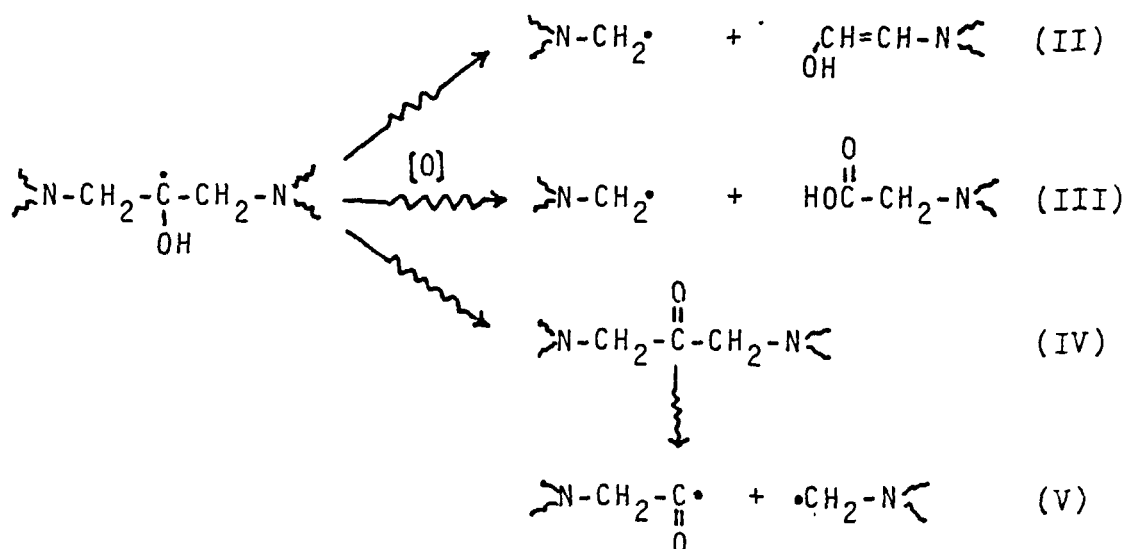
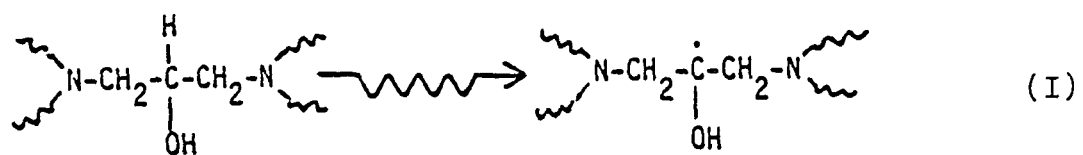


Figure 4.7. Possible chain scission reactions of TGDDM-DDS epoxy under radiation.

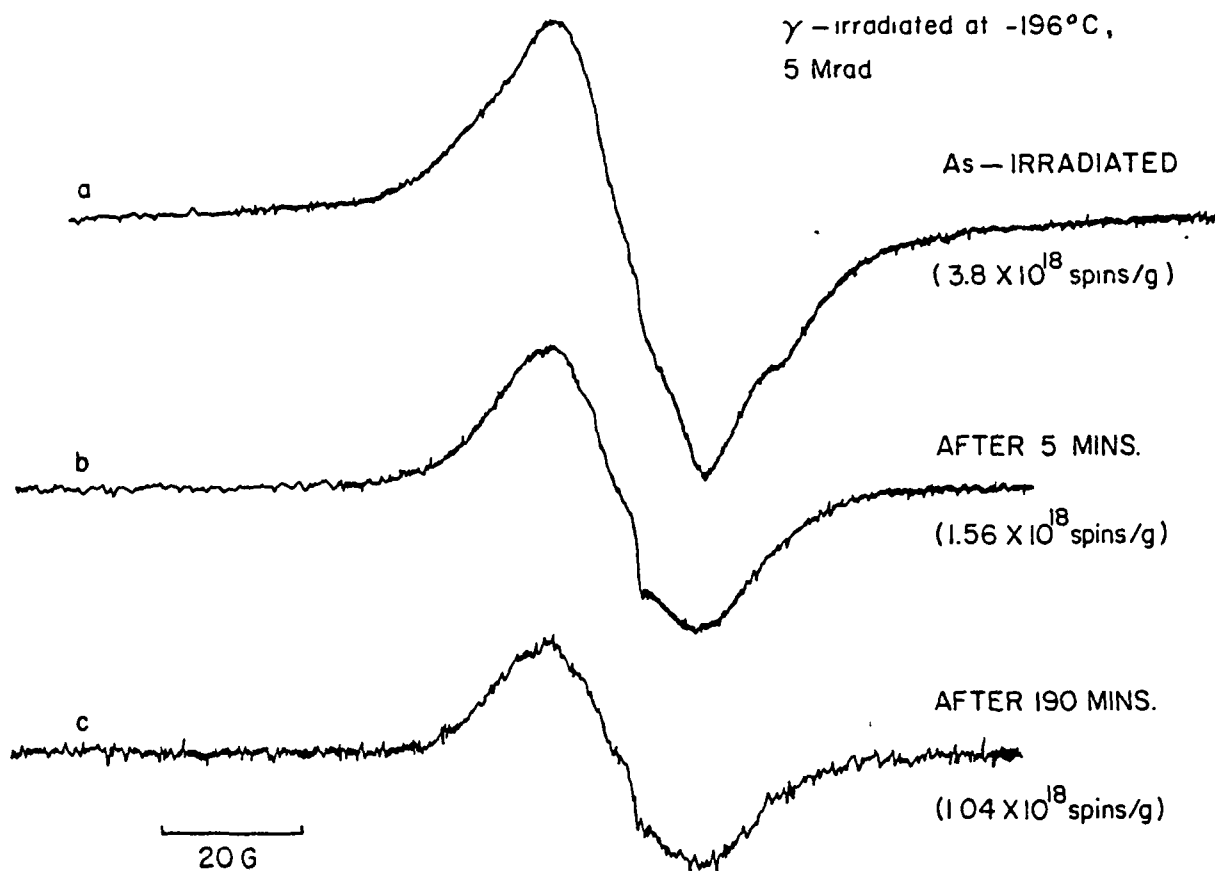


Figure 4.8. ESR spectra of TGDDM-DDS epoxy cured at 137°C (2 hrs) and then 160°C (5 hrs) and with a 5 Mrad dose of γ-radiation in liquid nitrogen (77°K). (a) as-irradiated (b) after 5 minute exposure to air at room temperature and (c) after 200 minute exposure.

The concentration at 5 minutes was 1.56×10^{18} spins/g and decreased very slowly to 1.04×10^{18} spins/g at 200 minutes (see Figure 4.8c). These results are consistent with the results observed by Schaffer [48] and Kent [64].

In order to identify radicals by analyzing the ESR line shape, the spectrum (Figure 4.8b) was subtracted from the original spectrum (Figure 4.8a). The resulting difference spectrum between the original and a 5 minutes decay is shown in Figure 4.9. This quintet-like ESR line shape with an apparent hyperfine splitting constant of approximately 12-20 G is probably due to alkyl-type radicals ($-\text{CH}_2-\dot{\text{C}}-\text{CH}_2-$) which are generally reactive and decay rapidly. As the temperature rises, the radicals may combine with other radicals or react with dissolved oxygen or hydrogen (or hydrogen radicals) produced by irradiation and trapped in the epoxy at liquid nitrogen temperature. The fast decaying characteristics of alkyl radicals in other polymers has been discussed by several authors [41-42, 54-55]. Another possible explanation of the quintet-like spectrum (Figure 4.9) is that it consists of signals from several different types of radicals each of which decay relatively fast. Gupta et al. [46] have suggested a quintet spectrum with a hyperfine constant of 19.2 G for an alkyl radical ($-\text{CH}_2-\dot{\text{C}}-\text{CH}_2-$) in the irradiated TGDDM-DDS epoxy (slightly cured at 177°C for 15 minutes). They have also suggested a broad doublet and a triplet, both of which have a line width

DIFFERENCE SPECTRUM

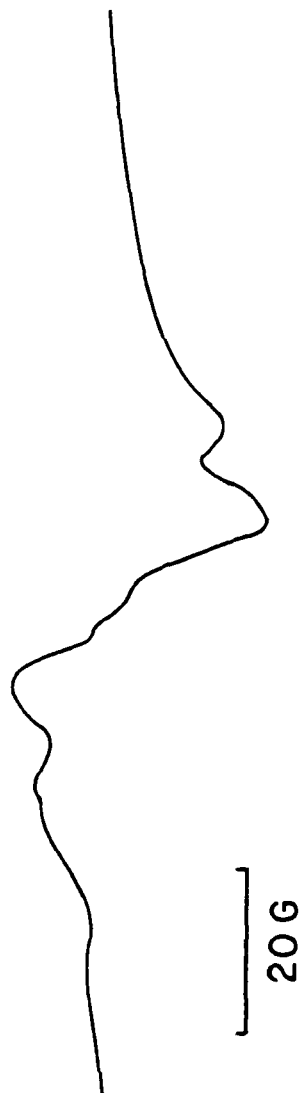


Figure 4.9 The difference spectrum between spectrum-a and spectrum-b in Figure 4.8.

of 30 G, for other types of alkyl radicals, $\begin{array}{c} \text{OH} \\ | \\ -\dot{\text{C}}\cdot \\ | \\ \text{H} \end{array}$, or $\begin{array}{c} \text{H} \\ | \\ -\dot{\text{C}}\cdot \\ | \\ \text{H} \end{array}$,

which could be produced at polymer chain-ends by main-chain scission (see Table 2.3).

On the other hand, the observed broad singlet spectrum (Figure 4.8c) after prolonged exposure (200 minutes) to air is probably due to the oxygenated radicals such as alkoxy ($-\dot{\text{C}}\text{O}\cdot$) or peroxy ($-\dot{\text{C}}\text{OO}\cdot$) radicals which are mostly trapped in the highly crosslinked regions of the irradiated epoxy. A broad singlet of a line width of 30 G was suggested for a alkoxy radicals in the irradiated TGDDM-DDS epoxy system by Gupta et al. [46]. However, the line width of the broad singlet observed in the present study is about 22 - 25 G.

A high concentration of radicals were observed in the as-cured TGDDM-DDS epoxy sample. The concentration of the stable radicals produced during the curing process is in the range of $0.2\text{--}0.7 \times 10^{18}$ spins/g and increases slightly with curing time and curing temperature. Schaffer [48] and Kent [64] have reported a concentration of ca. 0.3×10^{18} spins/g for the as-cured sample of the same epoxy system. The ESR line width (ΔH_{pp}) for these stable radicals is also about 22-25 G which is the same as the line width of the broad spectrum from long-lived radicals in the irradiated epoxy sample. Coulter et al. [49] observed a stable singlet line ($\Delta H_{pp} = 15$ G, as measured from the reported spectrum) for a slightly cured but not irradiated TGDDM-DDS sample. They

have suggested that the singlet spectrum is probably due to alkyl radicals ($-\text{CH}_2-\dot{\text{C}}-\text{CH}_2-$) which results from the loss of a tertiary hydrogen from the carbon of alkyl side-chains in TGDDM. As previously mentioned, the alkyl radicals are characteristically quite reactive [20a] so that they may quickly react with oxygen and transform into oxygenated radicals such as alkoxy ($-\dot{\text{C}}\text{O}\cdot$) or peroxy ($-\dot{\text{C}}\text{OO}\cdot$) radicals. Therefore, it is more likely that the stable broad singlet line observed in the as-cured epoxy as well as in the irradiated epoxy is due to oxygenated radicals rather than alkyl type radicals suggested by Coulter et al. [49].

4.1.4 Radical Decay in Irradiated TGDDM-DDS Epoxy

Figure 4.10 shows the change of radical concentration versus exposure time to air at various temperatures in TGDDM-DDS epoxy irradiated with a 5 Mrad dose of gamma-radiation at -196°C . The epoxy samples used in this experiment were cured at 150°C for 1 hour and postcured at 177°C for 5 hours. In each case there is an initial fast decay followed by a much slower decay. Similar radical decay behavior in the irradiated TGDDM-DDS epoxy was also observed by Schaffer [48] and Kent [64]. As the decay temperature at which the irradiated samples are exposed to air increases, the ratio of fast decaying to long-lived species increases. The decay rate during the initial 5 minutes apparently increases with decay temperature whereas

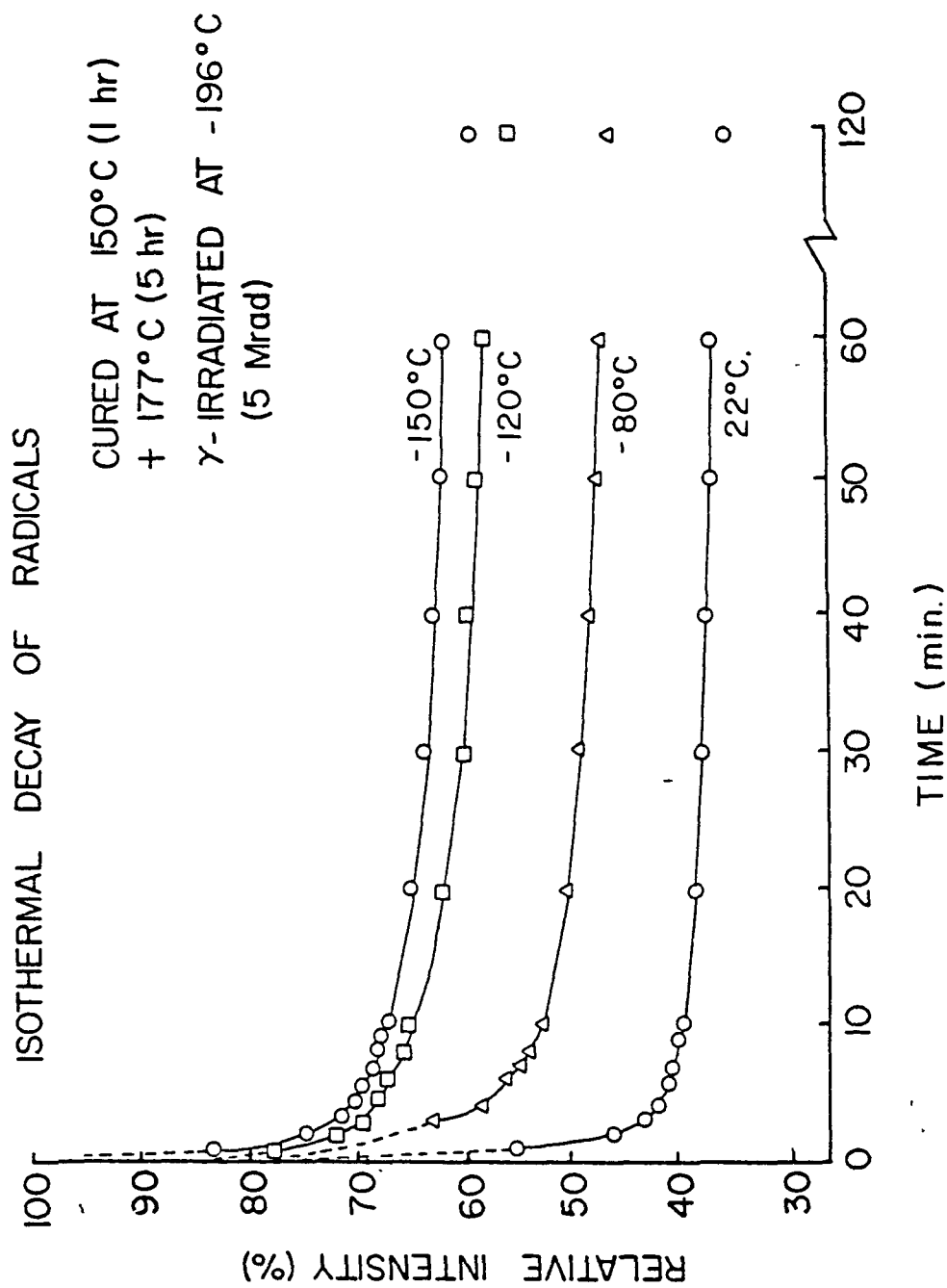


Figure 4.10 Isothermal decay of radicals in the irradiated TGDDM-DDS epoxy.

the decay rate at the later stage (after 10 minutes) is not apparently temperature-dependent. As the first-order and second-order plots (see Figures 4.11 and 4.12) of the isothermal decay curves indicate, the decay reaction does not follow any simple kinetic rule but shows two distinct decay stages with different reaction rates at a given temperature. There is a transient region of decay rates in the 5 to 10 minutes range. The observed decay behavior indicates that there are at least two kinetically distinguishable radical species trapped in the TGDDM-DDS epoxy irradiated in liquid nitrogen (-196°C).

The line shape of this sample was a broad feature (see Figure 4.13) and the asymmetric wiggled line shape (see Figure 4.8a) was not observed in this case. This is probably due to higher curing temperature (150°C for 1 hour, then 177°C for 5 hours) used for this sample than for the case of Figure 4.8a (137° for 2 hours, then 160° for 5 hours). The ESR line shape of as-irradiated epoxy changed with curing conditions. As the curing temperature and curing time increased the spectrum became a smoother line (see Figures 4.14 and 4.15). This is probably due to the crosslinking density effect of the cured epoxy. As the curing temperature or curing time increases, the crosslinking density in the epoxy is expected to increase and thus more broadening of ESR line may result. No noticeable change except the disappearance of long tails in

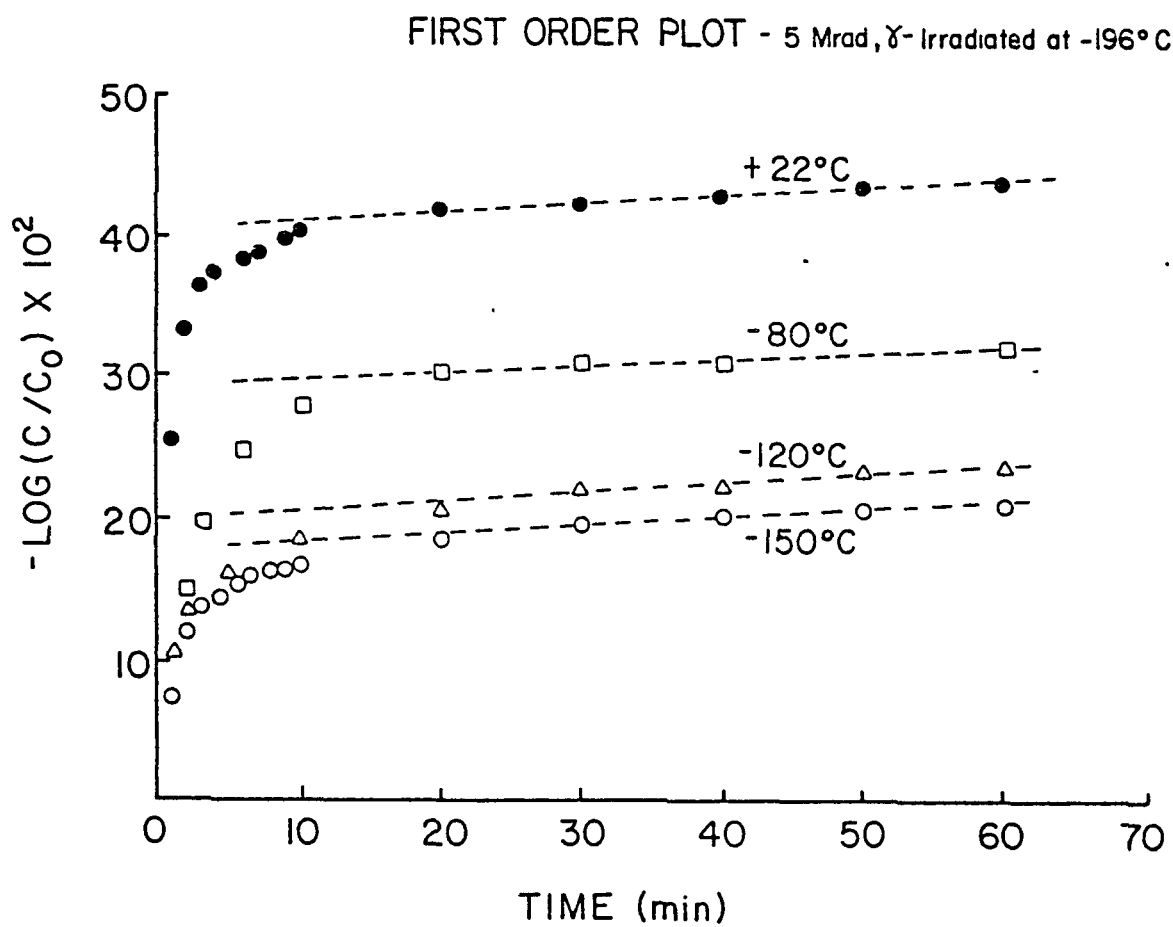


Figure 4.11 First-order plot of the isothermal decay curves in Figure 4.10.

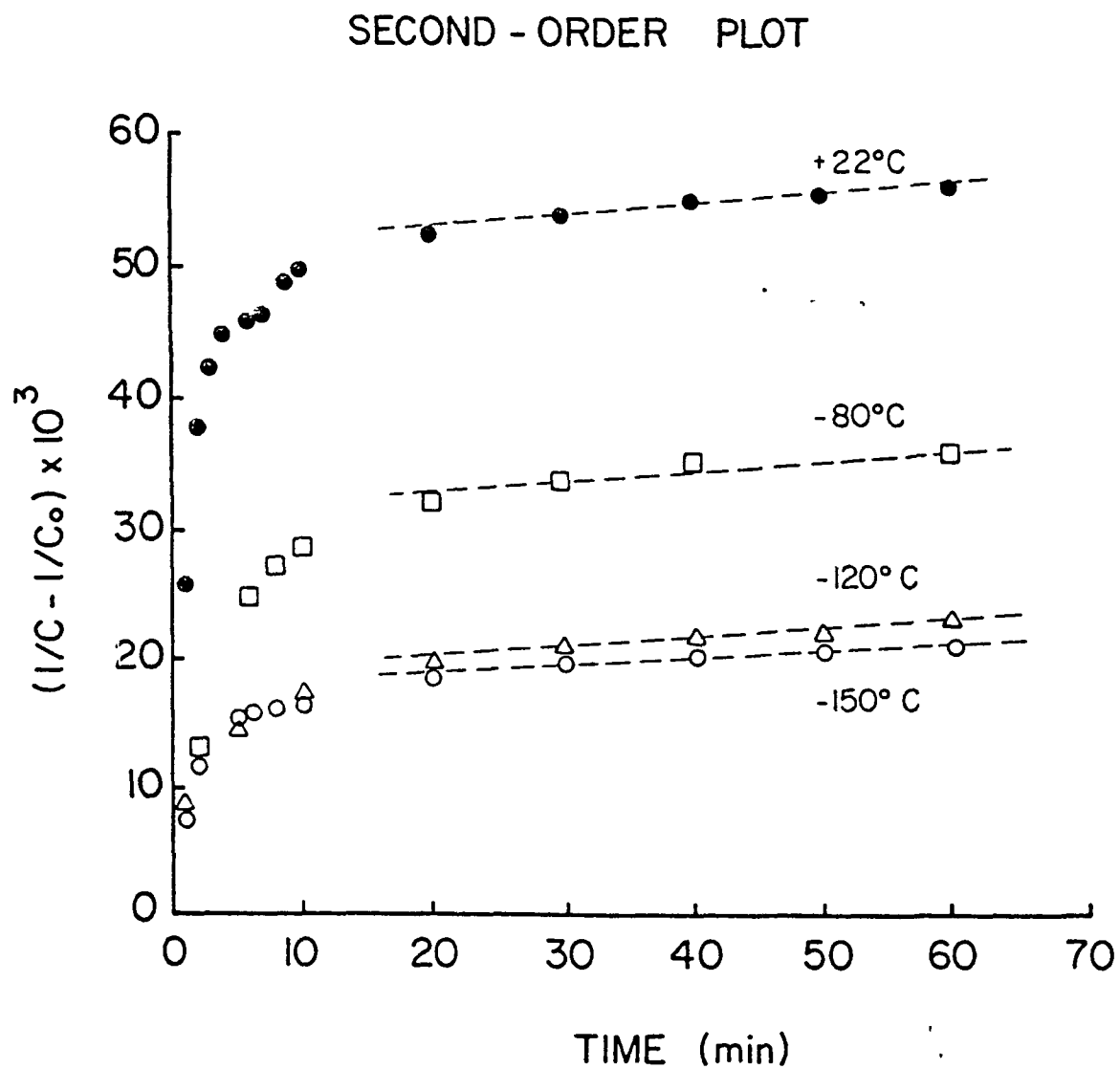


Figure 4.12 Second-order plot of the isothermal decay curves in Figure 4.10.

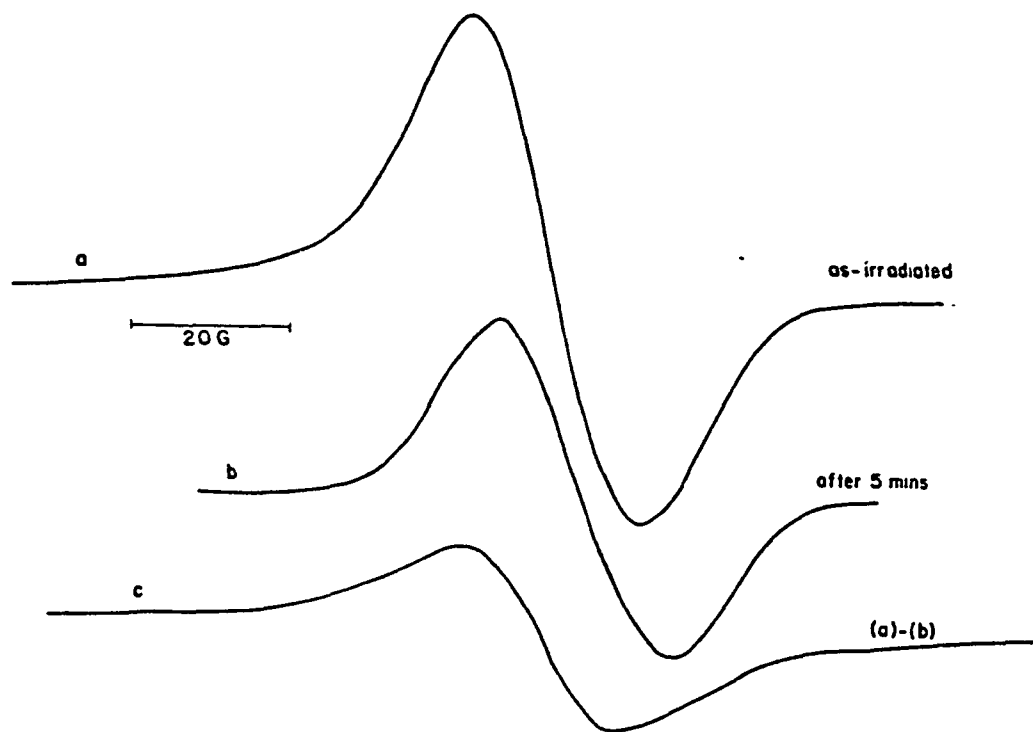


Figure 4.13 ESR spectra of TGDDM-DDS cured at 150°C (1 hr) and then 177°C (5 hrs) and γ -irradiated with a dose of 5 Mrad at -196°C . (a) as-irradiated, (b) after 5 minutes at -150°C , and (c) difference spectrum between (a) and (b).

CURING TEMPERATURE VS LINE-SHAPE

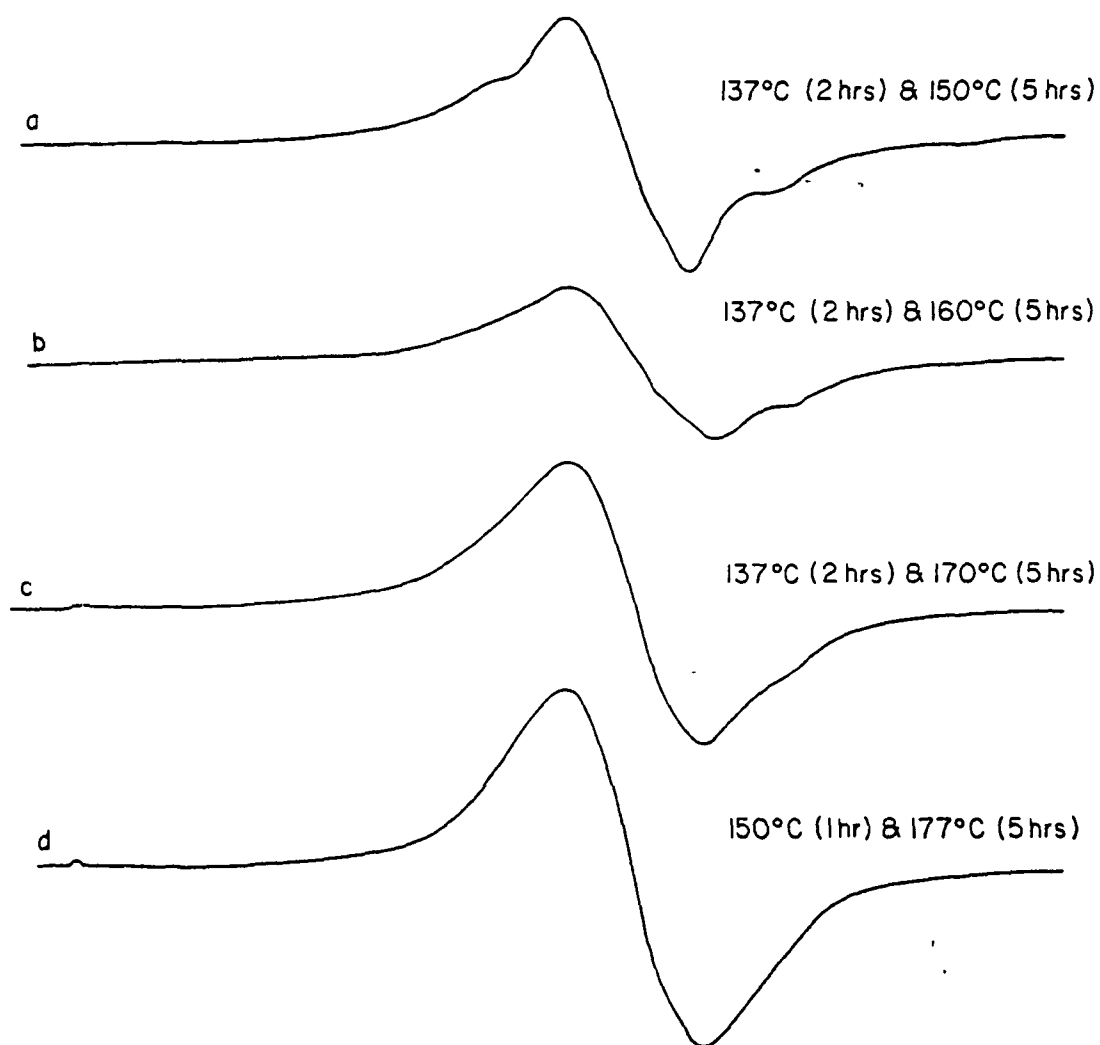
5 Mrad (γ -irradiation at -196°C)

Figure 4.14 ESR line shape of TGDDM-DDS epoxy cured at various temperatures, and irradiated with a dose of 5 Mrad of γ -radiation. ESR spectra were measured at -196°C .

CURING TIME VS. LINE-SHAPE
(γ -irradiation at -196°C)

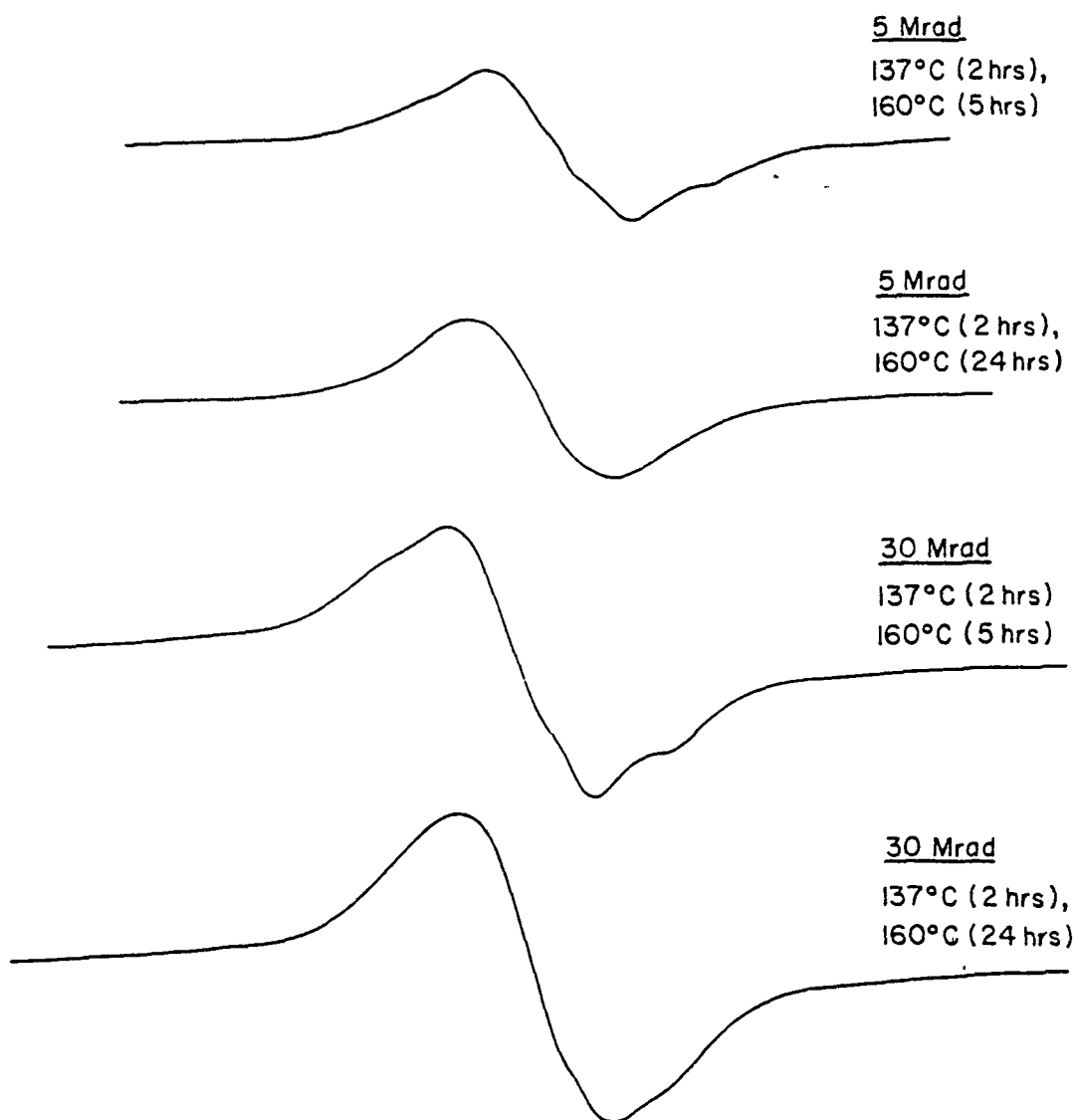


Figure 4.15 ESR line shape vs. curing time of TGDDM-DDS epoxy irradiated with 5 Mrad and 30 Mrad at -196°C . Spectra were measured at -196°C .

the ESR line shape was observed during this decay period over the decay temperature range considered.

In section 4.1.3, the fast-decaying fraction of the ESR spectrum (Figure 4.9) was assigned to the relatively reactive alkyl type radicals. However, the rate of radical disappearance is not only associated with the chemical structure of the radicals but also associated with the mobility of polymer radicals and the diffusivity of reactive gases such as hydrogen produced by irradiation or dissolved oxygen. The mobility of radicals and the diffusivity of reactive gases are primarily controlled by the physical state of polymer where the radicals are trapped. Therefore, the overall radical decay kinetics in the irradiated epoxy having an inhomogeneous network structure would be very complex.

As the temperature rises, a greater fraction of total radicals decay out at the early stage. The additional fraction of radicals disappearing at the higher temperature seem to be the same type of radicals as the fast-decaying radicals disappearing at lower temperature because the ESR line shapes of the former and the latter are similar to each other. The initial fast-decaying species are primarily due to the reactive radicals including alkyl radicals and also due to less reactive but mobile radicals located in less crosslinked regions or voids in the epoxy. Radical pairs or radical ions, if any, will undergo recombination reactions

at this early stage. Existence of free electrons as suggested by Schaffer [48] appears to be rare because most free electrons trapped in polymers show a very sharp ESR peak with a line width of less than 4 G [63] which is not observed in the present study. Thus, the fraction of fast decaying species is affected by: (1) the presence of trapped oxygen or hydrogen which reacts quickly with radicals and (2) the effect of crosslinking density on the recombination of radicals. At a given temperature, the trapped oxygen or hydrogen (or hydrogen radical) is depleted quickly reacting with radicals and the radicals which are mobile enough to recombine disappear also. Thereafter, changes in the radical concentration occur much slowly due to slow diffusion of oxygen either in highly crosslinked regions or from exterior and decreased probability of radical recombination, e.g., through a hydrogen hopping mechanism especially in highly crosslinked regions. As the temperature increases, the additional amount of radicals which have been trapped in more crosslinked regions may acquire enough energy to react and disappear at the early stage. At the later stage, on the other hand, the change of decay rate constants with temperature is negligible. It is expected that at this later stage the overall radical decay rate constant is predominantly governed by the decay rate constant of radicals trapped in highly crosslinked regions of the irradiated epoxy. Since all the temperatures

employed for the isothermal decay curves are below the glass transition temperature of the epoxy system ($T_g \sim 200^\circ\text{C}$), the increase of the decay temperature may not significantly affect the decay rate constant in the higher crosslinked regions at the later stage.

4.1.5 Effect of Curing Conditions on Radical Decay

The effect of crosslinking density on radical decay behavior of irradiated epoxy as a function of curing temperature, curing time, and radiation dose was also examined. Figures 4.16 and 4.17 show plots of radical concentration versus time for various epoxy samples cured at various temperatures and for various curing times, respectively. The concentration of the long-lived radical species trapped in the irradiated epoxy increases with curing temperature but shows less dependency on curing time. The scattering of data points for the initial radical concentration is probably due to the handling of the sample, i.e., due to an uncertain elapse of time (< 1 minute) involved during transferring the sample from the liquid nitrogen to the ESR cavity.

It is known that as the curing temperature increases the extent of curing reaction of an epoxy system increases at any given curing time [120-121]. Once the epoxy system reaches the vitrification point, further extension of the curing time at a given temperature does not significantly

CURING TEMPERATURE EFFECT ON RADICAL DECAY (AT 23°C)

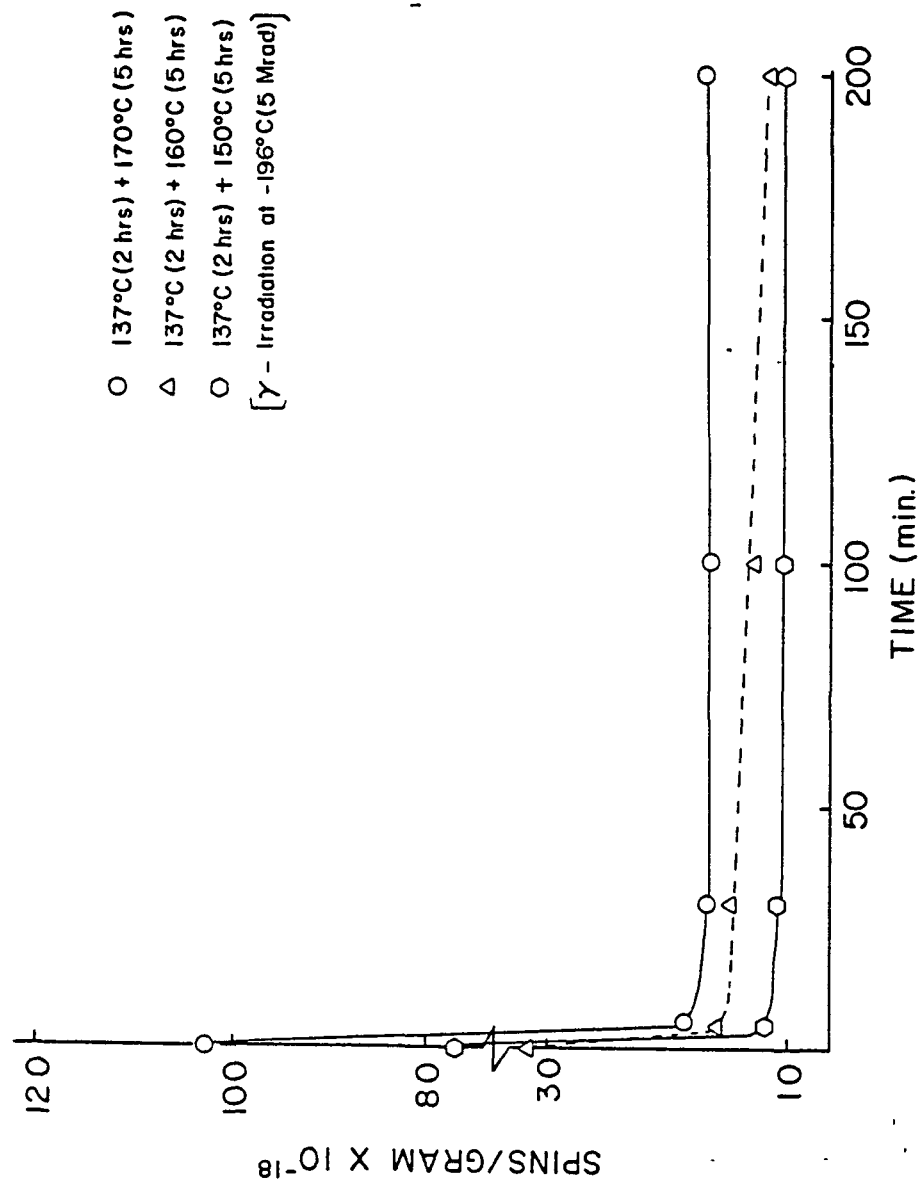


Figure 4.16 Radical decay in air at room temperature (23°C) of TGDDM-DDS epoxy samples cured at various temperatures.

CURING TIME EFFECT ON RADICAL DECAY (AT 23°C)

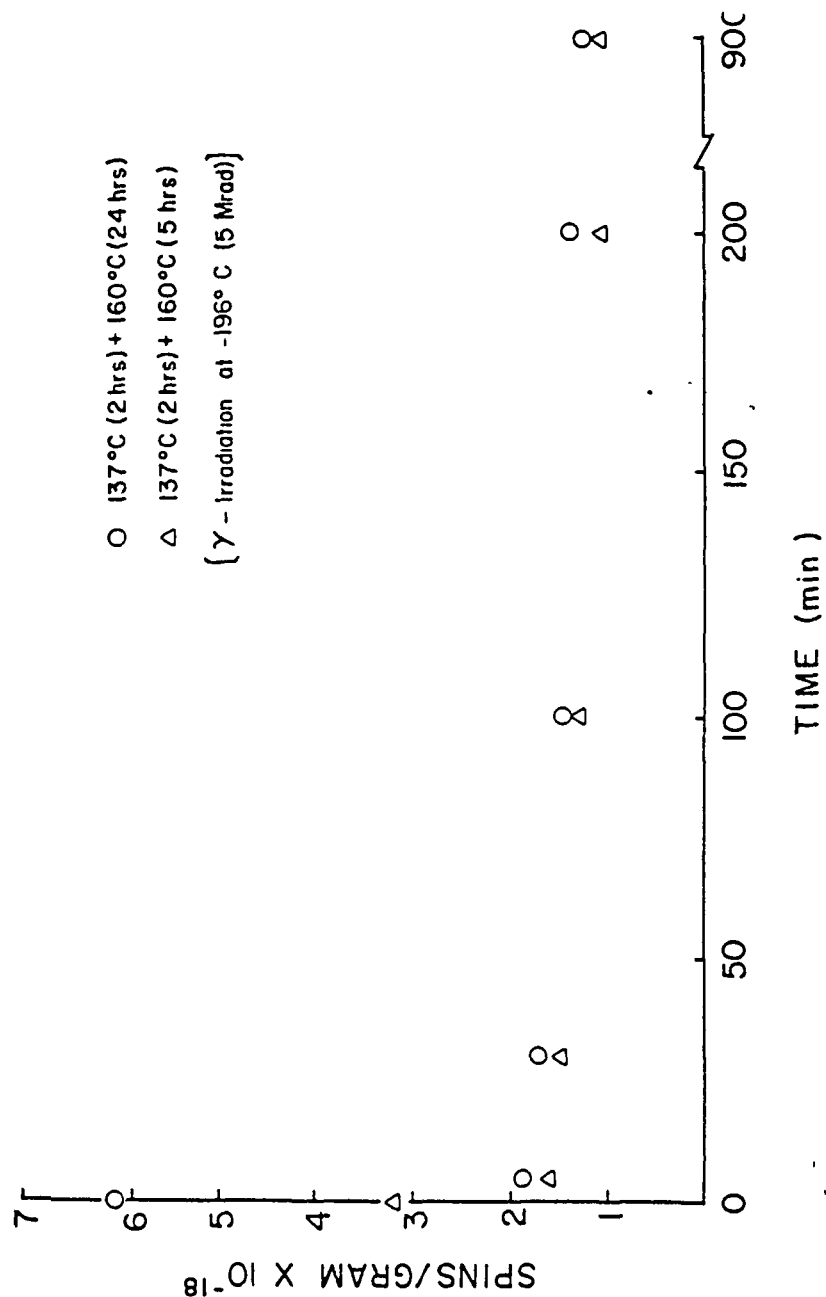


Figure 4.17 Radical decay in air at room temperature (23°C), of TGDDM-DDS epoxy cured with different curing times.

increase the extent of reaction due to the lack of diffusional transport of the reactive sites such as secondary amines. Crosslinking at this stage occurs mainly through the formation of ether linkages by the reaction between hydroxyl and epoxy groups. Further reaction of the secondary amine occurs only when the curing temperature becomes higher than the glass transition temperature of the 'on-curing' system [122]. The observed increase of long-lived radical concentration with curing temperature in the irradiated epoxy may reflect the crosslinking density effect on radical decay reactions.

Since the cured epoxy may contain unreacted functional groups as illustrated schematically in Figure 4.18, i.e. as 100 % reaction is never achieved for various reasons, it will undergo additional curing reaction upon exposure to high energy radiation. Figure 4.19 shows the effect of irradiation dose on the radical decay behavior in the epoxy. The concentration of long-lived radicals increases with irradiation dose. This result is consistent with Kent's [64] observation and support Netravali's observation [123] that additional crosslinking occurs upon irradiation of cured epoxy. However, it can not be ruled out that the increase of the long-lived radicals at higher dose levels could also be attributed to higher radical yields at higher irradiation dose.

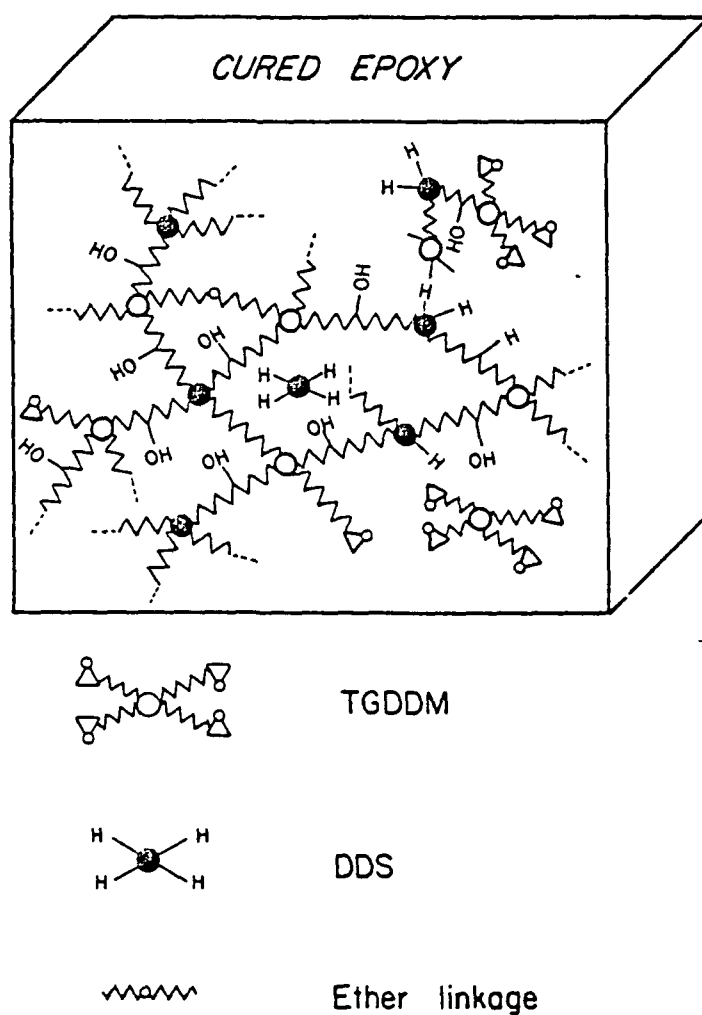


Figure 4.18 A schematic representation of cured TGDDM-DDS epoxy network.

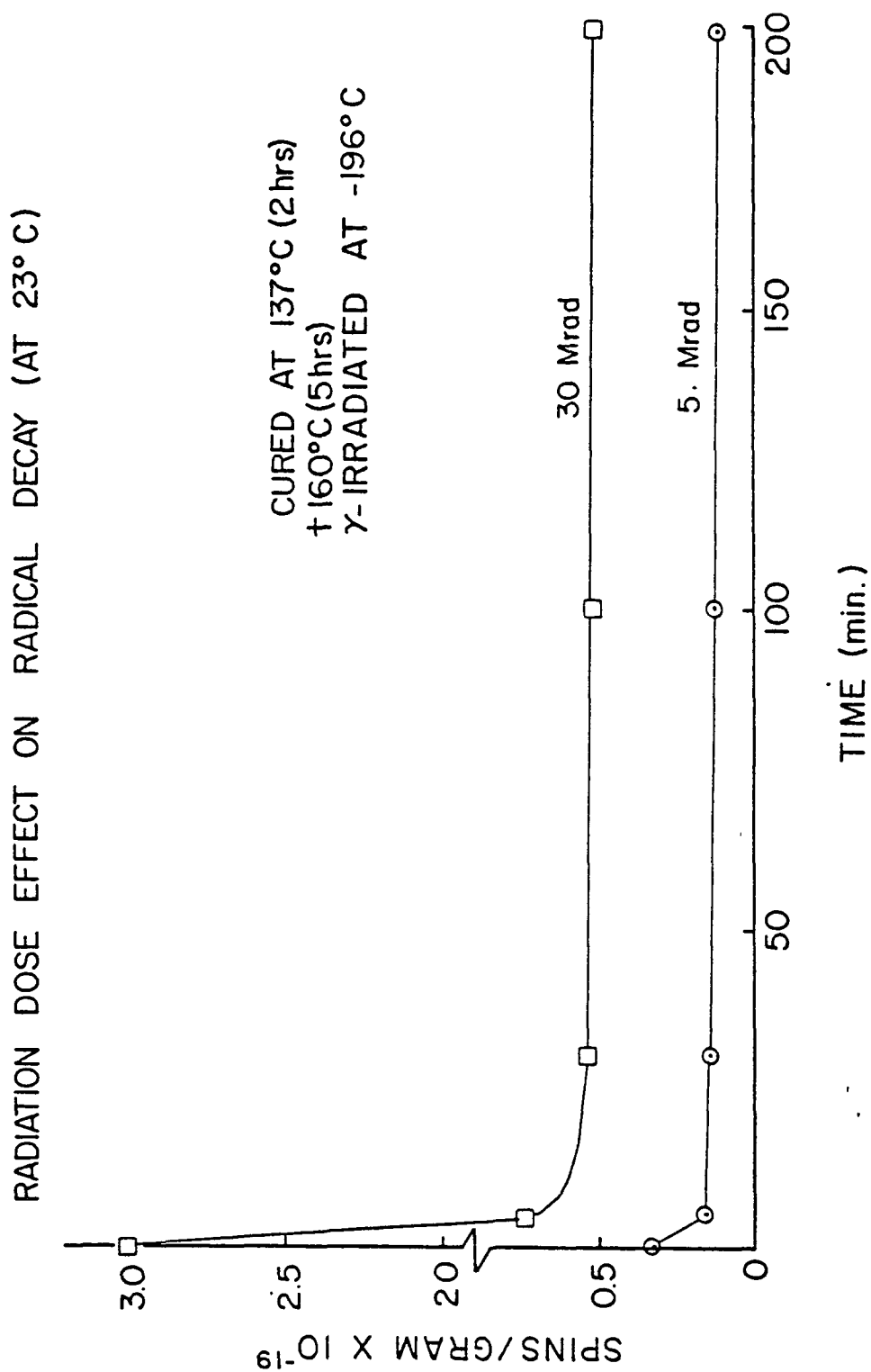


Figure 4.19 Radical decay in air at room temperature of TGDDM-DDS epoxy γ-irradiated with various radiation doses.

4.1.6 ESR Spectra of Graphite Fiber and Composites

It was impossible to resolve any ESR spectral change of the graphite fiber and the composite after irradiation because even unirradiated graphite fiber contains a large concentration of free radicals $10^{20} - 10^{21}$ spins/g, which is approximately two orders of magnitude higher than the radical concentration of the irradiated epoxy with over 1,000 Mrad of 1/2 MeV electrons ($10^{18} - 10^{19}$ spins/g). The unirradiated composite contains about the same concentration of radicals as in the unirradiated graphite fiber presumably due to radicals in the graphite fiber and the background over-shadows any spectral change in the composite as a result of irradiation.

The ESR spectra of T-300 graphite fiber and an epoxy/graphite fiber composite (T300/5208) irradiated by 1/2 MeV electrons at room temperature are shown in Figure 4.20. The line shapes of both spectra are singlets and are similar. The line width of the singlet for graphite fiber is about 4 G and its g-factor is 2.0023 being close to that for free electrons. The ESR line width and the g-factor of the composite are about 5 G and 2.000 ± 0.001 , respectively. This slight difference in line width and the g-factor between the graphite fiber and the composite is probably due to the different environments in which the radicals are residing. For instance, when there is a chemical reaction between graphite fiber and epoxy at the interface, the

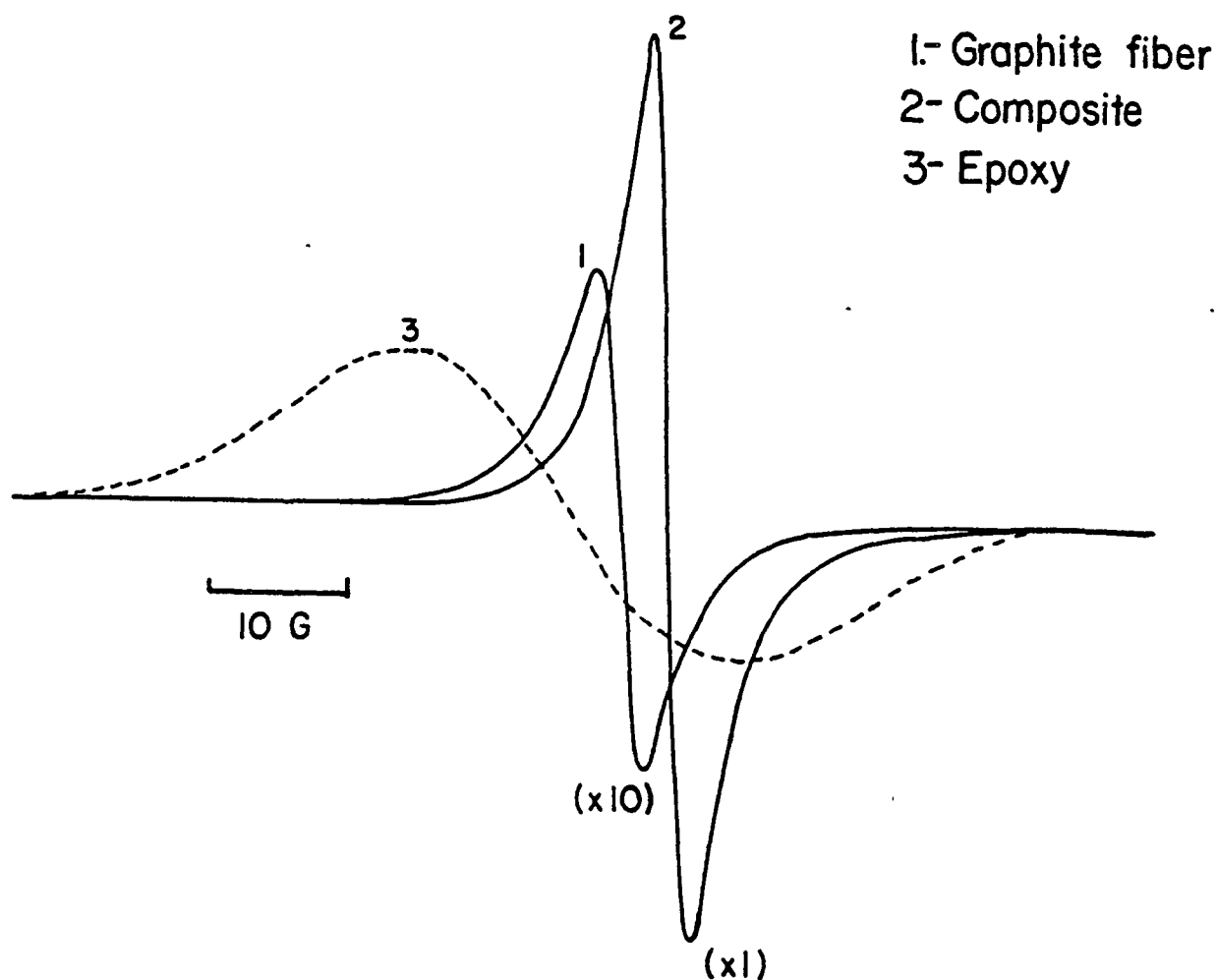


Figure 4.20 ESR spectra of (1) graphite fiber (~1 mg) and (2) T300/5208 composites (~4 mg) irradiated with a 9,000 Mrad dose of 1/2 MeV electrons at room temperature in air, and (3) TGDDM-DDS (~170 mg) epoxy γ -irradiated with 5 Mrad and exposed to air for several months.

radicals just beneath the surface of the graphite fiber may migrate to the interface and thus a variation in the environments of the unpaired electrons occurs as suggested for the case of carbon black/rubber by Fugimoto et al. [114]

If the large concentration of free radicals in the graphite fiber, which is presumably produced during the oxidation process in the preparation of graphite fiber, eventually interact with free radicals produced in the irradiated epoxy at the fiber/epoxy interface, (for example, by formation of chemical bonds or chemisorption of radicals), then enhancement of the bond-strength of the composite after irradiation, as observed by many authors [2, 116, 118], may be explained. If there is a chemical reaction between the radicals in the graphite fiber and radicals produced in the epoxy at the interface, then there should be a change in the radical concentration of the composite after irradiation. However, no confirmation of the reaction between radicals in the epoxy and the fiber was made in the present study. Although the exact nature of the reaction between radicals on the graphite fiber and those generated in the epoxy matrix by irradiation has never been discussed, chemical bond formation, or chemisorption of polymer radicals, on the surface of carbon black which also contains free radicals in rubber has been discussed by several authors [124-128].

4.2 Surface Analysis

Although the exact nature of the epoxy/graphite fiber interaction at the interface is not well defined, it is expected that there are polar-polar interactions including hydrogen bonding formation between two phases. The polar-polar interaction between the two phases depends on the surface polarity of the component materials which may change upon exposure to ionizing radiation. In this section, how the polarity of epoxy and graphite fiber changes with radiation dose will be discussed, and possible radiation processes causing the polarity changes in the TGDDM-DDS epoxy system are proposed on the basis of ESCA and IR results.

4.2.1 Surface Energy Measurements

Tables 4.1 shows the contact angle measurements of various liquids on TGDDM-DDS epoxy irradiated at room temperature with 1/2 MeV electrons at various dose levels. The epoxy samples were cured at 150°C (1hr) and post cured at 177°C (5 hrs). From the Young-Dupre equation (2.52), the work of adhesion W_a was calculated (see Table 4.2). Surface tensions of the test liquids were obtained from the literature [85] (see Table 3.1). Figure 4.21 shows the plot of $W_a/2\alpha_L$ vs. β_L/α_L for TGDDM-DDS epoxy irradiated with various doses. The polar and dispersion contributions to the total surface energy were determined using the slope

Table 4.1 Contact angles (degree) of 1/2 MeV electron-irradiated epoxy (TGDDM-DDS) measured with various liquids.

Test Liquids	Contact Angles					
	Dose (Mrad) x 10 ⁻³					
	0	0.4	1	2	5	10
Water	100.6	72.0	25.0	27.2	26.3	13.5
Ethylene-Glycol	70.9	53.3	28.3	17.4	16.0	12.7
Hexadecane	38.8	23.3	13.3	6.8	4.7	4.8

Table 4.2 Work of adhesion W_a of Liquid/Epoxy interface versus radiation dose (1/2 MeV electrons)

Liquid	Dose (Mrad)	W_a (dyne/cm)	β_L/α_L	$W_a/2\alpha_L$
Water	0	59.3	1.53	6.35
	400	95.2		10.2
	1000	138.8		14.9
Ethylene-glycol	0	64.1	0.81	5.92
	400	77.2		7.13
	1000	90.8		8.38
Hexadecane	0	49.1	0.00	4.67
	400	52.9		5.03
	1000	54.5		5.19

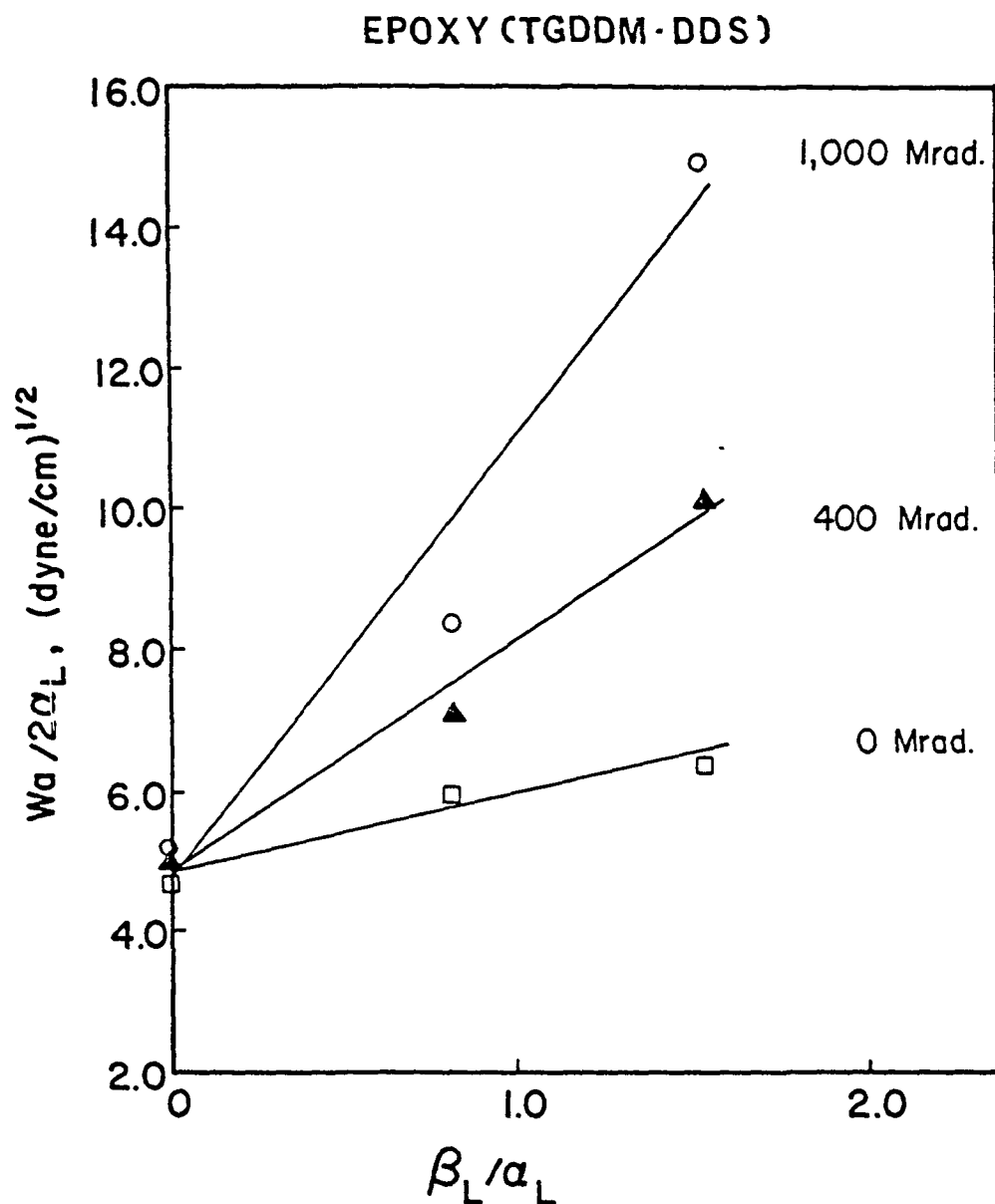


Figure 4.21 Plot of $W_a/2\alpha_L$ against β_L/α_L of TGDDM-DDS epoxy. Samples were irradiated with 1/2 MeV electrons at room temperature.

and the intersect of the linear plot of $W_a/2\alpha_L$ vs. β_L/α_L and equation (2.59) as described in section 2.4.1. Table 4.3 lists the surface energies of the epoxy determined from Figure 4.21. Figure 4.22 shows a plot of the surface energies including the polar and dispersion components versus radiation dose. The surface energy of irradiated epoxy increases monotonically with radiation dose up to 1000 Mrad and then levels off. The total surface energy increase is mainly due to the increase of the polar component upon irradiation whereas the dispersion component remains almost constant with dose, as expected. This indicates that polar groups, e.g., carbonyl groups, are produced on the surface of the sample by irradiation.

The surface energy changes of graphite fiber with radiation dose were also examined by the same procedure as for the epoxy. The surface energy increase of the graphite fiber with dose up to 10,000 Mrad is not significant probably due to its stability under exposure to ionizing radiation (see Tables 4.4-4.6 and Figures 4.23 and 4.24).

In order to examine the role of oxygen in the increase in the polarity of the epoxy surface upon irradiation, samples were irradiated with 1/2 MeV electrons in three different environments: (1) in air-filled Ziplog bags, (2) in nitrogen-filled Ziplog bags, and (3) in vacuum-sealed aluminium foil bags. Figure 4.25 shows the change in contact angle (measured with water) of the epoxy surface

Table 4.3 Surface energy of irradiated epoxy (TGDDM-DDS) vs. radiation dose (1/2 MeV electrons)

Dose Mrad	Surface Energy (dyne/cm)			
	Dispersion	polar	Total	Polar/Total
0	22.9	1.2	24.1	0.05
400	23.3	11.3	34.6	0.33
1,000	21.0	39.7	60.7	0.65
2,000	22.6	38.0	60.5	0.63
5,000	22.7	38.2	60.8	0.63
10,000	21.9	43.3	65.2	0.66

EPOXY (TGDDM-DDS)

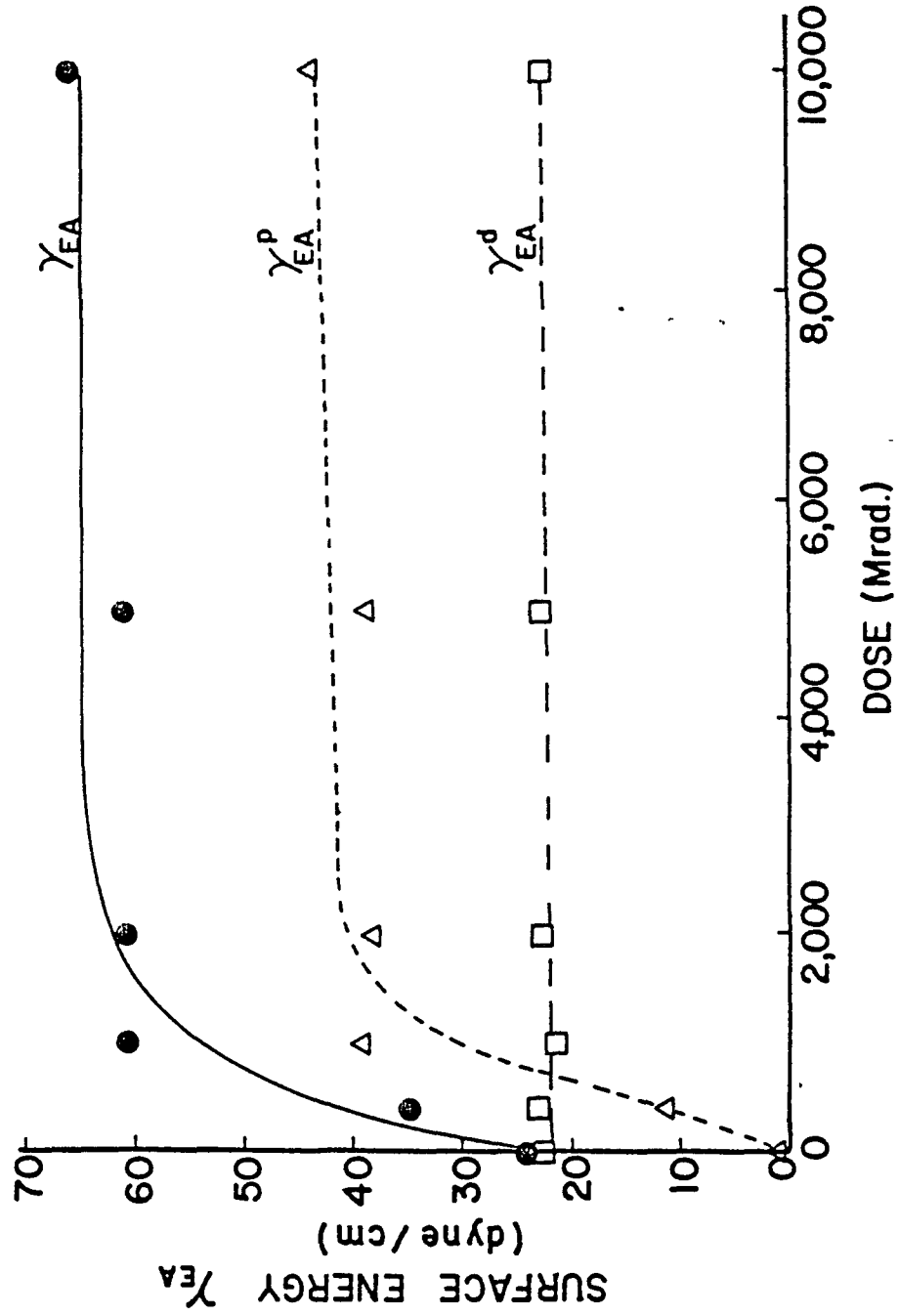


Figure 4.22 Surface energy changes of TGDDM-DDS epoxy with radiation dose.

Table 4.4 Contact angles (degree) of 1/2 MeV electron-irradiated graphite fiber (T-300) measured with various liquids

Test Liquids	Contact Angles .			
	Dose (Mrad) x 10 ⁻³			
	0	1	5	10
Water	38.6	23.4	21.7	17.5
Formamide	17.7	18.4	9.7	16.5
Ethyleneglycol	21.1	15.2	10.6	19.6
Tricresylphosphate	38.2	30.6	36.5	28.3
Hexadecane	30.2	32.3	28.2	29.8
1-Bromonaphthalene	12.2	-	4.9	-
Hexane	10.1	-	0.0	-

Table 4.5 Work of adhesion W_a of graphite fiber versus radiation dose (1/2 MeV electrons)

Liquids	Dose x 10 ⁻³ Mrad	W_a (dyne/cm)	$W_a/2SL$	$\beta L/SL$
Water	0	129.7	13.89	1.53
	1	139.6	14.94	
	5	140.4	15.04	
	10	142.2	15.23	
Formamide	0	113.8	10.01	0.89
	1	113.6	9.99	
	5	115.8	10.18	
	10	114.2	10.04	
Ethylene-glycol	0	93.4	8.66	0.80
	1	94.8	8.76	
	5	95.8	8.84	
	10	93.8	8.66	
Tricresyl Phosphate	0	73.0	5.83	0.21
	1	76.1	6.08	
	5	73.8	5.89	
	10	81.1	6.14	
1-Bromo-naphthalene	0	88.2	6.60	0.00
	1	-	-	
	5	89.0	6.66	
	10	-	-	
Hexadecane	0	51.5	4.90	0.00
	1	50.9	4.85	
	5	51.9	4.94	
	10	51.6	4.91	
Hexane	0	36.5	4.26	0.00
	1	-	-	
	5	36.8	4.29	
	10	-	-	

Table 4.6 Surface energy of irradiated graphite fiber (T-300) versus radiation dose (1/2 MeV electrons)

Dose (Mrad)	Surface Energy (dyne/cm)			
	Dispersion	Polar	Total	Polar/Total
0	21.2	34.5	55.7	0.62
1,000	20.1	42.3	62.3	0.68
5,000	20.0	42.6	62.6	0.68
10,000	19.3	44.6	64.0	0.70

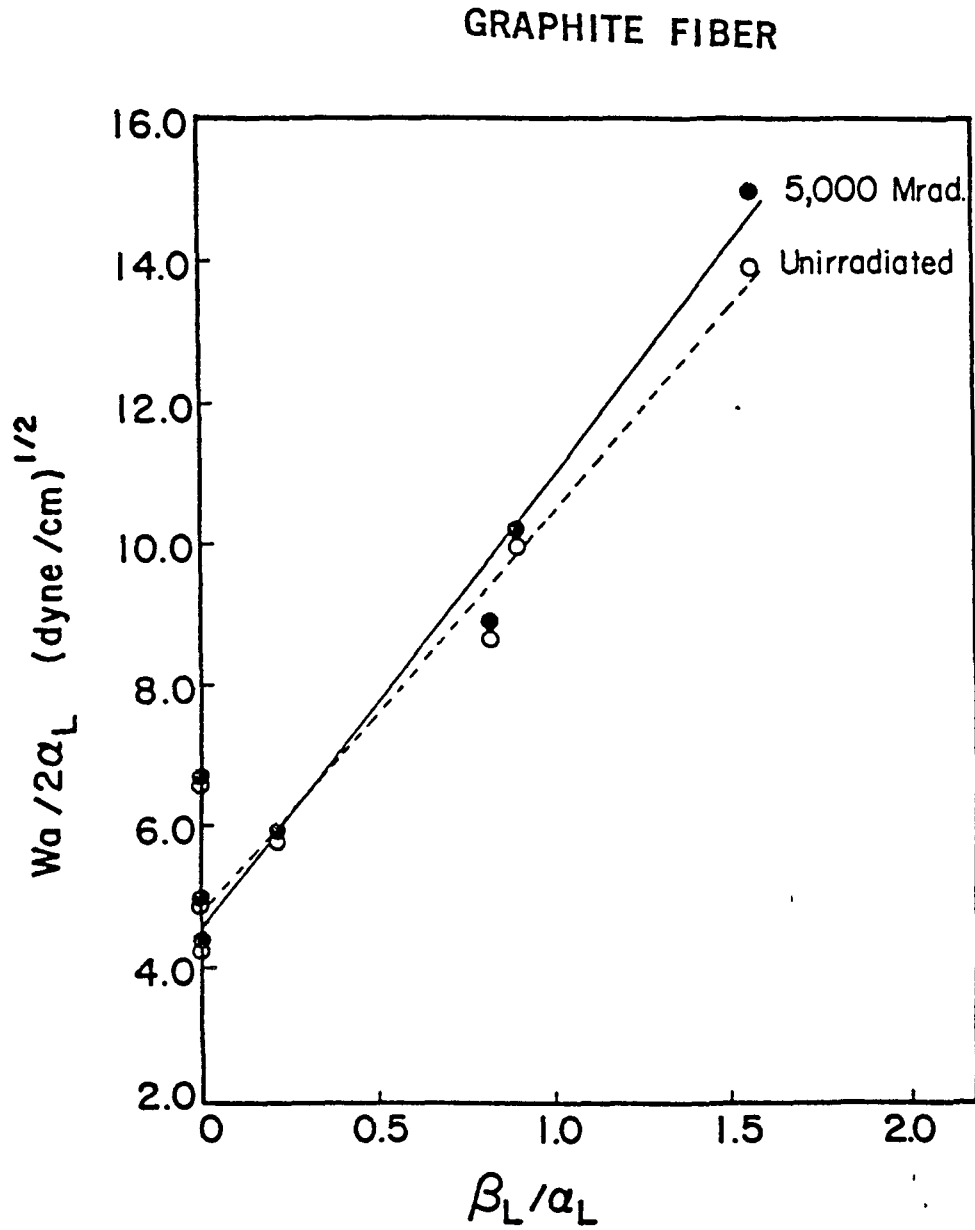


Figure 4.23 Plot of $W_a / 2\alpha_L$ against β_L / α_L of T-300 graphite fiber. Samples were irradiated with 1/2 MeV electrons at room temperature.

GRAPHITE FIBER

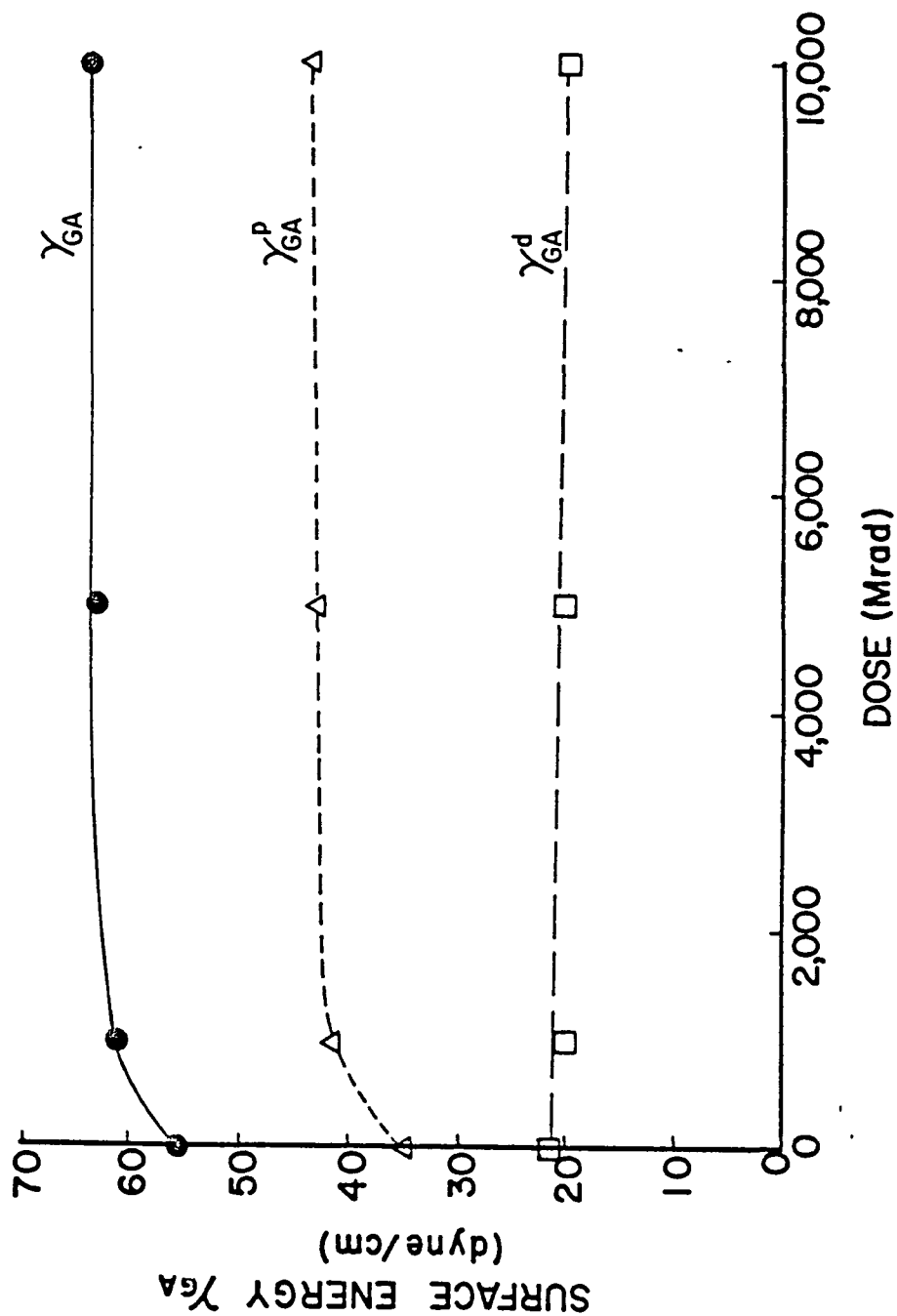


Figure 4.24 Surface energy changes of T-300 graphite fiber with radiation dose.

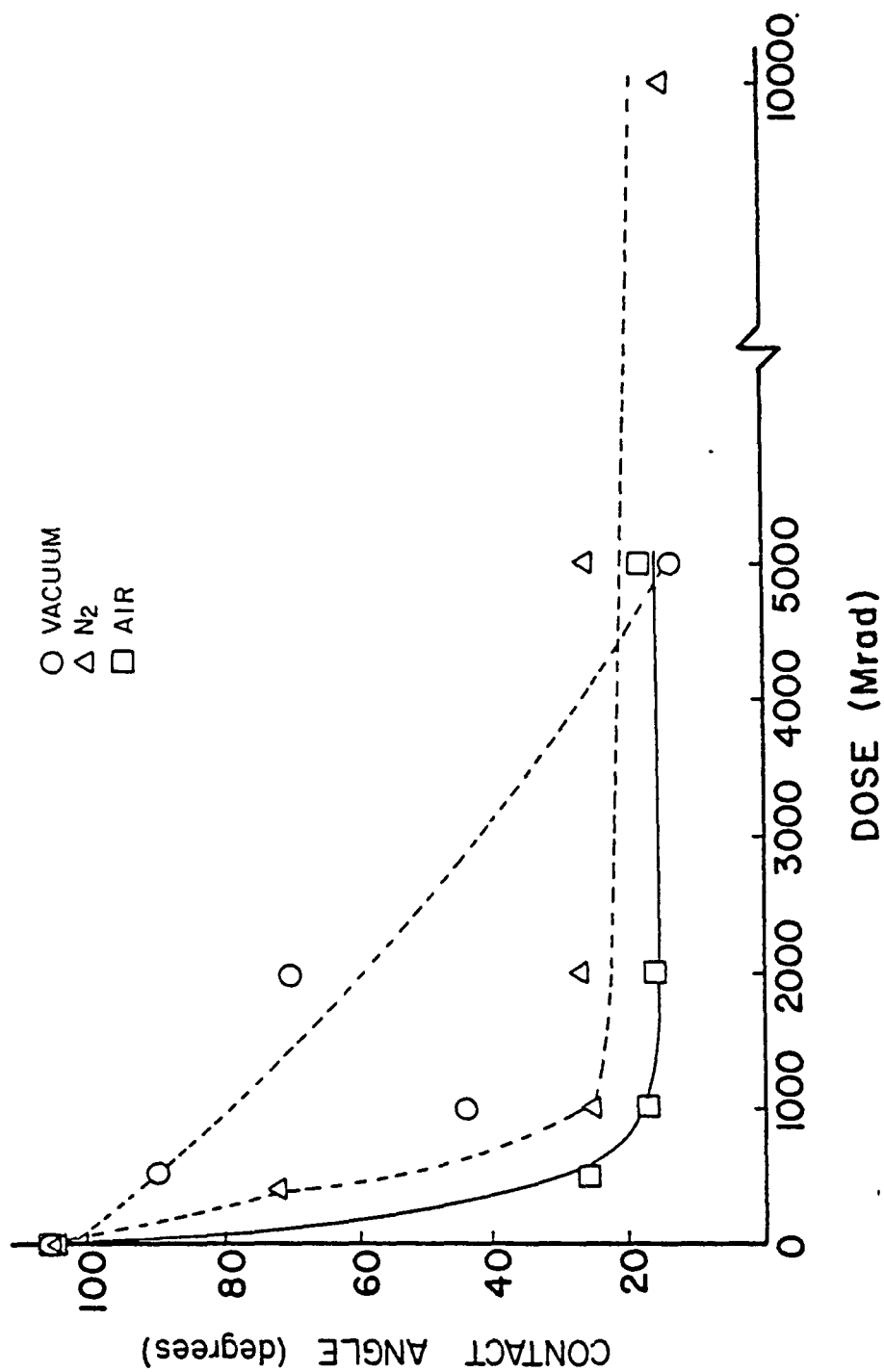


Figure 4.25 Contact angle changes (with H₂O) with radiation dose of TGDDM-DDS epoxy irradiated with 1/2 MeV electrons: □ in air, △ in nitrogen-filled bag, and ○ in vacuum.

with radiation dose in the different environments. For the samples irradiated in air-filled or in nitrogen-filled Ziplog bags, the contact angle decreases rapidly with dose, while for samples irradiated in vacuum-sealed aluminium foil bags the contact angle decreases more slowly but eventually reaches the same values of the samples irradiated in the air or in the nitrogen condition. This result indicates that oxygen is probably the most important factor determining the change in surface energy of the epoxy upon exposure to high energy radiation. The unusually low contact angle value at the 1,000 Mrad dose level of a sample that has exposed under the condition (3) is probably due to some pinholes or imperfect bonding in the vacuum-sealed aluminium foil bag which permitted air (or oxygen) to penetrate into the sample during irradiation. Even if samples were sealed tightly, oxygen might diffuse through the thin layers of aluminium foil and ultimately the contact angle reaches the same value as in the air condition.

4.2.2 ESCA Analysis of Irradiated Surfaces

If the surface energy increase with irradiation dose is mainly due to the polar groups produced by oxidation, the oxygen content on the irradiated surface should increase after irradiation. The same result can be expected for the interface, i.e., a shear-fractured surface, of the composite if oxygen is involved at the interface during irradiation.

Table 4.7 shows relative oxygen contents to carbon of both the epoxy surface and the fracture surface created by an interlaminar shear test of T-300/5208 composites. A significant increase in oxygen content was observed on both the epoxy surface (37 % increase) and the fractured surface of the composite (51 % increase) after irradiation. A similar oxygen content increase in the T-300/5208 composite after irradiation was observed by Wolf [116] although she examined only the outermost surface of the composite. Also the contact angle of water on the fractured surface of the epoxy decreases upon irradiation (see Table 4.8). This contact angle decrease is consistent with the increase in polarity of epoxy surface and graphite fiber after irradiation with 1,000 Mrad. Therefore, it may be concluded that oxidation reactions also occur at the interface of the composite upon irradiation. However, it should be noted that due to the high concentration of long-lived radicals, surface oxidation may occur after the shear test is completed and the surface is exposed directly to air.

4.2.3 IR Spectroscopy

In order to examine what kinds of chemical structure modifications occur in TGDDM-DDS epoxy upon irradiation and to examine what functional groups cause the increase in the surface polarity in the epoxy, the infrared (IR) absorption spectra of an as-cured sample and an irradiated sample were compared (see Figures 4.26 and 4.27).

Table 4.7 Relative atomic concentration of oxygen (O) and carbon (C) on TGDDM-DDS epoxy and T300/5208 composite as Determined by ESCA

Sample	C	O	O/C (Irradiated) O/C (Control)
Epoxy			
As-cured	1	0.237	1.37
10,000 Mrad	1	0.324	
Composite (Fracture Surface)			
Control	1	0.237	1.51
10,000 Mrad	1	0.358	

Note: Average value of two measurements

Table 4.8 Contact angles (degree) of water on shear-fracture surface and outermost surface of T300/5208 uniaxial composites irradiated with 1/2 MeV electrons in aluminium-foil Bags.

	Control	7,500 Mrad
Fracture surface		
Fiber Direction		
Advancing	61.7	45.2
Receding	-	-
Lateral Direction		
Advancing	85.0	59.0
Receding	84.0	59.0
Outermost		
Advancing	88.0	54.3
Receding	83.3	53.6

TGDDM-DDS EPOXY

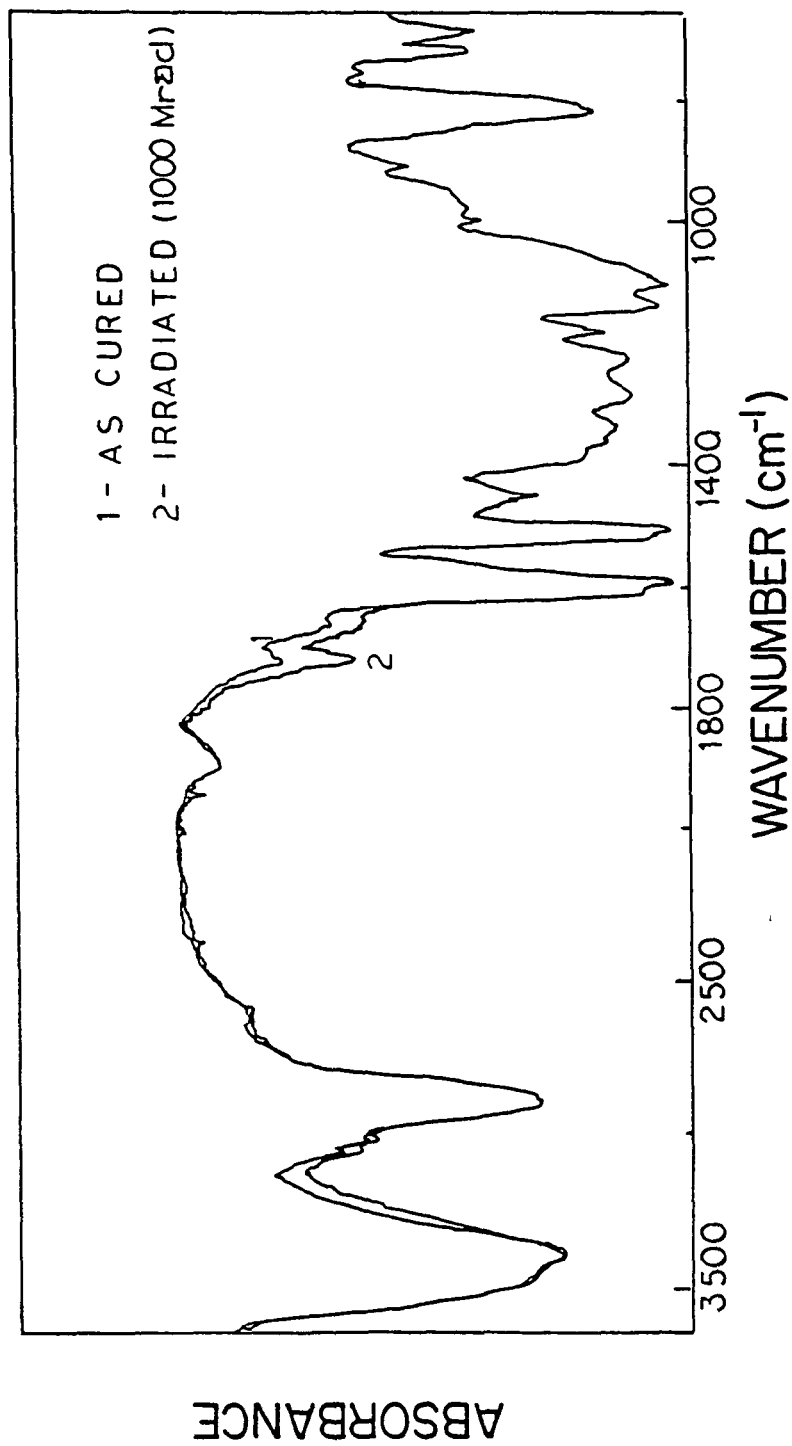


Figure 4.26 IR spectra of TGDDM-DDS epoxy: (1) as-cured and (2) irradiated with a 1,000 Mrad dose of 1/2 electrons in air.

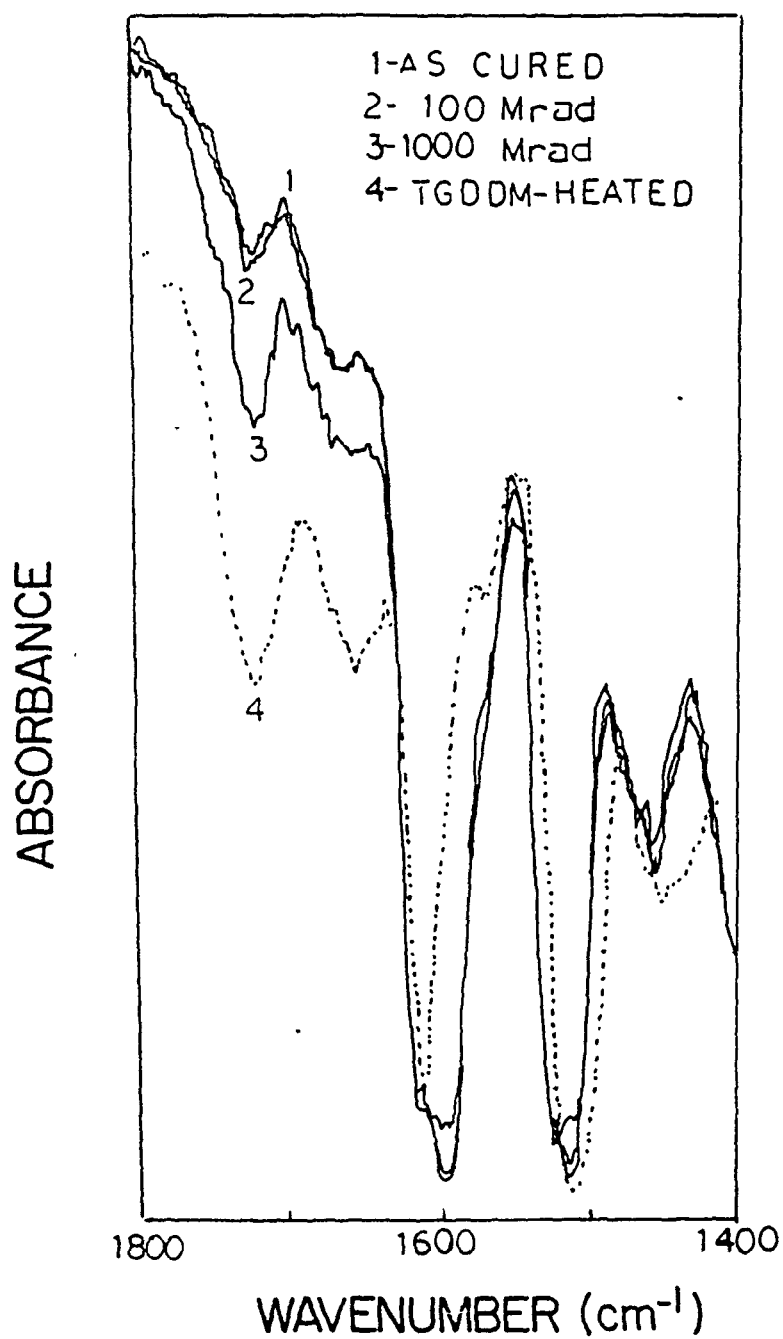


Figure 4.27 Growth of carbonyl peak at 1720 cm^{-1} upon irradiation. Samples were irradiated with $1/2 \text{ MeV}$ electrons in air at room temperature.

The IR spectrum (spectrum 1 of Figure 4.27) of the as-cured TGDDM-DDS epoxy shows two main carbonyl peaks, at 1720 cm^{-1} and 1660 cm^{-1} . The IR peak at 1720 cm^{-1} generally corresponds to either aliphatic ketones or carboxylic carbonyls, and the peak at 1660 cm^{-1} is attributed to amide or aromatic carbonyl groups [29-32]. Since these carbonyl peaks are not present in the uncured TGDDM-DDS mixture (see Figure 4.28), the carbonyl groups in the unirradiated sample must be produced during the curing process, probably by oxidation.

Upon irradiation of the cured epoxy with electrons, the intensity of the peak at 1720 cm^{-1} increases more than 110 % (in peak height) with a radiation dose of 1,000 Mrad while the 1660 cm^{-1} peak changes negligibly ($< 5\%$) with the same irradiation dose (see Figure 4.27). The same carbonyl peaks at 1720 cm^{-1} and 1660 cm^{-1} are observed for the pure TGDDM that was heated in air at 150°C for 1 hr and consecutively heated in air at 177°C for 5 hrs (see Figure 4.29). It is noteworthy that, as shown in Figure 4.29, there is a significant increase in the absorption near 3300 cm^{-1} which is attributed to $-\text{OH}$ groups with a concurrent decrease in the epoxy group absorption near 905 cm^{-1} . This may indicate that a self-polymerization occurs in TGDDM epoxy prepolymer by the heat treatment. However, the IR spectrum of DDS after heat treatment with the same condition as for the pure TGDDM does not change noticeably (see Figure 4.30). These

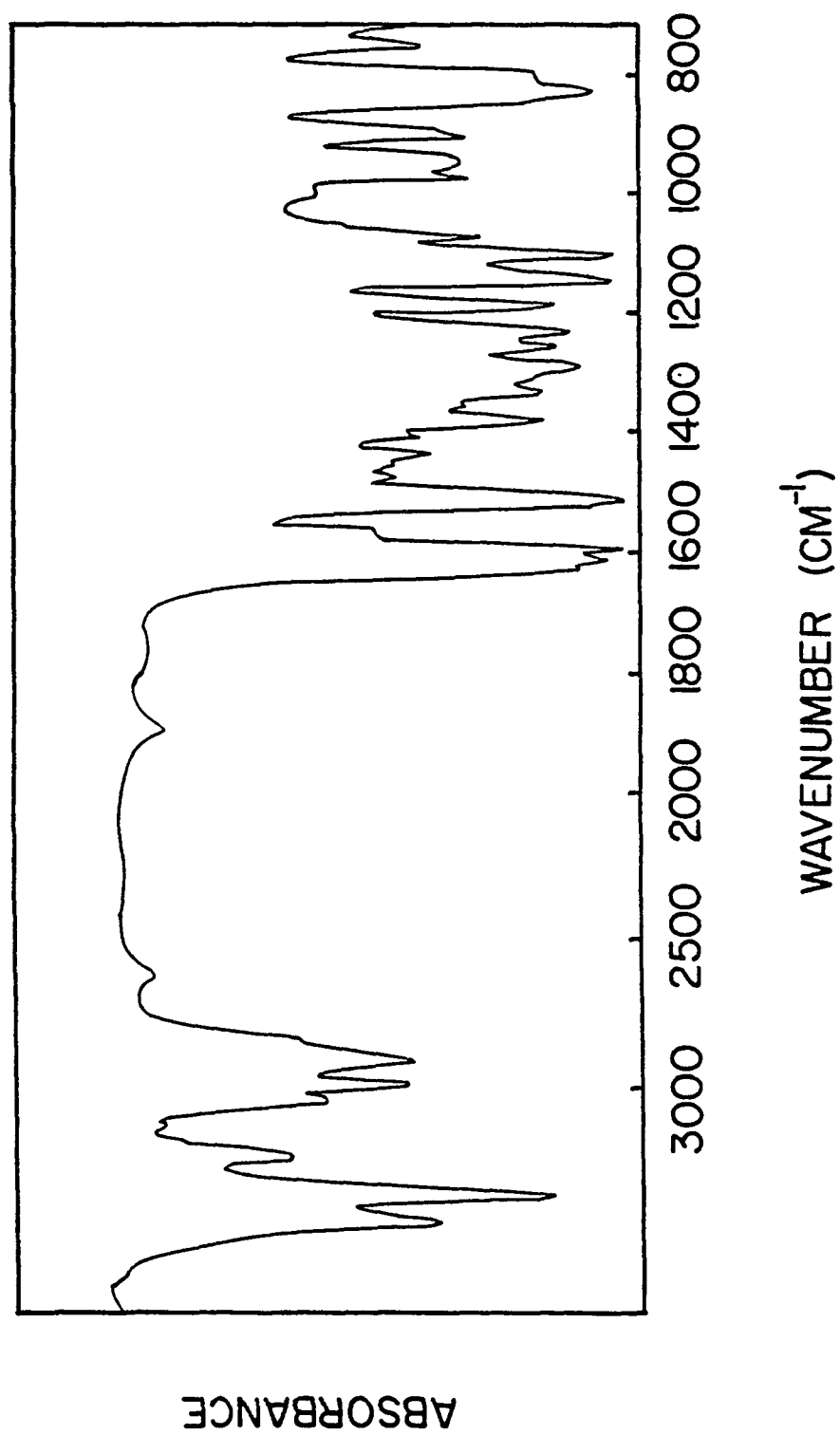


Figure 4.28 IR spectrum of the as-mixed TGDDM-DDS.

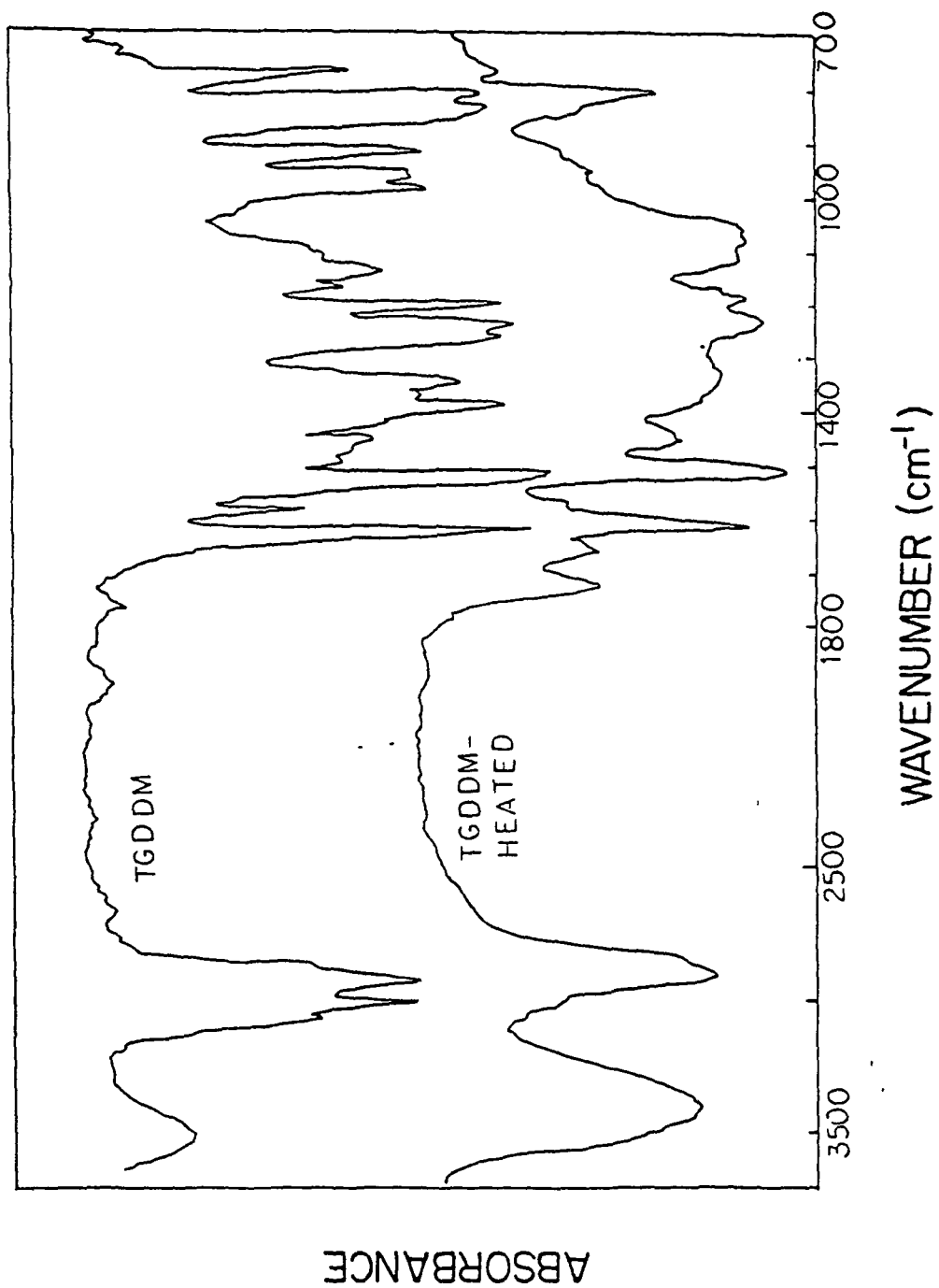


Figure 4.29 IR spectra of pure TGDDM and heat-treated TGDDM at 150°C for 1 hr and 177°C for 5 hrs in air.

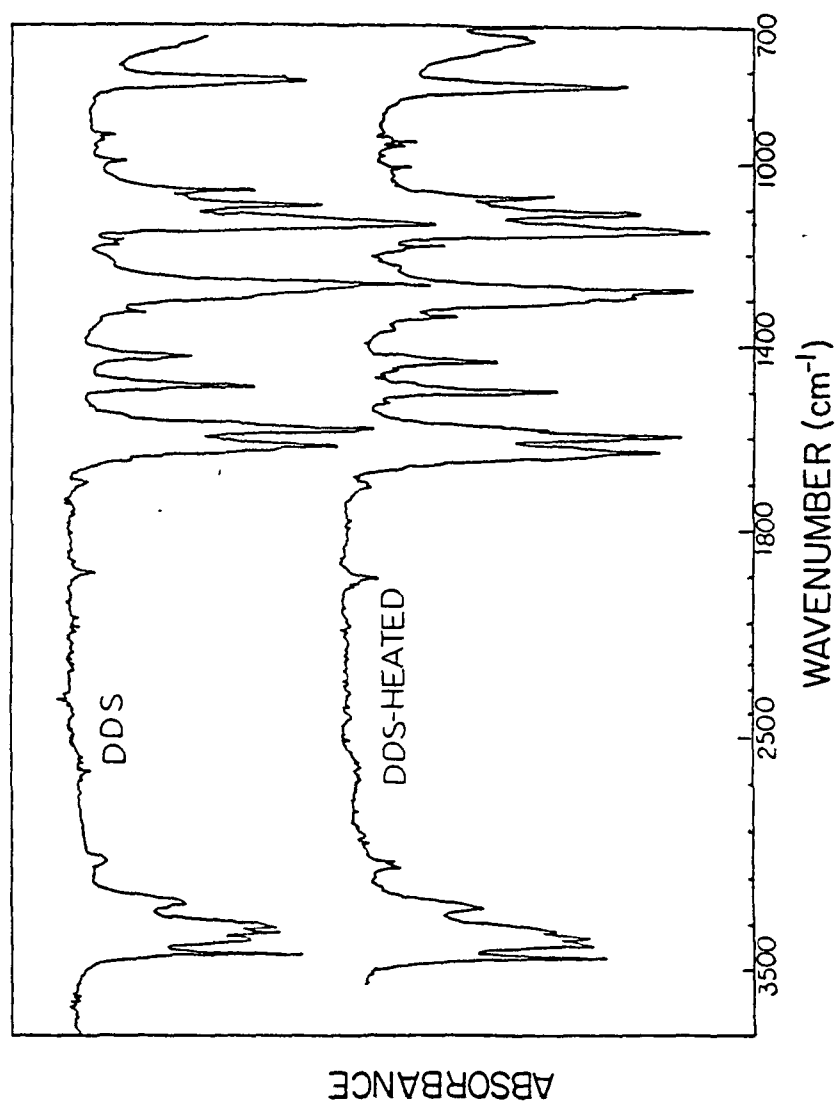
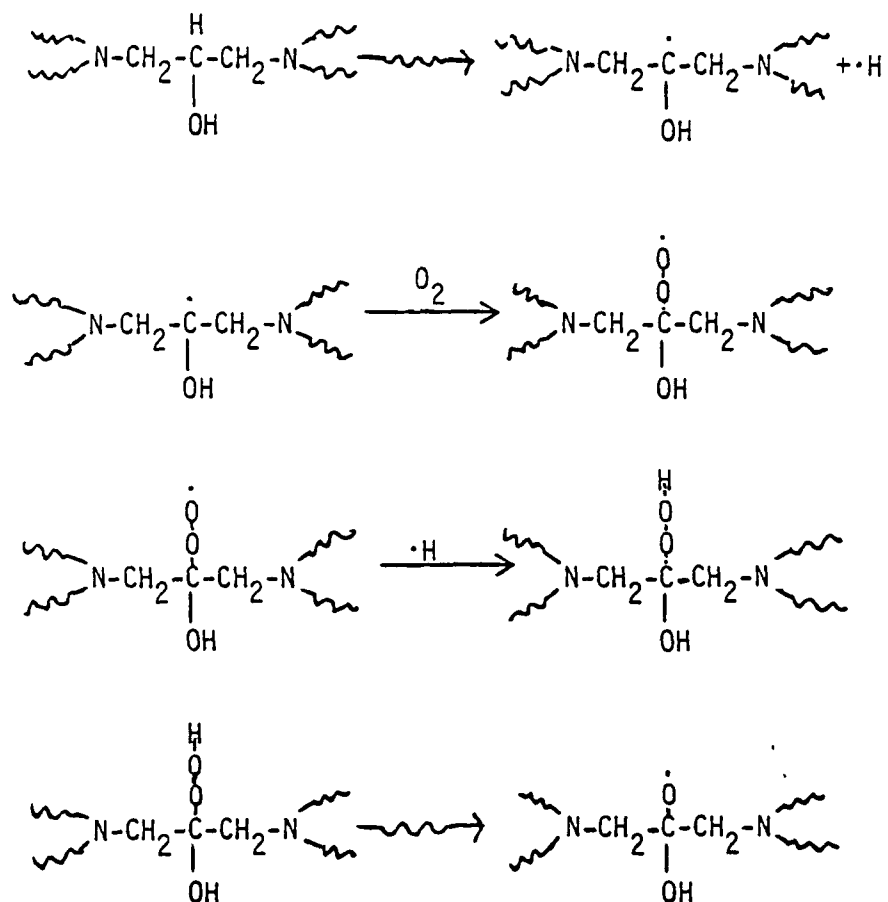
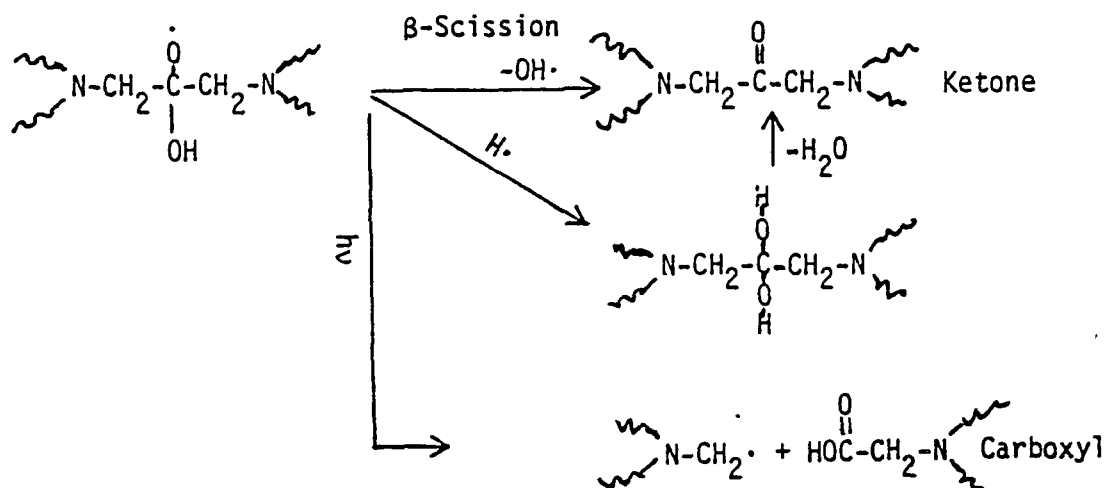


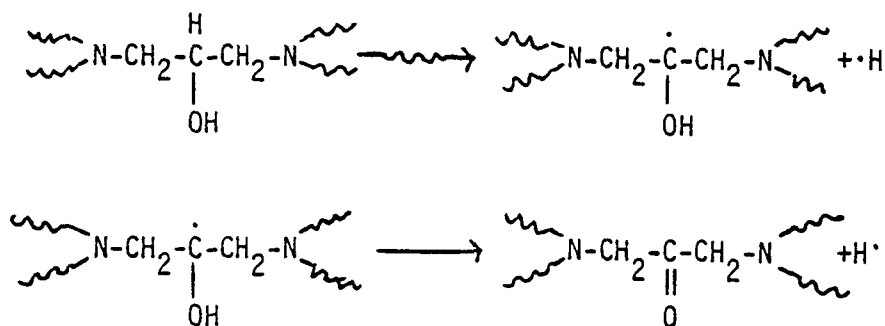
Figure 4.30 IR spectra of pure DDS and heat-treated DDS at 150°C for 1 hr and 177°C for 5 hrs in air.

results suggest that the formation of the carbonyl groups at 1720 cm^{-1} upon irradiation of the TGDDM-DDS epoxy probably occurs on the TGDDM structural unit, mainly at the carbon where the -OH group is attached. A possible reaction scheme leading to the formation of carbonyl groups in TGDDM-DDS epoxy is:





Formation of carbonyl groups in the absence of oxygen is also possible:



Formation of carbonyl groups through this reaction sacrifices the $-\text{OH}$ groups which is also polar. Since the polarity of the carbonyl group (dipole moment, $\mu = 2.5$) is higher than the hydroxyl group ($\mu = 1.6$) [129] the increase in polar

contribution to the surface energy with irradiation is also expected with this reaction.

Bellenger et al. [29-31] assigned the absorption band near 1665 cm^{-1} of an irradiated DEEBA-based epoxy to amide carbonyls, but George [32] assigned it to aromatic carbonyls. The IR spectrum (Figure 4.31) of 4,4'-diamino diphenyl methane (DDM), which is the precursor in the preparation of TGDDM and has no site for amide formation, does not show the 1660 cm^{-1} peak on heating in air at the same temperatures as used for curing of the TGDDM-DDS epoxy. This indicates that the methylene bridge between two phenyl rings in DDM is inert to thermal changes and thus the possibility of formation of the aromatic ketone through oxidation of the methylene bridge in the irradiated TGDDM-DDS epoxy may be small since the photooxidation mechanism of polymers is largely similar to the mechanism of thermooxidation [20a]. Therefore the observed 1660 cm^{-1} peak in cured or in irradiated TGDDM-DDS epoxy seems to be associated with amide carbonyl groups rather than aromatic ketones. However, this reaction must be a minor one since the peak at 1660 cm^{-1} does not change significantly upon irradiation (see Figure 4.27). Possible reactions for amide formation in cured or in irradiated TGDDM-DDS epoxy are:

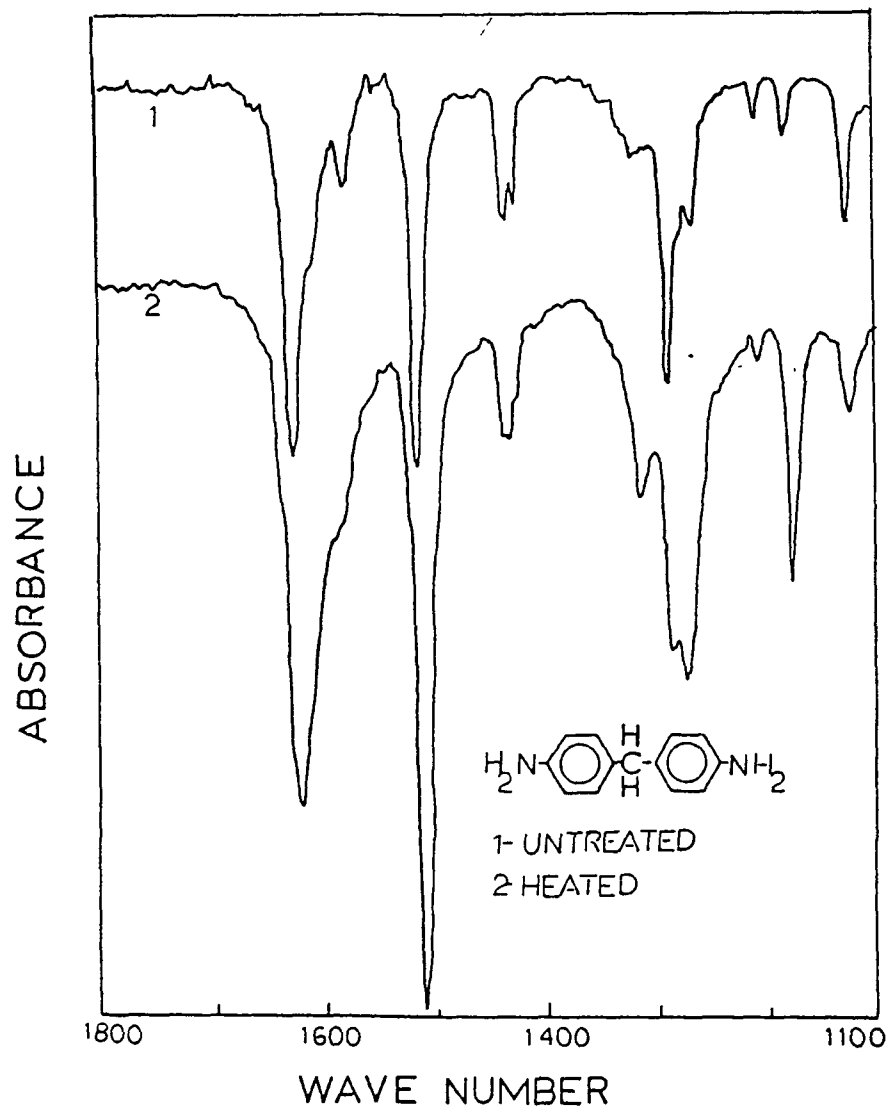
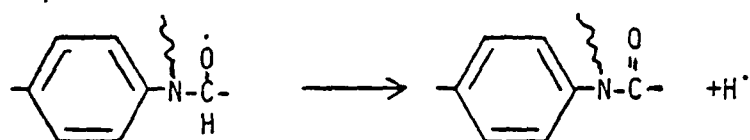
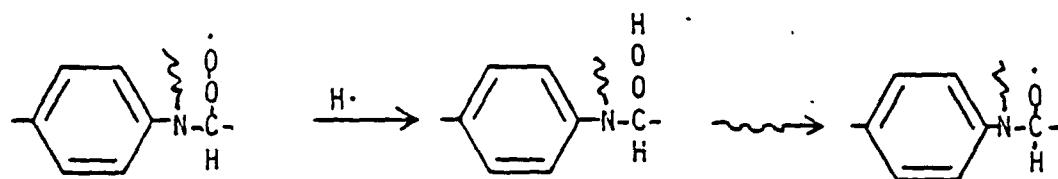
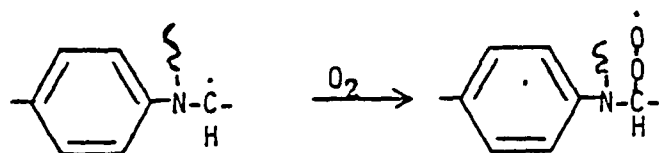
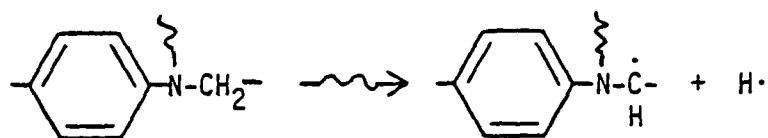


Figure 4.31 IR spectra of DDM: 1) pure and 2) heat-treated at 150°C for 1 hr and 177°C for 5 hrs in air.



5. CONCLUSIONS

Electron spin resonance (ESR) spectra of TGDDM-DDS epoxy irradiated with gamma-radiation at liquid nitrogen temperature (77°K) has a line shape with very broad shoulders (ca. 160-180 G) superimposed on a slightly asymmetric signal with peak to peak linewidth ca. 22-25 G. If the sample is heated to room temperature, then the radicals decay with two characteristic rates, one termed fast-decaying and one slow-decaying. The fast-decaying component has a quintet-like line shape and the slow-decaying component has a broad singlet. Measurements of isothermal decay curves of the radicals at various temperatures reveal clearly the two distinct decay rates indicating that at least two kinetically-different radical species are produced in the irradiated TGDDM-DDS epoxy and are consistent with earlier work [48,64]. As the decay temperature rises, the fraction of the fast-decaying species increases without changing the ESR line shape significantly. The decay rate constants of long-lived species does not appear to be temperature-dependent. The long-lived radical concentration is increased with curing temperature, with irradiation dose and, to less extent, with curing time since all these three factors are expected to increase the crosslinking density of the epoxy. However, the fraction of long-lived radicals decreases with radiation dose. It can

be concluded from these results that the fast-decaying species are most likely associated with reactive alkyl

radicals such as $-\text{CH}_2-\dot{\text{C}}-\text{CH}_2-$, $-\text{CH}_2\cdot$ or $-\overset{\text{H}}{\underset{\text{OH}}{\text{C}}}\cdot$

trapped in various regions with different crosslinking density. Some radicals trapped in relatively high-crosslinked regions of epoxy cannot react (or react extremely slowly) at a given temperature due to restricted mobility or to the restricted diffusion of reactive gases such as oxygen or hydrogen into the regions. As the temperature rises, a higher fraction of polymer chains in the epoxy will be sufficiently mobile to permit more radicals to recombine and/or to permit the trapped gases to diffuse more easily to react with the radicals, and therefore appear as fast-decaying species. The long-lived radicals is mainly attributed to oxygenated radicals such as alkoxy ($-\dot{\text{C}}\text{O}\cdot$) or peroxy ($-\dot{\text{C}}\text{OO}\cdot$) radicals which are trapped in the highly-crosslinked regions of the epoxy. The oxygenated radicals are presumably produced by oxidation during or after irradiation.

The ESR spectrum of TGDDM-DDS epoxy irradiated at room temperature with gamma-radiation or 1/2 MeV electrons show a additional narrow component which is not observed for the sample irradiated in liquid nitrogen. Even continuous vacuum treatment during irradiation does not eliminate this narrow component. This narrow ESR spectral component can be

attributed to the acyl type radicals ($-\dot{C}=O$) which may be produced preferentially at higher temperature, especially in the presence of oxygen whether from dissolved oxygen or from oxygen diffused from outside the sample.

The T-300 graphite fiber contains a large concentration of radicals ($> 10^{20}$ spins/g). A similar concentration of radicals also exist in T300/5208 composite due to the radicals in the graphite fiber. These radicals are suspected to react at the epoxy/fiber interface with radicals generated in irradiated epoxy resulting an increase in interfacial strength of the composite after irradiation.

The surface energy of TGDDM-DDS epoxy increases monotonically with irradiation dose up to a dose of about 1,000 Mrad mainly due to an increased concentration of polar groups. The polar groups are mostly carbonyl groups as confirmed by IR showing the increase in the absorption peak at 1720 cm^{-1} with irradiation. The formation of the carbonyl groups should occur on the TGDDM structural unit, probably at the carbon where the -OH group attached. This carbon should be the most vulnerable position for chain-scission of TGDDM-DDS epoxy to radiation or heat.

T-300 graphite fibers show only a slight increase in surface energy with dose probably due to their stability under exposure to the high energy radiation.

The rate of surface energy increase with radiation dose

appears to be accelerated by the presence of oxygen. Electron spectroscopy for chemical analysis (ESCA) shows that the oxygen content at the epoxy surface increases with radiation dose indicating involvement of oxygen during irradiation. The fracture surface (fiber/epoxy interface) of the irradiated composite also shows an increase in oxygen content and a decrease in contact angle measured with water. These results would provide another reason for the increase in the interfacial strength of composite with irradiation since the increase of polarity (or polar-polar interaction) at the fiber/epoxy interface will also enhance the interfacial strength of the composite.

An amide formation at the TGDDM structural unit of cured epoxy is also possible either with heat treatment or with ionizing radiation as confirmed by IR (1660 cm^{-1}).

6. RECOMMENDATIONS

The involvement of oxygen in the sample during irradiation was confirmed in a qualitative manner in this experiment. Diffusivity or permeability of reactive gases such as oxygen and hydrogen into the epoxy system must be evaluated in order to estimate the amount of oxygen in the sample at certain radiation condition. It is very difficult to remove all the reactive gases from the epoxy sample due to their low diffusivities in cured epoxy. Therefore rather oxygen-rich or hydrogen-rich environments can be considered for investigation of their effect on radiation processes. The effect of pressure of the reactive gases on radical formation and decay reaction can also be examined.

The interaction of radicals in graphite fiber with those in epoxy at the interface must be studied. A precise measurement of radical concentration in the composite sample before and after irradiation should be necessary. Other types of composites containing radical-free fibers such as Kevlar may be compared with this graphite fiber/epoxy composite in terms of interfacial strength change upon irradiation.

Characterization of crosslinking density or crosslinking density distribution of the cured epoxy is highly recommended in order to draw more detailed information from the observed results in the present investigation.

7. REFERENCES

1. Sykes, G. F. and Milkovich, S. M.,
Proc. of ACS, Div. of Polymeric Materials:
Science and Engineering, Vol. 52, 1985.
2. Leung, C. L., Composite for Extreme Environments,
ASTM STP 768, (ed. Adsit, N. R.), American Society of
Testing Materials, 110, 1982.
3. Chapiro, A., Radiation Chemistry of Polymeric Systems,
Interscience Publishers, New York, a. Ch.I, b. Ch.II
c. Ch.IX, 1962.
4. Charlesby, A., Atomic Radiation and Polymers, Pergamon
Press, a. Ch.3, b. Ch.28, 1960.
5. Spinks, J. W. T. and Woods, R. J., An Introduction to
Radiation Chemistry, John Wiley Sons, New York,
a. Ch.1, b. Ch.2, c. Ch.4, d. Ch.8, 1976.
6. Ranby, B. and Rabek, J.F., ESR Spectroscopy in Polymer
Research, Springer-Verlag, Berlin Heidelberg, a. Ch.1,
b. Ch.7, 1977.
7. Wilson, J., Radiation Chemistry of Monomers, Polymers
and Plastics, Mercel-Dekker, Inc., New York, a. Ch.1,
b. Ch.2, c. Ch.3, 1974.
8. Williams, F., The Radiation Chemistry of Macromolecules,
(ed. Dole, M.), Academic Press, New York, Vol.I,
9. Walsh, W. K. and Rutherford, H. A., Textile Research
Journal, 37, 89, 1967.
10. Naranong, N., Effect of High Energy Radiation on
Mechanical Properties of Graphite Fiber Reinforced
Composites, M.S. Thesis, N. C. State University,
Raleigh, NC, 1980.
11. Makhlis, F.A., Radiation Physics and Chemistry of
Polymers, John Wiley & Sons, a. Ch.III, b. Ch.IV, 1975.
12. Charlesby, A., Nature, 171, 167, 1953.
13. Lawton, E. J., Buche, A. M., and Balwit, J. S., Nature,
172, 76, 1953.
14. Miller, J. Polym. Sci., 14, 503, 1954.
15. Danno, A., J. Phys. Soc. Japan, 13, 722, 1958.

16. Billmeyer, F. W., Textbook of Polymer Science, John-Wiley & Sons, Ch. 7, 1971.
17. Tobolsky, A. V., Prettyman, I. B., and Dillon, J. H., J. Amer. Chem. Soc., 72, 1942, 1950.
18. Tobolsky, A. V., Prettyman, I. B., and Dillon, J. h., J. Appl. Phys., 15, 380, 1944.
19. Jenkins, R. V., Polymer Letters, 2, 1147, 1964.
20. Ranby, B. and Rabek, J. F., Photodegradation, Photo-oxidation and Photostabilization of Polymers, John Wiley Sons, a. Ch.3, b. Ch.4, 1975.
21. Li, S. K. L. and Guillet, J. E., Macormolecules, Vol. 17, No. 1, 14, 1984.
22. Burnay, S. G., Radiat. Phys. Chem., 16, 389, 1980.
23. Hikita, K., Okamoto, S., and Ohya-Nishiguchi, H., Shikizai Kyokaishi, Vol.57, No.2, 49, 1984.
24. Keenan, M. A. and Smith, D. A., Appl. Polym. Sci., 11, 1009, 1967.
25. Mayor, F. R., Polym Prepr., Amer. Chem. Soc., Div. Polym Chem., 12, 61, 1971.
26. Tsuji, K. and Seiki, T., J. Polym. Sci. B, 8, 817, 1970.
27. Tsuji, K. and Seiki, T., J. Polym. Sci. A1, 9, 3063, 1971.
28. Tsuji, K. and Seiki, T., Polym. J., Vol.2, No.5, 606, 1971
29. Bellenger, V., Bouchad, C., Claveirolle, P. and Verdu, J., Polymer Photochemistry, 1, 69, 1981.
30. Bellenger, V. and Verdu, J., J. Appl. Polym. Sci., 28, 2599, 1968.
31. Bellenger, V. and Verdu, J., J. Appl. Polym. Sci., 28, 2677, 1983.
32. George, G. A., Sacher, R. E., and Sprouse, J. F., J. Appl. Polym. Sci., 21, 2241, 1977.
33. Conley, R.T., J. Appl. Polym. Sci., 9, 1107, 1965.

34. Eichler, V. J. and Mleziva, J., *Angew. Makromol. Chem.* 19, 31, 1971.
35. Carrington, A and McLachlan, A. D., *Introduction to Magnetic Resonance*, Chapman and Hall, 1979
36. Wertz, J. E. and Bolton, J. R., *Electron Spin Resonance: Elementary, Theory and Practical Applications*, McGraw-Hill, 1972
37. McConnell, H. M., *J. Chem. Phys.*, vol.34, No.1, 13, 1961
38. Walter, R. I., Codrington, R. S., D Adamo, Jr., A. F. and Torrey, H. C., *J. Chem. Phys.*, Vol.25, No.2, 319, 1956.
39. Hana, M. W., McLachlan, A. D., Dearman, H. H., and McConnell, H. M., *J. Chem. Phys.*, Vol.37, No.2, 361, 1962
40. Ohnishi, S. I., Ikeda, I., Sugimoto, S. I., and Nitta, I. J., *J. Polym. Sci.*, 47, 503, 1960
41. Onishi, S. I., Sugimoto, S. I., and Nitta, I., *J. Polym. Sci. A*, 1, 625, 1963.
42. Onishi, S. I., Sugimoto, S. I., and Nitta, I., *J. Polym. Sci. A*, 1, 625, 1963.
43. Hori, Y., Shimata, S., and Kashiwabara, H., *J. Polym. Sci.-Phys.*, 22, 1407, 1984
44. Igarashi, M., *J. Polym. Sci.-Chem.*, 21, 2405, 1983
45. Jain, P. L., *J. Polym. Sci.*, Vol.31, No.122, 210, 1958
46. Gupta, A., Coulter, D. R., Tsay, F. D., Moacanin, J., *Proc. of Intern. Sympo. on Spacecraft Materials in Space Environment*, 191, 1983.
47. Ovenall, D. W., *J. Polym. Sci. B1*, 37, 1963.
48. Schaffer, K. R., *Characterization of Cured Epoxy Resin Exposed to High energy Radiation with Electron spin Resonance*, M.S. Thesis, N. C. State University at Raleigh, NC, 1981.

49. Coulter, D. R., Gupta, A., Tsay, F. D., Moacanin, J., and Liang, R., Proc. of the AIAA 21st Aerospace Sciences Meeting, 1983.
50. Nara, S., Shimada, S., Kashiwabara, H., Shoma, J., J. Polym. Sci. A2, 6, 1435, 1968.
51. Nara, S., Kashiwabara, H., and Shoma, J., J. Polym. Sci. A2, 5, 929, 1967.
52. Fujimura, T., Hayakawa, N., and Tamura, N., J. Macromol. Sci.-Phys., B16(4), 511, 1979.
53. Waterman D. C., and Dole, M., J. Phys. Chem., vol.74, No.9, 1913(1970)
54. Fujimura, T., Hayakawa, N., and Kuriyama, I., J. Appl. Polym. Sci., 27, 4085, 1982.
55. Fujimura, T., Hayakawa, N., and Kuriyama, I., J. Appl. Polym. Sci., 27, 4093, 1982.
56. Dole, M., Hsu, S. D., Patel, V. M., and Patel, G. N., J. Phys. Chem., Vol.79, 23, 2473, 1975.
57. Basheer, R. and Dole, M., Intern. J. chem. Kinetics, 13, 1143, 1981.
58. Basheer, R. and Dole, M., J. Polym. Sci.-Phys., 21, 111, 1983.
59. Shimada, S. and Kashiwabara, H., Polym. J., 6, 448, 1974.
60. Wuenche, P., Linberg, J., and Roth, H. K., J. Macromol. Sci.-Phys., B22(2), 169, 1983.
61. Eda., B., Nunome, K., and Iwasaki, M., J. Polym. Sci.-Polym.Lett., 7,71, 1969
62. Mayo, F. R., Macromolecules, 11, 942, 1978.
63. Keyser, R. M., Tsuji, K., and Williams, F., The Radiation Chemistry of Macromolecules (ed. Dole, M.), Vol.I, Ch.9, 1972.
64. Kent, G. M., X-ray and ESR Characterization of the Effect of High Energy Radiation on Graphite Fiber Reinforced Composite Materials, M.S. Thesis, N.C. State University, Raleigh, NC, 1982.

65. Racich, J. and Kautsky, J.,
J. Appl. Polym. Sci., 20, 2111, 1976.
66. Morgan, R. J. and O Neal, J. E.,
Polym. Plast. Tech. Eng., 10(1), 49, 1978.
67. Mijovic, J. and Kautsky, J.,
Polymer, 20, 1095, 1979.
68. Misra, S. C., Manson, J. A. and Sperling, L. H.,
Epoxy Resin Chemistry, Amer. Chem. Soc., p139, 1979
69. Misra, S. C., Manson, J. A. and Sperling, L.H.,
Epoxy Resin Chemistry, Amer. Chem. Soc.,
p157, 1979.
70. Bell, J. P.
J. Appl. Polym. Sci., 27, 3503, 1982.
71. Brown, I. M. and Sandreczki, T. C.,
Polymer Prepr., 22, 2, 284, 1981.
72. Brown, I. M., Lind, I. C., and Sandreczki, T. C.,
AD-A116542, MDC-Q0759, 1981.
73. Sandreczki, T. C. and Brown, I. M.,
Macromolecules, 17, 1789, 1984.
74. Morgan, R. J.,
Development in Reinforced Plastics-1,(ed. Pritchard, G.),
Ch.7, Applied Science Publisher Ltd., London, 1980
75. Brown, I. M., Lind, A. C., and Sandreczki, T. C.,
AD-A099225, MDC-Q0721, 1980
76. Brown, I. M., Lind, I. C., and Sandreczki, T. C.,
AD-A073590, MDC-Q0673, 1979
77. Adam, N. K.,
Contact Angle, Wettability and Adhesion,
Adv. in Chem. Series 43, p52, 1964.
78. Aveyard, R. and Haydon, D.A.,
An Introduction to the Principles of Surface
Chemistry, Cambridge Univ. Press, N.Y.,
Ch.6, 1972.
79. Wu. S., Adhesion and Adsorption, (Lee, Ed.) p53-64
80. Fokes, F.M. J. Phys. Chem., 66, 382(1962)

81. Kaelble, D. H.,
Proc. 23rd. Int. Cong. of Pure and Appl. Chem.,
8, 265, 1971
82. Furusawa, K., Shimura, Y., Sasaki, K.,
and Tsuda, K., Kogyo Gijutsuin Seni Kogyo
Shikensho Kenkyu Hokiku, 131, 11, 1981.
83. Wesson, S.P. and Jen, J. S.,
16th. National SAMPE Tech. Conf., 16, 375, 1984.
84. Kammer, H. W.,
Acta Polimerica, B-34, 112, 1983.
85. Dynes, P. J. and Kaelble, D. H.,
J. Adhesion, 6, 195, 1974.
86. Wu. S., J. Polym. Sci, C-34, p19-30(1971)
87. Penn, L., Bystry, F., Lee, S., and Karp, W.,
Polym. Prepr., 189
88. Tabor, D.,
Surface Physics of Materials, Vol.II
(ed. Blakely), Academic Press, Ch. 10, 475, 1975.
89. Levine, M., Ilkka, G., and Wiess, P.,
J. Polym. Sci., B2, 915(1964)
90. Schulman, F. and Zisman, W. A.,
J. Colloid Sci., 7, 465, 1952.
91. Drzal, L. T., Mescher, J. A. and Hall, D. L.,
Carbon, vol. 17, No. 5/A, 375(1979)
92. Donnet, J.B. and Gent, A. N.,
Proc. 23rd. Int. Cong. Pure and Appl. Chem.,
8, 233, 1971.
93. Gent, A. N. and Tobias, R. H.,
J. Polym. Sci., 22, 1483, 1984.
94. Weyl, W. A.,
Proc. 23rd. Int. Cong. Pure and Appl. Chem.,
8, 303, 1971.
95. Jubramanian, R. V., Jakubousky, J. J., and
Williams, F. D.,
J. Adhesion, 9, 185, 1978.
96. Chwastiak, s. and Bacon, R.,
Polym. Prepr., 22(2), 222, 1981.

97. Shimbo, M., Ochi, M., and Matsuura, M.,
Kobunshi Ronbunshu, Vol. 38, No.3, 129, 1981.
98. McMahon, P. E. and Ying, L., NASA Contractor Report
3607 (NAS 1-15749), 1982.
99. Mozzo, G. and Chabard, R.,
23rd. Annual. Tech. Conf. Reinforced Plastics and
Composites Div., SPI Inc., Sec.9-C,1, 1968.
100. Neumann, A. W. and Tanner, R.,
Proc. 5th. Int. Cong. on Surface Activity,
2, 727, 1968.
101. Ranby, B., Polymer Surfaces (ed. Clark, D. T.
and Feast, W. J.), John Wiley Sons, Ch.15, 1978.
102. Willis, H. A. and Veronica, J. I. J.,
Polymer Surfaces (ed. Clark, D. T. and Feast, W. J.),
John Wiley & Sons, Ch. 15, 1978.
103. Paralusz, C. M.,
ASTM Standardization News, February, 42, 1985.
104. Garton, A.,
J. Polym. Sci., 22, 1495, 1984.
105. Park, R. L., Surface Physics of Materials, Vol.II.
(ed. Blakely), Academic Press, Ch.8, 377, 1975.
106. Clark, D. T., Polymer Surfaces,
(ed. Clark, D. T. and Feast, W.J.) John Wiley & Sons,
Ch.16, 1978
107. Wolsky, S. P. and Czanderna, A. W.,
Method and Phenomena, Vol.1, Method of Surface Analysis,
Elsevier Sci. Pub. Co., N.Y., 1975
108. Gahde, J., Loeschke, I., and Richter, K. H.,
Acta Polimerica, 34, 5, 260. 1983.
109. Peeling, J. and Courval, G.,
J. Polym. Sci., 22, 419, 1984.
110. Hammer, G. E. and Drazel, L. T.,
Applications of Surface Science, 4, 340, 1980.
111. Hopfgarten, F.,
Fiber Sci, and Technology, 11, 67, 1978.
112. Hon, D. N. S.,
J. Appl. Polym. Sci., 29, 2777, 1984.

113. Nuzzo, R. G. and Smolinsky, G.,
Macromolecules, 17, 1013, 1984.
114. Barber, M., Evans, E. L. and Thomas, J. M.,
Mature, Vol.227, September12, 1131, 1970.
115. Waltersson,K.
Composite Science and Technology 22, 223-239(1985)
116. Wolf, K., PhD.thesis, N. C. State University at
Raleigh, NC, 1982.
117. Tsay, F., Hong, S. D., Patel, V. M., and Patel, G. N.,
J. Polym. Sci.-Phys., 20, 763, 1982.
118. Park, J. S., Bulletin, American Physical Society,
Vol.30, No.3, 1985
119. Giori, C., Yamauchi, T., Rajan, K., and Mell, T.
AIAA 21st Aerospace Science Meeting, Paper 83-0590,
Jan., 1983.
120. Gillham, J. K., Polym. Eng. Sci. 19, 676, 1979
121. Mijovic, J., Kim, J., and Slaby, J.
J. Appl. Polym. Sci., Vol. 29, 1449-1462(1984)
122. Gupta, A., coulter, C. D., Liang, R.H., Yavrouian, A.,
Tsay, F. D., and Moacanin, j.
J. Appl., Polym, Sci., Vol.28, 1011-1024(1983)
123. Netravali, A., Fornes, R. E., Gilbert, R. D., and J. D.
Memory, J. Appl. Polym. Sci, Vol.30, 1573-1578(1985)
124. Fugimoto, K., Inomata, I., and Fujiwara, S.
Nippon Gomu Kyokaishi, Society of Rubber Industry,
Japan. Journal, Vol.46, 232, 1973.
125. Spackman, J. W. C. and Charlesby, A.
Proc, Rubber Technology Conference, Vol.4, 24, 1962.
126. Ellis, B., and Baugher, J. F.,
J.. Polym. Sci.-Phys. Ed. Vol.11, 1461, 1973.
127. Kecki, Z. and Lancman,L.
Przemysl Chemiczny,46/2.94, 12967.
128. Chatterji, A.K.,
Polym. Preprints, Div. Polym. Chem., 7, 535, 1966.
129. Kaelble, D. H., Adhesion and Cohesion, (ed. Weiss,P.),
Elsevier, Amsterdam, 240, 1962.

APPENDICES

Table A. Radical concentration, ESR line shapes and g-factors of TGDD-DDS epoxy and T-300 graphite fiber, and T300/5208 composites

Radiation	Dose (Mrad)	sample	Irradiation condition	Radical conc. (spins/g x 10 ⁻¹⁸)	Line-shape (ΔH_{pp})
	0	E-1	-	0.5	broad (22-25 G) no tail
		E-3	-	0.7	-
γ -radiation	5	E-1	N ₂ (1)	3.18	1.56 wiggled, long tails
		E-2	N ₂ (1)	6.04	1.87 broad (22-25 G) long tails
		E-3	N ₂ (1)	11.5	1.98 broad (22-25 G) long tails g=2.0042 +0.002
	30	E-1	N ₂ (1)	29.9	5.17 wiggled, long tails
		E-2	N ₂ (1)	33.5	7.3 broad (22-25G) long tails
	100	E-3	N ₂ (1)	25.0	7.2 broad (22-25 G) long tails
		E-3	A(RT)	5.0	< 2.0 (27day) composite of narrow (13 G) and broad (22- 25 G) lines
		E-3	V(RT)	-	-
		E-3	CV(RT)	-	-
			(continued)		

Table A. (continued)

elect- rons	160	E-3	A(RT)	35.0	-	composite of narrow (13 G) and broad (22- 25 G) lines
	490	E-3	A(RT)	30.0	-	
	5000	E-3	A(RT)	25.0	-	
		G	N ₂ (RT)	>100	-	singlet (4 G) g=2.0023 +0.001
		C	N ₂ (RT)	>100	-	singlet (5 G) g=2.0000 +0.001
	9000	G	N ₂ (RT)	>100	-	
		C	N ₂ (RT)	>100	-	same as for un- irradiated samples

Note:

E-1: epoxy cured at 137°C (2 hrs), then 160°C (5 hrs)
 E-2: epoxy cured at 137°C (2 hrs), then 160°C (24 hrs)
 E-3: epoxy cured at 150°C (1 hr), then 177°C (5 hrs)
 G : T-300 graphite fiber
 C : T300/5208 uniaxial composites
 N₂(l): in liquid nitrogen
 V(RT): in a vacuum-sealed ESR tube at room temperature
 CV(RT): under continuous vacuum at room temperature
 A(RT): in air at room temperature
 N₂(RT): in a nitrogen-filled bag at room temperature

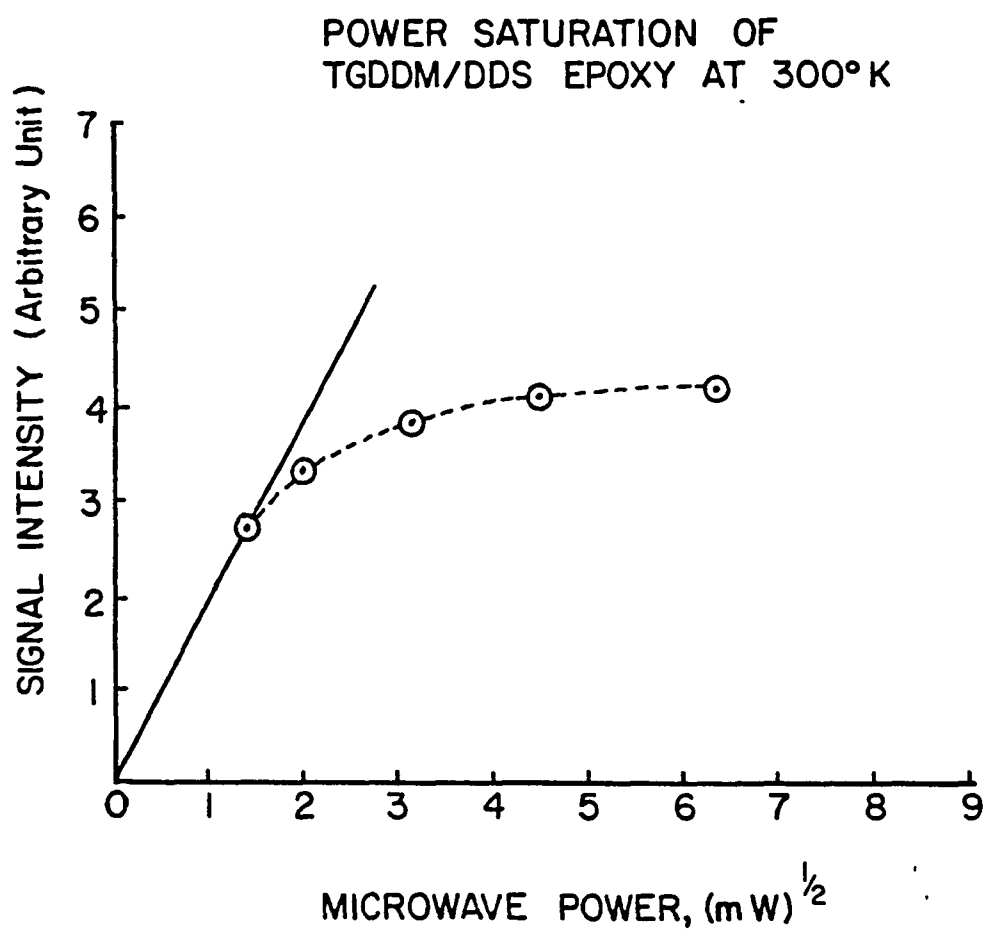


Figure A. Power saturation behavior of long-lived radicals in TGDDM-DDS epoxy irradiated with a dose of 5 Mrad of γ -radiation. ESR measurements were made at room temperature.

EFFECTS OF RADIATION ON THE INTERFACIAL STRENGTH OF COMPOSITES

JONG SHIN PARK

TABLE OF CONTENTS

1. INTRODUCTION
2. ADHESION
 - 2.1 Mechanical Theory
 - 2.2 Electrostatic Theory
 - 2.3 Donor-Acceptor Bonds at Interfaces
 - 2.4 Adsorption Theory
 - 2.5 Condition for Interfacial Separation vs. Cohesive Failure
3. INTERFACES IN COMPOSITES
 - 3.1 What is Interface?
 - 3.2 Physical Factors influencing Interfacial Strength
 - 3.2.1 Surface Friction
 - 3.2.2 Surface Energy of Interfaces
 - 3.2.3 Surface Roughness and Porosity
 - 3.2.4 Properties of constituent Material
 - 3.2.4.1 Resin Properties
 - 3.2.4.2 Fiber Properties
 - 3.3 Chemical Factors influencing Interfacial Shear Strength
 - 3.3.1 Chemical Bonding
 - 3.3.2 Coupling Agent
 - 3.4 Effects of Radiation
 - 3.4.1 Radiation Effects on Carbon Fibers
 - 3.4.2 Radiation Effects on Epoxy Resin

3.4.3 Radiation Effects on Composites

3.5 Theoretical Analysis of Interfacial Shear Strength of
Fiber-Resin Composites

3.5.1 Determination of the Strength and Shear Modulus
of the Interface

3.5.2 Load to Pull-out When considering the friction
between fiber and matrix

3.5.3 Shear Stress Distribution along the Interface

3.5.4 Work of Interfacial Fracture

4. REFERENCES

1. INTRODUCTION

Although graphite fibers have excellent mechanical properties among which are high stiffness and strength coupled with light weight ,these properties only become of interest if high translation of these properties can be achieved in a usable structural form, such as composites. Once a particular fiber is shown to have promising specific properties, as is the case for graphite fiber, the next step is to form a composite with a well characterized resin matrix such as an epoxy resin system, and then evaluate it. Resultant composites are usually characterized initially by determining the moduli and strength in tension, compression, flexure, and shear to obtain knowledge of the translation efficiency of the reinforcement in the composites. As far as the translation efficiency is concerned, the interface between fiber and matrix plays a profound role in the behavior of composite materials. Most mechanical properties and the failure mode of composites are strongly influenced by the interfacial bond.

It is at the interface where stress concentrations develop because of differences in thermal expansion coefficients and cure shrinkage between fiber and resin. The interface can also serve as a nucleation site, a preferential adsorption site, and as a surface for chemical reaction. Accordingly, considerable efforts has been made

for decades to understand the interface, to control it, and even specifically modify it. However, the exact nature of the interface is incompletely understood, not only in advanced composites containing high performance fibers such as boron and graphite[28], but also in the more established glass fiber reinforced plastics[29].

To obtain a basic understanding of the interfacial bond, some current theories of adhesion are discussed in this review. Adhesion is defined as 'the state in which two surfaces are held together by interfacial forces which may consist of valence forces or interlocking action, or both.' [30] Two theories are most prominent, one of which is the mechanical bonding and the other the chemical bonding. Chemical bonds, once regarded as unnecessary to explain adhesive strength, are nowadays seen to be quite common and, for ionic bonds, to be closely linked with electrostatic theory.

The interface will be considered as a zone between two constituents, which is often referred as the interphase. A variety of physical and chemical factors which might affect the strength of the interphase are discussed in detail. Some theoretical considerations of the interfacial shear strength are also reviewed and modified to apply to the geometry of double-notched specimen used in interlaminar shear tests. Because the final objective of this study is to determine the effects of radiation on the interfacial

strength of graphite fiber composites, articles dealing with the radiation effects on composites are also reviewed.

2. ADHESION

2.1 Mechanical Theory

The mechanical view of adhesive action is well typified by the layman's approach to gluing wood. The wood is cleaned and roughened in order that the glue may penetrate irregularities of the surface and thus lock into it. Abrasive treatments of surface prior to adhesive bonding in order to increase surface area is a mechanical approach. The electroless method of plating certain plastics with metals may be taken as a very good example of adhesion where mechanical interlocking is thought to be an essential feature of the process. Marcus[24] reviewed theories about the mechanism of this bonding action differentiating between chemical interaction and mechanical interaction. The mechanical theory explains that the chromic-sulphuric acid solutions used in the surface-conditioning operation oxidize or dissolve the butadiene portion of the ABS plastic, leaving a microscopic system of odd-shaped cavities in the surface, fulfilling a function of anchoring the metal coating to the plastic.

Perrins and Pettet[25] reported a comprehensive investigation of the factors concerned in adhesion. They tried to separate the mechanical influence from the chemical influence on adhesion. They showed that both a mechanical component and a proper chemical surface must be taken together to produce the highest bond strength. These

results support those who claim both chemical and mechanical factors play a role and that both are important. Andrews and Kinloch[26] also treated the peel strength adhesion tests as multiplicative functions.

However, some critics rejected the explanation of the effectiveness of chemical finishes which is hypothesized to achieve the chemical bonding between glass fiber and resin for the following reasons. According to McGarry[1], no measurable influence of a finishing agent on glass-resin joint strength has been found. A cohesive failure occurred in glass-epoxy joint studies even when no finishing agent was used. No improvement of such ideally efficient joints was sensible unless the cohesive strength of the components were increased. Irrespective of the finish used, the polyester-glass joints always broke cleanly at the interface in a thin layer of imperfectly polymerized resin caused by local contamination of the reaction by the water present on the glass surface. Internal cracking from tensile loading, because of resin brittleness, occurred extensively, irrespective of the finishing agent used.

Finally, the beneficial results associated with effective finishes are equally explainable on the basis of improved wetting and impregnation of the yarn structure by the liquid resin since the inferior mechanical properties of incompletely impregnated laminates are widely recognized.

There exists good direct evidence that the primary contribution of the finishes is to serve as wetting agents.

The higher the meniscus which forms on glass fibers with one end immersed in liquid resin, the better the finish on the fiber, and the smaller is the contact angle[1].

Mechanical factors have also been shown to be important in adhesion to textiles. Wake[15] established that the important mechanical feature in the adhesion of rubber to textiles woven from spun staple was the embedding in the rubber of the protruding fiber ends of the staple yarn.

2.2 Electrostatic Theory

The principal proponents of this theory have been Russian scientists led by Derjaguin[18]. The principle of the treatment is to consider an adhesive in intimate contact with an adherend, one half of a normal adhesive joint, as it were, and to regard the surface of the adhesive as one plate of a condenser and the adherend as the other plate. To separate these plates work must be done against any electrical charge separation occurring between them. The energy of the condenser is then equated to the work of adhesion, assuming that no other factor such as Van der Waals forces have to be overcome to carry out the separation.

The condenser energy, A , per unit area is given by

$$A = 0.5 Q \Delta V$$

where Q = charge per unit surface area and,

$$\Delta V = (dV/dh) h$$

the voltage drop across the distance h , the gap as the plates begin to separate. But $dV/dh = 4\pi Q/e$, where e = the dielectric constant of the medium between condenser plates. Hence $A = (\frac{he}{8\pi}) (dV/dh)^2$ or $A = 2\pi Q^2 h/e$.

Weaver[17] showed that when gold is bonded to glass, bond strengths were achieved which resulted from Van der Waals forces only, but that in the case of oxidizable metals in the presence of oxygen the increased adhesion must be due to

some form of additional chemical bonding. He confirmed the existence of an electrical component of adhesion by investigation of metal on a polymer surface. If electrostatic forces contributed to adhesion, then their contribution must be in addition to the Van der Waals forces and not solely responsible for the observed adhesion strengths. Several experimentalists have attempted to partition the strength between these two, and have assumed that they are additive.

von Harrach and Chapman[27] measured charge densities remaining after removing a thin metallic film from a glass microscope slide. From these measurements they deduced the electrostatic contribution to the work of adhesion. They found only 5% of the total was electrostatic for gold, 12.5% for silver and 17% for copper.

Wake[15] concluded that particle adhesion can result from electrical charges as well as dispersion forces but that when films of adhesive substances adhere to substrates, the electrical phenomena observed when they are peeled do not contribute appreciably to the force required to cause separation.

2.3 Donor-Acceptor Bonds at Interfaces

There are a number of situations in which the chemical

constitution of one substance allows it to interact with another in a specific way not available to it for interaction between identical molecules. Typical of such interactions are those between acid and base. The importance of this sort of interaction as well as its difference from dispersion interactions has been stressed by Fowkes[13]. According to him, nearly all intermolecular interactions at interfaces can be reduced to two phenomena; London dispersion forces and electron donor-acceptor(acid-base) interactions. Hydrogen bonds are included in acid-base interactions, and dipole phenomena are usually negligibly small. Donor-donor and acceptor-acceptor interactions are negligibly small compared to donor-acceptor interactions.

The effect of hydrogen bonding is to enhance attractive forces across the interface beyond the level which would be expected from a consideration of the surface free energies of the two phases considered separately. Thus, although the work of adhesion can be considered as the sum of components representing dispersion, polar and acid-base interactions, these cannot be expressed simply as functions of the surface free energies of the contacting substances. In hydrogen bonding, the length of the hydrogen-acceptor bond can vary considerably. Also some substances exhibiting hydrogen bonding with other substances can also bond to themselves, as is the case with water. Thus the contribution to surface energy may provide only an approximate estimate

of the contribution to an interfacial interaction.

Because these donor-acceptor interfacial interactions all involve redistribution of electrons and are confined to the interface they become a form of electrostatic adhesion. To the extent that this contributes to the force required for separation, an electrostatic term needs to be added to the work of adhesion if separation were indeed to occur at the interface.

2.4 Adsorption Theory

The essence of the adsorption theory of adhesion is that surface forces are involved and that, moreover, where polar molecules or groups are used, these are oriented at the interface. Further, chemisorption may occur and is believed to occur where adhesion is particularly strong even though physical adsorption could provide for more than the observed strength of adhesive joints. If the adsorption theory is correct, then a correlation would be expected between the energy of adsorption and the adhesive bond. In fact, most polar adhesives are better than non-polar adhesives and the heats of wetting of ionic or polar surfaces by small molecules increases with increasing polarity.

C-3

Additionally, in the exceptional case of surfaces of low surface free energy, a linear relation has been shown between the critical surface tension of the surface of the solid and the bond strength in direct tension for a particular epoxy resin[16]. But there is a lot of information about the adsorption of polymer molecules from solution onto solid surfaces and even more about the adsorption of polar molecules on liquid surfaces.

If a molecule is large enough to contain both a dipolar group and other groupings of atoms which are not polar in nature then this molecule, placed at an interface between two phases across which a change of dielectric constant occurs, will orient itself with its non-polar part in the medium of lowest dielectric constant. In the case of completely non-polar symmetrical molecules, orientation will not be involved and there may be no preferential adsorption from solution, though removal of solvent will leave the molecules adsorbed. The reduction in surface free energy when a liquid is allowed to wet the surface of a solid can be argued to be adsorption. If this is so, the whole development of the argument for wetting as a necessary precondition for adhesion is a statement of adsorption being a necessary condition for adhesion. However, the adsorption theory also involves orientation on the surface and should cover those examples where particularly strong adhesive bonds could be associated with chemisorption.

2.5 Condition for interfacial separation vs. cohesive failure

A controversy has been in progress for some years as to whether true interfacial failure between two phases can occur[19,20,21]. Bikerman[19] has contended that failure will always occur within one phase or the other, on two general grounds. The first basis was a consideration of the failure locus; he used a probabilistic argument, considering the direction of propagation of failure on a molecular scale, and also the natural roughness of a solid-solid interface. He claimed that there is small likelihood that a failure locus would follow the path defined by the true interface.

This argument is based on the implicit assumption of a brittle-fracture model; its validity is probably limited to interfaces between phases both of which are very brittle, and not to solids which are thermoplastic.

Bikerman gave a second general reason as to why true interfacial failure is so rare as to be of no practical importance. Denoting the intermolecular attractive constants in the Van der Waals equation as a_1 , a_2 , and a_{12} , he wrote the Berthelot-Van Larr equation[22],

$$\frac{a_1}{a_{12}} = \frac{a_{12}}{a_2}$$

and concluded that, in the example of metal-polymer interface, attraction between metal and polymer is greater than that between polymer and polymer.

It is well known[21] that the geometric mean relationship for intermolecular forces,

$$a_{12} = \sqrt{a_1 a_2}$$

is valid only when the intermolecular forces are of the same type, e.g. London dispersion forces, or dipole-dipole (Keesom) forces.

According to Good[23], it is obvious that if the cohesive forces of both phases are strong, i.e, covalent bonds in one phase or the other, or ionic or metallic bonds, and if the elastic constants of the two phases are similar, then if interfacial failure is to be avoided, the forces across the interface must also be strong forces, e.g. covalent or ionic forces.

This clearly refutes Bikerman's contention that a strong interaction across the interface is unnecessary for a strong bond.[19]

Good also illustrated the conditions for true interfacial separation by supposing that there is a drastic mismatch of properties between the phases and that there is a dynamic deformation-strengthening mechanism in the weaker phase.

For example, phase 1 is strong and has a high modulus, and phase 2 is a lightly crosslinked rubber with a low modulus which, at some elongation, crystallizes so that its modulus rises sharply. When this system is placed under a tensile load, the material of phase 2 undergoes deformation by Poisson contraction as well as by tensile elongation. Since the interfacial contact constrains the polymer from lateral motion in the vicinity of the interface, the result is a multiplication of stress applied to the interface and to the adjacent material in phase 2. But the increase in modulus of phase 2 with deformation has the effect of strengthening that phase; and it further increases the concentration of stress at the interface. There is no mechanism for strengthening the interface by deformation. So with increasing load, long before the stress reaches a level required to break chemical bonds in the polymer, the stress on the interface will exceed the adhesive force across the interface; and interfacial failure will occur even if there are strong covalent or ionic bonds across the interface.

3. INTERFACES IN COMPOSITES

3.1 What is Interface?

It is important to establish what is meant by the term interface. The interface can be defined as the adhesive bond across the boundary of two materials in intimate contact. The strength of the bond may be measured in a relative manner by the force required to separate the materials. Or, if upon the application of stress normal to the interface, a clean separation does not occur and one of the materials breaks, we may presume that the interfacial strength is stronger than the cohesive strength of the weaker of the two materials [33].

Sharpe[32] recognized that the adherend-adhesive interface is not a planar singularity but a region or "interphase" with properties different from the bulk adhesive. This would be so even if the adherend were ideally smooth and chemically homogeneous and if the adhesive were a single component polymer because the molecular configuration of a polymer at an interface is different from its molecular structure in bulk[31]. But adherend surfaces are never smooth or homogeneous and adhesives are seldom well defined polymers. These factors have a profound influence on the properties of the interfacial region. For example, if the adhesive fills in the surface roughness, the depth of interfacial region should be at least as great as the rugosity of the adherend surface. The transition from interfacial structure to bulk structure may extend over distances of hundreds or even thousands of angstroms from the interface[38].

Kwei[31] studied the sorption of water vapor by epoxy polymers filled with titanium dioxide. The principal conclusion drawn from the calculation is that the unfilled polymer has higher free energy, enthalpy, and entropy content than the filled polymer. The inference is very strong that the transformation of a filled polymer to the unfilled state is accompanied by increases in both enthalpy and entropy per unit weight of polymer. It appears that there might exist in the filled state local ordering of the polymer segments rather than the well defined, periodic order observed in crystalline polymers. Kwei proposed a model to describe the interaction between the polymer and the filler as follows.

1. There exists between the filler and polymer chains an interaction which manifests itself in a decrease in the chemical potential of the polymer.
2. The interaction must be a function of distance, i.e., the interaction decreases rapidly with distance so that a polymer segment at a distance greater than r from the center of the filler would experience negligible interaction and has all the properties of an unfilled polymer and may be called "free" polymer. Chain segments at distances smaller than r from the center of the filler could fall within the sphere of influence of the filler particle and may be called "bound" polymer. The chemical potential of the chain segments in the

bound layer is assumed to increase with distance from the center of the filler particle.

3. Solvent molecules have a greater tendency to mix with the free polymer than the bound polymer because the free energy of mixing with the former is more negative.

The calculations based on above model showed that the influence exerted by the filler particle probably is not limited to the immediate vicinity of the particle surface. The distance of effective interaction between a filler particle and the surrounding polymer in the solid state was estimated to be about 1500A. It is generally acknowledged that the configuration of adsorbed polymer molecules is not necessarily the same as the configuration of the same polymer chains in solution or in bulk. It appears possible that the packing of the polymer molecules on top the adsorbed layer may be different from the packing of chains in the unfilled state. According to his calculation, a higher state of order exists in the packing of polymer chains near the filler surface. It is not entirely unexpected that the order of polymer packing might decrease progressively with increasing distance from the filler surface.

The chemical composition of the adhesive in the interfacial region is also likely to be different from the bulk because of the selective adsorption of one of the

components. There is evidence that in amine-cured epoxies, the amine is preferentially adsorbed by glass[39] and by metal substrates[40]. Enrichment of the interface with amine would cause the resin in this region to be cured differently than the bulk. Furthermore, any excess amine left at the interface could affect the chemical phenomena associated with stress-corrosion[41]. Even if there were no preferential adsorption, the adherend could still influence the solidification of the adhesive polymer. Fitchmun et al.[42] showed that the polymer crystal structure which develops at the interface differs considerably from the bulk crystal structure. Even in the case of amorphous, thermosetting polymers which solidify by a chemical reaction, the adherend may influence the chemical nature and kinetics of the cure reaction in the immediate vicinity of the interface[43].

3.2 Physical Factors influencing Interfacial Strength

3.2.1 Surface Friction

There are natural relationships between the so-called 'surface properties' and the 'bulk properties' of materials. From a molecular point of view, this is not at all surprising since the molecular properties of a surface must obviously be related to the molecules that make up the whole

material. As an illustration of this last point, consider a specific 'surface property', namely frictional resistance. The coefficient of friction for a pair of surfaces is a measure of the resistance to the sliding of one body over the surface of the other. When two surfaces are in physical contact, they are in actual molecular contact at only a minute fraction of the total surface. The reason for this is that even the most highly polished surfaces are rough on an atomic scale. A finely ground, super finished silver plate may have surface asperities of up to 100 to 1000Å, compared to a distance of 2 to 3Å between molecular layers in the crystal lattice. Thus, Figure 1 is a reasonable qualitative picture of two surfaces in contact. A relatively simple model can be used to predict the coefficient of friction for such a pair of identical surfaces. Idealize each contact point between the two surfaces as a flat surface in contact with a round asperity, as shown in Figure 2. When a load is applied, the round asperity will penetrate the flat surface causing an indentation. On a macroscopic scale, Figure 2 shows the exact geometry used in a standard Brinell hardness test. In such a test the Brinell hardness number, σ_H is defined as the applied load per unit cross-sectional area of indentation.

$$\sigma_H = \frac{F}{A}$$

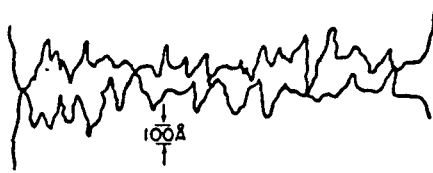


Fig.1. Roughness on a submicroscopic scale; only a small fraction of the contacting surfaces exhibiting solid-solid contact even on finely ground surfaces. [14]

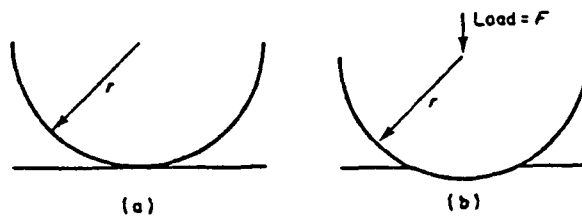
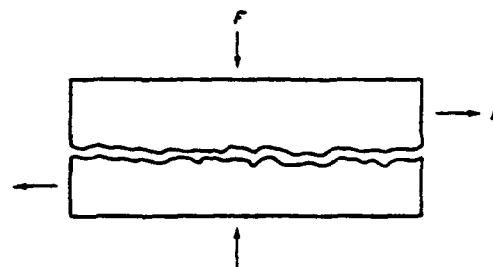


Fig.2. A model for the points of contact between two solid surfaces. Also the geometry of a Brinell hardness test. (a) Sphere resting on flat surface; (b) Sphere pressed into surface by a force F . [14]



$$\text{Contact area} = F/\sigma_H = A_R = \frac{\text{Force}}{\text{Bearing pressure}}$$

$$\text{Slippage force} = f = \tau_y A_R = (\text{Shear stress of junction}) (\text{Contact area})$$

$$= \left(\frac{\tau_y}{\sigma_H} \right) F = \beta F$$

β = coefficient of friction

Fig.3. Frictional adhesion. [14]

If we visualize that the contact points of a pair of surfaces penetrate in a similar fashion, the cohesive junctions are created by plastically deforming the surface until sufficient surface area of contact is formed to support the load without further deformation (Figure 3). If the bearing pressure is equated to the Brinell hardness number, the total contact area required A_R is;

$$A_R = \frac{F}{\sigma_H}$$

where F is the force normal to the surfaces. In order to slide the two surfaces relative to one another, these junctions must be destroyed in shear. If the yield strength of the junction in shear is τ_y , the force required to slide the two surfaces relative to one another, f , is

$$f = \tau_y A_R = \frac{\tau_y}{\sigma_H} F \quad (1)$$

By definition the static coefficient of friction β is

$$f = \beta F \quad (2)$$

By comparing Eqs (1) and (2),

$$\beta = \frac{\tau_y}{\sigma_H}$$

It becomes clear that yield stress, hardness and frictional resistance are interrelated. The reason for this is that all of these properties are tied together by the common bond of molecular interaction. Thus, understanding of the molecular nature of the material can give us some insight into some physical property relationships.

3.2.2 Surface Energy of Interfaces

Adhesive layers, inclusions in solids, grain boundaries in polycrystalline materials, or other similar situations are liquid-liquid, liquid-solid, and solid-solid interfaces. The properties of such interfaces can normally be described as triple junctions. A few illustrations are shown in Figure 4. Type(a) represents an inclusion of B in the grain boundary between two regions of material A. In the absence of a grain boundary in A, this would represent an inclusion B in a homogeneous matrix of A. Since surface energy and surface tension are synonymous in isotropic materials, the equilibrium state for the junction can be described by making a force balance about the point of intersection for the three regions;

$$\gamma_{AA} = 2\gamma_{AB} \cos \frac{\theta}{2}$$

where γ_{AA} is the tension in the A-A interface and γ_{AB} is the tension in the A-B interface. For the case where A is homogeneous with no boundaries, $\gamma_{AA}=0$, and $\theta = 180^\circ$. Thus, if B is an isotropic fluid capable of attaining an equilibrium shape, it would take on a spherical shape in a homogeneous fluid matrix.

Figure 4(b) shows a triple junction, or meniscus, for liquid B in a capillary tube A. The case with a small contact angle represents good wetting of the capillary wall, while the case with a large contact angle represents

poor wetting of the capillary wall. Figure 4(c) shows a fluid drop L on a flat solid surface S. Region V is either vapor or another liquid. The small contact angle represents good wetting while the large contact angle represents poor wetting. At equilibrium;

$$\gamma_{sv} = \gamma_{sl} + \gamma_{lv} \cos \theta$$

or

$$\cos \theta = \frac{\gamma_{sv} - \gamma_{sl}}{\gamma_{lv}} \quad (3)$$

Equation (3) fixes the limits for absolutely no wetting and also for spontaneous wetting. If $\gamma_{sv} \geq \gamma_{lv} + \gamma_{sl}$, θ must be zero, and spontaneous wetting can occur. If $\gamma_{sl} \geq \gamma_{sv}$, θ must be 180° , which means that L cannot wet S to any extent. Wetting is favored when the substrate is free of contamination so γ_{sv} is maximum, the adhesive has an affinity for the substrate (γ_{sl} is low) resulting in a low interfacial tension, or when the surface tension of the adhesive is low (γ_{lv} is low).

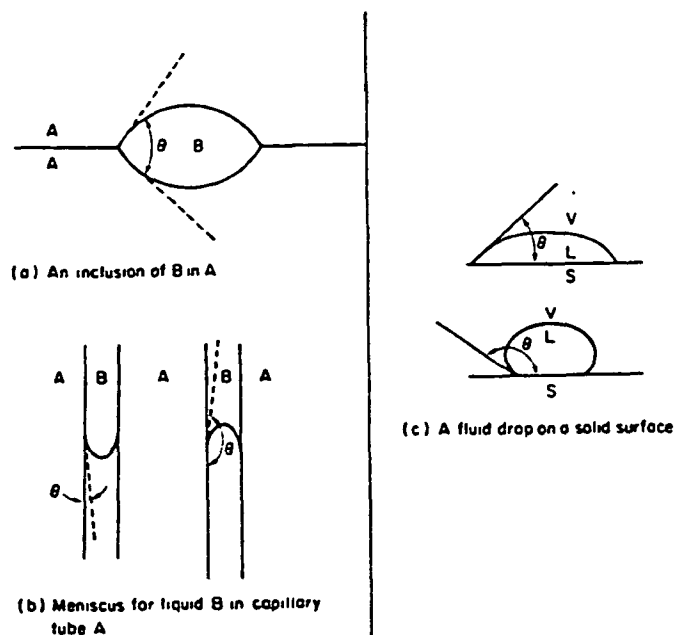


Fig.4. Triple junctions [14]

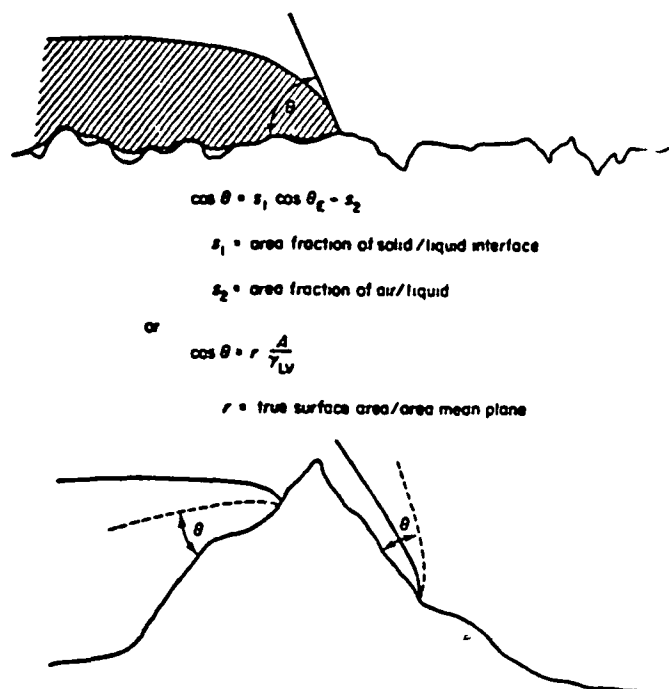


Fig.5. Effects of surface roughness.[14]

3.2.3 Surface Roughness and Porosity

Surface roughness modifies the wetting characteristics of solid surfaces because the fluid must move up and over asperities (Figure 5). For spreading on the rising side of an asperity, wetting is probably hindered due to gravitational forces whereas on the falling side it is probably aided. Most important is the possibility of air being trapped under a spreading fluid, thereby changing the equilibrium contact angle. There is no accurate way of predicting the net effects of roughness, but Wenzel[47] has suggested that the equilibrium contact angle of a rough surface is given as

$$\cos \theta = r \frac{\gamma_{sv} - \gamma_{sl}}{\gamma_{lv}} \quad (4)$$

where r is the ratio of the true surface area to the mean plane surface area.

Equation (4) suggests that if θ is less than 90° wettability is enhanced by roughness and if θ is greater than 90° wettability is hindered by roughness.

Wake[35] has shown that the adherence to fabrics based on continuous but variously shaped yarns is proportional to the surface area of the fabrics.

The rugosity is a positive factor only in so far as the substrate is perfectly wetted by the liquid. As a matter of fact, if the liquid cannot penetrate into the asperities of the substrate, the hardening of the resin is accompanied by the formation of interfacial cavities which are liable to initiate the failure of the interfacial bond. An increase in the specific surface area of graphite fibers achieved by nitric oxidation has been reported to improve the interlaminar shear strength of the corresponding composites[36].

According to Baier et al.[44], the innumerable small hills, valleys, and crevices in the surface of practically any real solid create problems which must not be neglected if strong durable, adhesive joints are desired. A viscous liquid can appear to spread well over a solid surface and yet have many gas pockets or voids in small surface pores and crevices where the liquid adhesive has formed a mantle over neighboring peaks without having fully penetrated into the valleys. Even if the liquid adhesive spreads spontaneously over the solid, there is no certainty that intimate contact of the liquid and solid interface will have occurred everywhere. This problem is magnified when the liquid rapidly polymerizes or hardens soon after being applied. When a liquid adhesive solidifies, the loss in joint strength caused by the interfacial voids is much

greater than would be expected from the ratio of the interfacial area occupied by voids to the area of the entire joint interface. This result arises from the action of internal and external stress concentrations.

Griffith[37] showed that adhesive joints may fail at relatively low applied stresses if cracks, air bubbles, voids, inclusions, or other surface defects are present. On application of an external load to the joint, stress concentrations arise that can be much higher than the mean applied stress. Real joints are better illustrated by Figure 7 than by Figure 6. If the gas pockets or voids in the surface depressions of the adherend are nearly all in the same plane and are not far apart (as is shown for the upper adherend of Figure 7), cracks can readily propagate from one void to the next, and the joint can break as easily as if it had a built-in zipper. For a strong adhesive joint, however, the kind of roughness shown on the lower adherend would be preferable (provided roughening of the surface did not result in excessive formation of voids) because crack propagation in the resin would have to follow a much longer, tortuous path to connect neighboring voids.

When a liquid spreads over a porous surface, it must wet the capillary passages in order to displace the air in the pores (Figure 8). In a cylindrical open pore of diameter d , the depth of penetration (D_p) is equal to;[14]

$$D_p = \sqrt{\frac{\cos \theta \gamma_{lv} d t}{4 \eta}}$$

ORIGINAL PAGE IS
OF POOR QUALITY

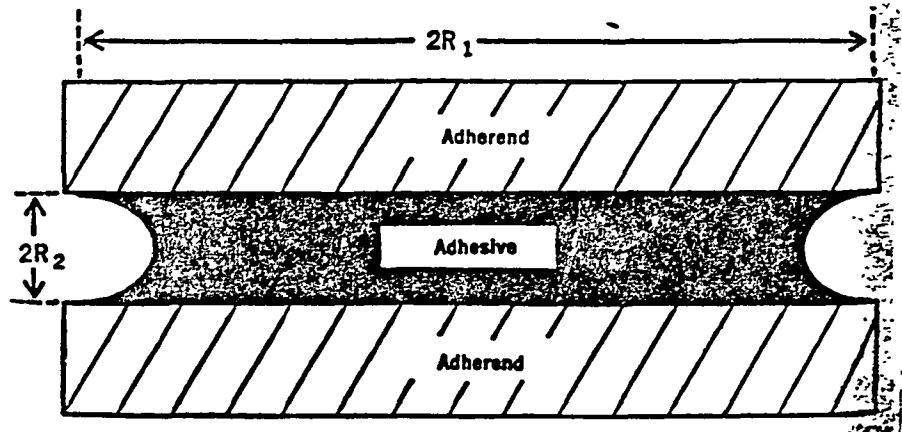


Fig.6. Idealized adhesive joint.[44]

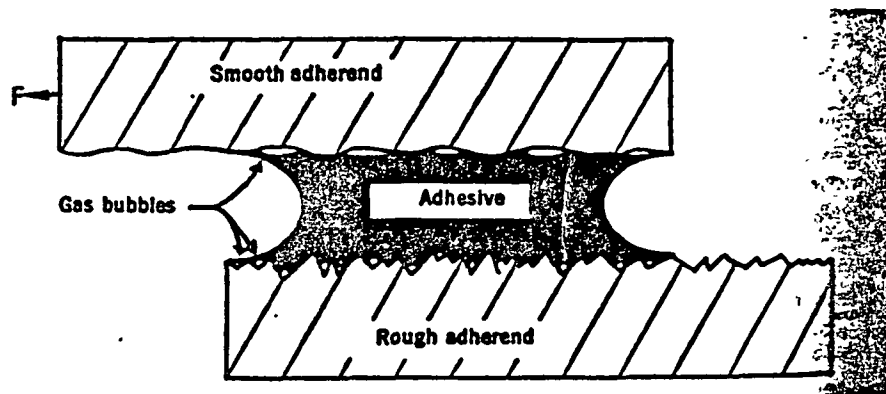


Fig.7. Effect of surface roughness on coplanarity of gas bubbles. [44]

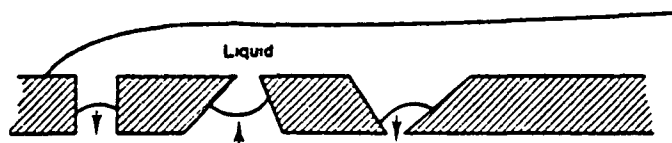


Fig.8. Effects of porosity. [14]

where t =time, and η =viscosity.

Thus as $\theta \rightarrow 90^\circ$, $d \rightarrow 0$, $\eta \rightarrow \infty$, it takes a very long time to fill a pore. If the pore is closed at one end, the gas is merely compressed, trapping a void at the interface. Pore shape also affects the wettability. Filling a diverging cone, for example, requires an increasing surface energy as one moves to a wider section; thus, filling diverging pores is not thermodynamically favorable.

3.2.4 Properties of Constituent Material

3.2.4.1 Resin properties

The interlaminar shear strength of composites seems to show a marked dependence on resin properties. One of the properties, for example, tensile strength of the resin showed a very strong positive correlation with interlaminar shear strength. Figure 9 [3] shows a smooth curve for the ILSS versus the tensile strength of eight different resins. At the lower portion of the curve up to strengths of approximately 7000 psi, the interlaminar shear showed almost a linear relationship with resin tensile strength. As a resin tensile strength of 10,000 psi or higher was achieved, the ILSS showed very little increase. Two

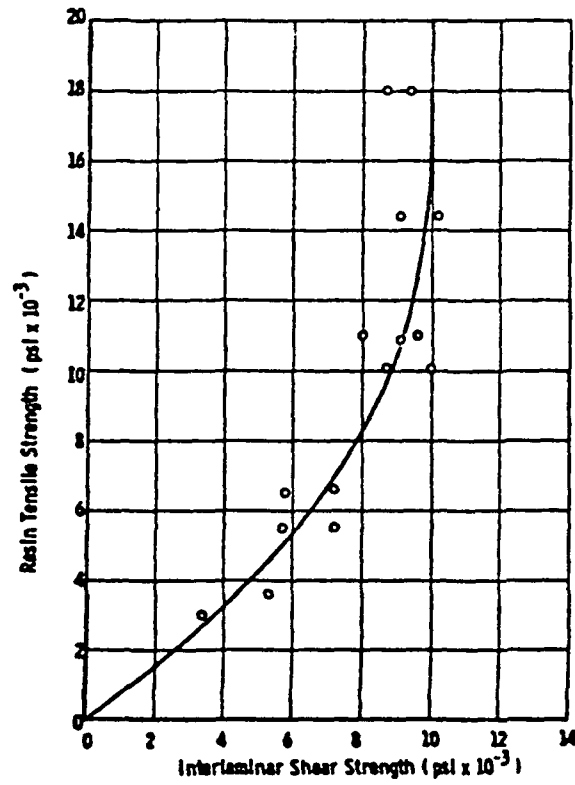


Fig.9. Influence of resin strength on interlaminar shear strength [3]

possible mechanisms were postulated; first, that the interfacial strength was stronger than the strength of resin and that the resin failure was occurring at the low levels of interlaminar shear. As the resin strength increased beyond 10,000 psi, this tendency was reversed. In this instance the interlaminar interface was failing and this was determining the interlaminar shear strength which did not increase appreciably even though the resin strength could be doubled. The second postulate was that voids were controlling the interlaminar shear. Resins with low levels of tensile strength have greater flexibility than high strength resins and the former would tend to be less influenced by voids. As the resin tensile strength increased, the resins became more brittle and failure through the void areas was more predominant. The energy necessary to propagate a crack through the voids was approximately equal whether the resin tensile strength was 10,000 or 18,000 psi.

3.2.4.2 Fiber properties

The decrease in interlaminar shear strength of graphite fiber composites as the moduli of graphite fibers increase has been found to be common.[61,62] Although the reason for this decrease in composite shear strength is still not fully understood, one hypothesis is that sites for bonding or chemical functionality is associated with the edge carbon

atoms. As the axial moduli of the filament increases this infers improved molecular orientation and thus, a decrease in exposed edge atoms. Therefore, possible chemical coupling at the fiber matrix interface is reduced[61].

According to Butler et al.[62], the decrease in interlaminar shear strength of graphite fiber composites could be explained by the preferred orientation of graphite crystallites on the fiber surface, since the surface energy decreases as the crystallites become more parallel to the fiber surface. Thus as the planes align with the fiber axis to yield a high modulus, the interlaminar shear strength of the fiber/matrix interface should decrease.

3.3 Chemical Factors influencing Interfacial Shear Strength

3.3.1 Chemical Bonding

It is reasonably well accepted that in order to have interfaces that are at least as strong as the constituent materials in shear, it is necessary to develop some kind of chemical bonding. Chemical bonding at an interface is developed by wetting the solid surface with a fluid. Once molecular contact has been attained, the two phases can interact through intermolecular forces. The magnitude of the interaction depends on the type of chemical bonds

formed. Chemical bonding can be classified into primary and secondary bonding. Primary bonds generally have bond energies of the order of 30-100 Kcal/g-mole and involve interatomic distance of $1-3 \text{ \AA}$. This leads to theoretical strengths of order of 10^6 to 10^7 psi. Primary bonding can be either ionic, covalent, or metallic. An ionic bond is an electrostatic interaction between highly electronegative (e.g. F) and highly electropositive (e.g. Na) atoms. When two such elements interact, the electronegative element draws an outer shell electron away from the electropositive element, thereby forming an anion and a cation. These will then coulombically interact to form an electrostatic bond.

A covalent bond is a true sharing of the electron orbitals of the interacting atoms. The outer shell electrons of such atoms lose their identity and form molecular orbitals that bind the nuclei of the interacting atoms. This manifests itself as a high electron density along the internuclear axis.

Metallic bonds are similar to covalent bonds in that outer shell electrons are shared by the nuclei of many atoms. The effects of primary bonding are of importance to composites technology. The mixing of a metal matrix with a metal or oxide reinforcement often results in intermetallic compound formation at interfaces. Such reactions have a marked effect on the composite properties. Likewise, organic matrices can be chemisorbed on to surfaces,

resulting in the formation of organic compounds at the interfaces.

Secondary, or Van der Waals, bonds (shown schematically in Figure 10(a)) generally have bond energies of the order of 0.5 to 10 Kcal/g-mole and involve interatomic distances of 3 to 5 Å. This leads to theoretical strengths of the order of 10^5 to 10^6 psi. These bonds are thus an order of magnitude weaker than primary bonds. Secondary bonding arises from electrostatic and inductive interactions between charges, dipoles, and multipoles in adjacent molecules or from London dispersion interactions (Van der Waals forces) between molecules. Qualitatively, when two relatively simple molecules, separated by a distance r , interact in this manner, the potential energy of interaction can be represented by a function of the form;

$$\phi_{12} = \frac{B}{r^m} - \frac{A}{r^n} = (-\phi_{12}^*) \left[\left(\frac{r^*}{r} \right)^m - 2 \left(\frac{r^*}{r} \right)^n \right] \quad (5)$$

where the first term is a net repulsion and the second term is a net attraction. The quantities A and B are constants, m is constant at about 10 to 30 (usually 12), and n is constant at about 1 to 7 (usually 6), depending on the type of secondary bond. Equation(5) generally looks like the curve shown in Figure 10(b). The minimum represents the maximum interaction potential and the distance at the minimum r represents the most stable distance between

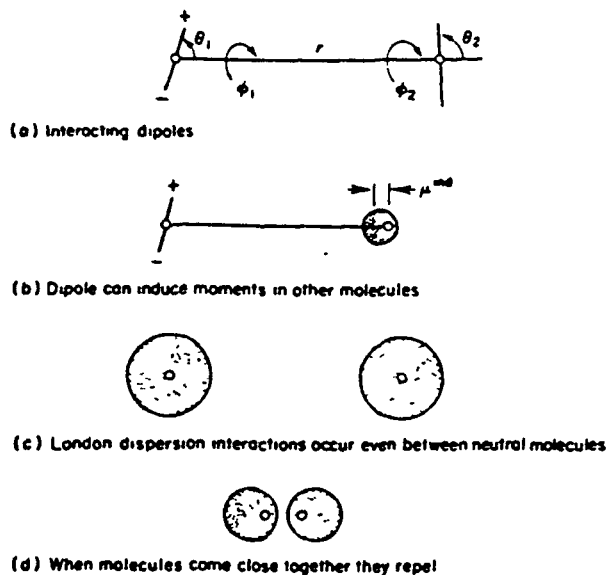


Fig.10(a). Secondary interaction. [14]

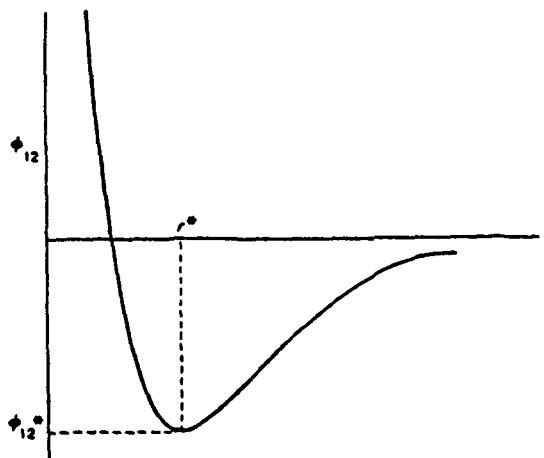


Fig.10(b). Schematic representation of the net interaction potential between two molecules. [14]

particles.

The interaction energy between two materials across an interface and the tensile strength of the resulting adhesive bond can be related to intermolecular forces, by considering the energy of absorption of a single molecule A at a distance (d) from a solid surface, as shown in Figure 11. The interaction between the molecule and an annular ring below the solid is $N_A 2\pi r dr dz$ where N_A is the molecular density. A potential function such as Equation (5) can be integrated over the whole solid to obtain the total energy of interaction of molecule A with the solid. To a zero order of approximation the maximum energy of absorption for Van der Waals bonding is given by:[14]

$$(\phi_{\text{absorption}})_{\text{max}} = 2.5 N_A N_L^{\frac{2}{3}} (\phi_{12}^*) (r^*)^3$$

where N_L = the density of the absorbed material.

If we assume $r^* = 3-4 \text{ \AA}$, $N_A = N_L = 4 \times 10^{22}$ particles/cc, and $\phi_{12}^* = 0.3-7.0$ Kcal/g-mole, the energy of absorption becomes[14]

$$(\phi_{\text{absorption}})_{\text{max}} = 60-2,000 \text{ ergs/cm}^2$$

Experimental data for the energy of adhesion of liquids to high energy solids show that dispersion bonding results in energies of $100-200 \text{ ergs/cm}^2$ [14]. Thus even the crude molecular model discussed here can predict the proper order of magnitude for the energy of interaction for two materials in molecular contact across an interface. Since the

ORIGINAL PAGE IS
OF POOR QUALITY

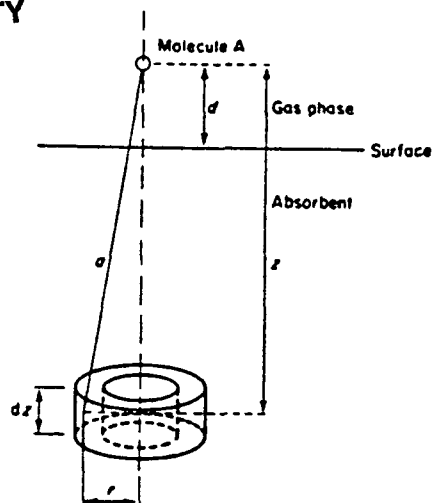


Fig.11. Interaction of a molecule with a plane surface.[14]

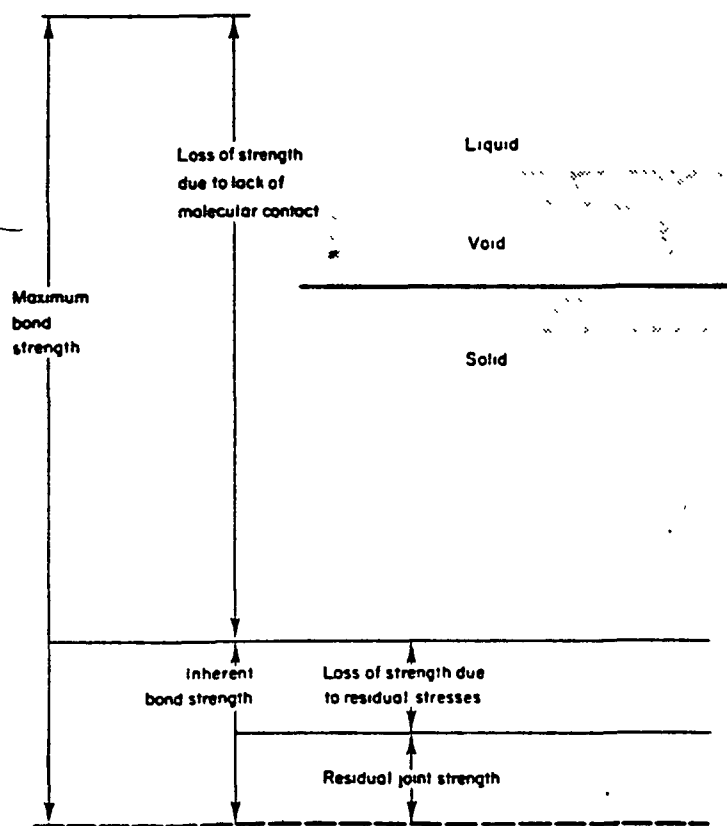


Fig. 12. Factors affecting adhesive bond strength.[14]

intermolecular force is related to the intermolecular energy by $f = -d\phi/dr$, a theoretical maximum tensile strength for the interface could be estimated by differentiating Equation(5) to obtain an equation relating force and interplanar separation and then evaluating the force at the maximum where $df/dr=0$. To a zero order approximation the maximum tensile strength for the interface is[14]

$$f_{\max} = 4.5 r^*{}^2 N_{ANL}^{2/3} \phi_{12}^*$$

Using the same numbers as before for the molecular constants, a theoretical maximum tensile strength $f_{\max} = 60,000-1,5000,000$ psi. Experimental data show that the actual tensile strength of an interfacial bond rarely exceeds 2,000 psi. Thus the actual tensile strength of an interfacial bond is only a small fraction of the theoretical bond strength, as shown schematically in Figure 12. The primary loss of strength is due to failure of the molecules to approach their proper bonding distances of a few angstrom units. This may be visualized as a microvoid at the interface which is then capable of concentrating stress and causing premature failure.

A second major loss in bond strength comes about from the development of residual stresses at the interface. Normally, a matrix is applied in the fluid state and then solidified by cooling or chemical reaction. This invariably

causes a differential shrinkage at phase boundaries that leads to undesirable stress concentrations. Since the energy calculations were reasonable, it can be assumed that if wetting and molecular contact is attained at an interface, even relatively weak Vander Waals forces should give a strong, cohesive interface. The low mechanical strength is thus controlled by factors other than molecular cohesion. In real composite materials, the phases are not always compatible and wetting and molecular contact are not necessarily attained. The low mechanical strength of an interface is most certainly caused by microscopic and submicroscopic defects. Probable causes of such defects will include; imperfect wetting, shrinkage on solidification, thermal stresses, dirty surfaces, and cracks and voids in the interfacial layer.

3.3.2 Coupling Agent

A coupling agent is a chemical applied to the surface of the reinforcing medium of a composite to improve adhesion between a matrix and a reinforcing medium. By this definition, a coupling agent can be considered to be an adhesive used to join two dissimilar surfaces. The mechanisms at both interfaces by which such adhesion can be achieved are determined by the three components and the physical state in which the coupling agent functions as an

adhesive.[48] The type of adhesion[49] involved then determines the magnitude of bond energies as illustrated in Figure 13.

If the adhesive strength is of chief concern, an ideal coupling agent should be chemically bonded to both the matrix and the reinforcing medium. It has been shown that this type of chemical bond exists in glass-reinforced thermosetting resins.[51] In a system in which a chemical bond can be readily formed, the contribution of physical adhesion to the total adhesive bond is relatively unimportant.

It is well known that the most effective coupling agents on glass fiber are the silanes. Figure 14 [2] postulates a possible chemical mechanism for forming a chemical link between a coupling agent and the glass surface. The chemical bridge is completed by the other functional group of the coupling agent (in this instance, an amino group) which will react with an epoxide resin. The evidence which supports this theory is the increased wet and dry strengths of composites with coupling agents, the requirement of chemical bifunctionality for effective coupling agents, and the chemical uniqueness of coupling agents. Therefore, an effective coupling agent for an epoxide resin may not be effective with another matrix. Surprisingly there is one facet of filament-resin interaction in which there appears to be universal agreement. Because of the exceptionally

large bond surface area which is characteristic of filamentous composites, almost all investigators believe a strong adhesive bond at the resin/glass fiber interface is a requirement for strong structural performance.

Wong[45] also proposed a mechanism of coupling by silanes of epoxies to glass fiber. According to him, the 'bonding layer' is formed by depositing a uniform and continuous film forming layer of an epoxy resin onto the coupling agent layer. The 'bonding layer' chemically bonds to the matrix epoxy resins which result in a maximum resin-glass bond strength. The 'compatibility layer' is the outermost layer and is an epoxy containing substance which is designed to enhance the complete wetting of the 'bonding layer' by the matrix epoxy resins. In this manner the glass-resin interface is composed of a monomolecular silane coupling agent layer which is continuous, uniform, close-packed and oriented.

However, the effect of coupling agents for the graphite fiber/epoxy system is ambiguous. Goan and Prosen[46] coated both oxidized and unoxidized graphite fibers with polymers and reactive monomers. The principle was that carboxyl and phenolic groups on the surface of oxidized graphite should be able to react with isocyanate groups in a urethane prepolymer. Other isocyanate groups in the coating would be available to couple with the resin. The polyisocyanates thus would act as bridging or coupling

agents between the fiber and the resin. However, when composites were made from fibers treated in this way, they exhibited no significant improvements over composites made from fibers which had not been treated with a coupling agent.

One glass finish, A-1100, gamma-aminopropyl triethoxysilane, when applied to an oxidized graphite surface, resulted in a composite with a shear strength slightly higher than composites made with oxidized fibers without coupling agents[46]. It was speculated that the phenolic hydroxyl groups on the oxidized fiber surface could react with the finish in a similar fashion to the silanol groups on the surface of glass[46].

Riess et al.[80] have proposed a method for surface treatment of carbon fibers in order to improve the fiber-matrix bonding. The method consists in grafting a copolymer bearing flexible segments (polyisoprene), and segments compatible with the epoxy matrix(styrene-maleic anhydride). The bonding between the carbon fiber surface and the elastomer segments of graft copolymer is attained by ionic(dipole-dipole) interactions. By means of this treatment, better adhesion and improvement in interlaminar shear strengths were reported.[80]

3.4. Effects of Radiation

3.4.1. Radiation effects on carbon fibers

Apparently, the first investigation of the effect of radiation on carbon fibers reported was by Allen, Cooper, and Mayer[63,64,65]. These investigators irradiated HTS(high tensile strength) and HM(high modulus) carbon fibers to a fast neutron flux of $2.2 \times 10^{17} \text{ n/cm}^2$ ($E > 2.9 \text{ MeV}$), and they found the tensile strengths of the two fibers to be increased by 12 and 5%, respectively, over unirradiated control strengths.

Jones[66] reported that the tensile strength of HM fibers was increased by 2% for a fast-neutron flux of $4 \times 10^{17} \text{ n/cm}^2$ ($E > 0.18 \text{ MeV}$) and was decreased by about 5% for the next reported flux of $3.2 \times 10^{20} \text{ n/cm}^2$.

Bullock[67] irradiated two types of carbon fibers (HTS and HM) in environments of air and liquid nitrogen. The tensile strength of HTS fibers irradiated in air increased sharply and was 17% greater than the strength of unirradiated control fibers at a flux of $8.5 \times 10^{17} \text{ n/cm}^2$, but then the strength began to decrease for additional neutron exposure in air and fell 25% below the control strength at the highest flux of $4.5 \times 10^{18} \text{ n/cm}^2$. However, when irradiated in liquid nitrogen where surface oxidation did not take place, the room-temperature strength of HTS fibers continued to increase and became almost 30% greater than the control

strength for a flux of 3×10^{18} n/cm². The tensile strength of HM fibers irradiated in air increased slowly but steadily with neutron exposure and was only 4% greater than the control strength at the highest flux of 4.5×10^{18} n/cm². The room-temperature strength of the HM fibers decreased by 13% when irradiated to a flux of 3×10^{18} n/cm² in liquid nitrogen.

Two competing processes were thought to bring about the rise and fall in strength of HTS fibers with radiation exposure; (1) fibers are being internally strengthened by fast neutrons which dislodge carbon atoms from their lattice sites in basal planes of tightly bound atoms, the displaced atoms come to rest in spaces between weakly bound lattice planes, and (2) radiation-enhanced oxidation is taking place at vacant lattice sites on fiber surfaces from which atoms have been displaced[66]. The internal strengthening process dominates for lower neutron fluxes(n/cm²-sec) where there is less radiation heating of fibers, but surface oxidation rapidly begins to take over for higher rates of radiation exposure.

It has been reported [76] that the chemical reactivity of graphite was increased by radiation, mainly by oxidation in the presence of carbon dioxide, oxygen, water vapor or all three. These oxidation products may consist of reactive species which are retained on the fiber surface and then interact with the matrix polymer, affecting the bonding

between the fiber-matrix interface.

3.4.2. Radiation effects on epoxy resins

When cured, epoxy resins are generally hard, extremely tough, and chemically inert. These resins are above average in radiation resistance, having withstood gamma ray doses up to 9.5×10^{10} ergs/g without deterioration.

Several factors appear to affect the radiation stability of epoxy resins. The structure of the polymer, the curing agent used, the presence of a filler all influence the stability of epoxy resins. In general, the greater the aromatic content, the greater the stability of the polymer. Thus, aromatic curing agents provide greater radiation stability than do aliphatic curing agents. A polymer based on epoxy resins having a greater number of aromatic groups is generally more stable than one based on a structure having fewer phenyl groups.

Mixer[60] studied the radiation stability of three epoxy systems, including DEBA (a diglycidyl ether of Bisphenol-A), Epon 1001 (a longer chain Bisphenol-A diglycidyl ether), and Epon X-131 [containing tetraglycidyl ether of tetrakis (hydroxyphenyl) ethane]. These resins were cured with primary aliphatic, secondary aliphatic, and primary aromatic amines. He found that Epon X-131 was the most radiation

resistant of the three epoxy resins when aromatic amines were used as curing agents. DEBA was the least radiation resistant. He found that

- (1) the aromatic amine product was far more stable than aliphatic amine products;
- (2) chain cleavage of the epoxy resins was in the aliphatic portion, i.e., in the glycidyl group rather than in the aromatic part of the molecule; and
- (3) the predominant effect of irradiation on epoxy polymer was crosslinking.

Morgan et al.[77] measured the flexural strength of cast epoxy resin as a function of gamma radiation doses. In combination with the aromatic diamine based hardeners, the glycidyl amine resin produced castings which showed little deterioration of flexural strength at doses up to 10,000 Mrads. However, the glycidyl ether/aromatic diamine systems showed a 50% reduction in flexural strength at about 4,000 Mrads.

3.4.3. Radiation effects on composites

Mckague et al.[69] reported that mechanical property improvement of carbon fibers by neutron irradiation[63,67,70,71] largely translated into composites reinforced with such fibers. Moreover, as an added benefit, fiber/matrix interfacial bonding determined by horizontal

shear strength test was improved in irradiated-fiber composites; this is of particular importance because chemical surface treatments of fibers to improve their bondability with an epoxy matrix often result in strength losses, whereas irradiation treatment increases both the strength and bondability of carbon fibers. They proposed a following model to explain the increase in shear strength of the irradiated-fiber composites. The carbon fiber/matrix interface can be divided into 3 regions[62];

- (1) the epoxy surface adjoining the fiber
- (2) the chemical interface between fiber and matrix
- (3) the first several atomic planes within the surface of the carbon fiber itself

Shear failures will occur in the weakest of these regions, of course and the first region can be eliminated as a source of failure in good resin systems, since electron micrographs do not reveal an epoxy layer left on fibers after shear failures[62]. The second region is certainly the weakest in composites in which the carbon fibers are not surface treated, but there is evidence that the chemical interface can be sufficiently strengthened through surface treatment to shift the zone of weakness into the surface layer of the carbon fiber itself[72]. The irradiation should provide strengthening in both of the critical interface regions(2 & 3). As to the chemical interface(2), the surfaces of high-modulus fibers are covered largely with basal planes of carbon atoms in which valencies of interior atoms are fully

saturated, so that such fibers do not bond well with epoxies. A greater number of the much more chemically active 'edge-type' atoms (having unsaturated valences) are exposed at vacant lattice sites left by the displacement of surface atoms, and this should enhance fiber to matrix bonding[61]. At the same time, the weak shear regions between the atomic planes within the carbon fiber itself(3) are being strengthened by the displaced atoms that come to rest within the interplanar regions.

Bullock et al.[73] also irradiated two types of carbon/carbon composites using a fast-neutron flux of 2×10^{18} n/cm² ($E > 1\text{MeV}$) in a helium atmosphere at 175° C. Shear strengths determined by the short beam shear method at room temperature were increased by 25% or more by irradiation, and this increase in shear strengths allowed the composites to be flexed to higher stress levels(15-25%) before undergoing permanent deformations. They found that stress-strain curves of as-received specimens were perfectly linear(with a slope of E) up to a transitional stress and thereafter they began to change slope as the stress increased less and less rapidly with increasing strain. In these nonelastic regions at higher strains, it has been suggested that the interlocking between fiber and matrix begins to break down, allowing fibers to move within the matrix. Thus more and more stress is gradually transferred into the brittle carbon matrix until crack growth becomes sufficient to cause its failure. This

behavior was verified by the experimental result that the onset of nonelastic bending shifted smoothly to higher stresses as the ILSS increased. This explains why flexural tests on irradiated specimens maintain linearity to higher stresses than do unirradiated specimens with lower shear strengths. Bullock et al.[73] also found that the transitional stresses became more uniform with radiation, and that the irradiated specimens failed more suddenly than did the control specimens. They verified this distinct change in failure mode by examining the fracture surfaces. The failure path through the control specimens was highly tortured, with a number of offsets occurring at fiber/matrix interfaces. The irradiated specimens had much smoother, more glass-like failure surfaces. They concluded that the weaker fiber/matrix interface of the control specimens could apparently better serve to arrest cracks.

Bullock[78] reported that finished carbon-epoxy composites could not be strengthened by neutron irradiation in air because of severe oxidative degradation of the epoxy matrix of the composite. The room-temperature flexural strength of composite specimens in the fiber direction decreased by almost 80% for a fast-neutron flux of 4.2×10^{17} n/cm²; beyond this minimum there was a strength increase of almost 70% by the time a flux of 7.5×10^{17} n/cm² was reached, but this still left the longitudinal flexural strength lower than the unirradiated control strength. When carbon-epoxy composites were irradiated in liquid nitrogen and then were

mechanically tested in liquid nitrogen without warmup, however, the longitudinal flexural strength increased by 80% over the control strength in liquid nitrogen. He concluded that the carbon-epoxy composites could be greatly strengthened by neutron irradiation in an liquid nitrogen environment, because of the increased strength and stiffness of the epoxy matrix at cryogenic temperatures.

Raff et al.[74] measured the joint strengths between stainless steel or copper and an epoxy resin as a function of gamma radiation dose. Their results showed that the joint strength could be increased up to 300% by ^{60}Co gamma radiation. They assumed that the changes in the metal-polymer interfaces might be caused by internal bombardment by the Compton electrons generated by the gamma irradiation, leading to atom displacements in the metals, and free radicals in the polymer.

Leung[75] measured the interlaminar shear strength of graphite/epoxy composites by the short beam method as a function of gamma-radiation exposure dosages. His data showed an initial increase, followed by a decrease, as the dosage increased. Leung concluded that exposure of graphite/epoxy composites to gamma radiation improved the fiber/matrix interfacial bonding initially.

Wolf[79] conducted interlaminar shear tests on T300/5208 and C6000/PMR15 composites. Both composites followed the same general trend which was an initial increase in ILSS (up

to 1,000 Mrad) followed by a sharp decrease with further radiation exposure. According to Wolf[79], the initial increase in ILSS with radiation exposure is probably due to relaxation of internal stresses created at the interface during composite fabrication. After the internal stresses are relieved, further radiation exposure leads to bond degradation due to chain scission, and thus the decrease in interlaminar shear strength at levels of radiation greater than 1,000 Mrad.

NOMENCLATURE

a	$CK(\frac{1}{A_f E_f} - \frac{1}{A_m E_m})$
A	cross-sectional area
b_i	Interface thickness
C	Circumference of fiber
E	Young's modulus
F	Force
G	Shear modulus
K	Constant
l	Fiber imbedment length
L	Debonded length
P	Axial load
q	Bonding shear force between fiber and matrix
r	Radial coordinate
r_o	Fiber radius
$r_1 - r_o$	Thickness of matrix
R	$[\frac{1}{A_f E_f} - \frac{1}{A_m E_m}]^{-1}$
u	Displacement
W	Work
x	Axial coordinate
α	$[\frac{2G_i}{b_i r E_f}]^2$
γ	Shear strain
ϵ	Normal strain
λ	Frictional stress
σ	Normal stress
τ	Shear stress

Subscripts

f	Fiber
m	Matrix
i	Interface
max	Maximum
ave	Average

3.5 Theoretical Analysis of Interfacial Shear Strength of Fiber-resin Composites

3.5.1 Determination of the Strength and Shear Modulus of the Interface [52]

The strength and the shear modulus of the fiber-matrix interface may be measured by using the equations of the shear-lag theory, in combination with the test data from the pullout tests on fibers that are imbedded in matrix to various lengths. The parametric relationship between the properties and geometry of the constituents and the shear strength of the bond may be obtained by considering the model shown in Figure 15.

The equilibrium of forces acting on an element dx requires that

$$F - (F + dF) + (2\pi r_0) dx \tau = 0$$

or,

$$\frac{dF}{dx} = 2\pi r_0 \tau \quad (6)$$

The strain in the fiber is

$$\epsilon = \frac{du}{dx} = \frac{F}{\pi r_0^2 E_f} \quad (7)$$

where E_f = fiber modulus.

The shear strain in the matrix is

$$\gamma = \frac{u}{b_i} \quad (8)$$

where b_i is the effective thickness of the interface.

Using the relationship between shear stress and strain

$$\gamma = \frac{\tau}{G_i}$$

in combination with Equation (8), and solving for τ ,

$$\tau = \frac{u G_i}{b_i} \quad (9)$$

Substituting Equation (9) into Equation (6), solving the resultant equation for u , differentiating u with respect to x , and substituting the result into Equation (7) gives,

$$F'' - \alpha^2 F = 0 \quad (10)$$

Where the primes denote differentiation with respect to x and

$$\alpha = \left[\frac{2 G_i}{b_i r_0 E_f} \right]^{\frac{1}{2}} \quad (11)$$

The solution of Equation (10) is

$$F = C_1 \sinh x + C_2 \cosh x$$

With the boundary conditions $F=P$ at $x=0$, and $F=0$ at $x=l$, the final solution for the shear stress at any point x is,

$$\tau = \frac{P \alpha}{2 \pi r_0} (\sinh \alpha x - \coth \alpha l \cosh \alpha x) \quad (12)$$

In terms of the average shear stress, $\tau_{ave} = P/2 \pi r_0 l$, Equation (12) may be expressed as

$$\frac{\tau}{\tau_{ave}} = \alpha l (\sinh \alpha x - \coth \alpha l \cosh \alpha x) \quad (13)$$

The maximum shear stress occurs at $x=0$, and from Equation (13),

ORIGINAL PAGE IS
OF POOR QUALITY

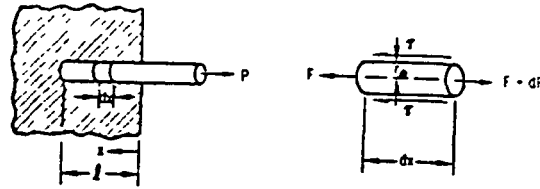


Fig.15. Filament imbedded in a matrix.[52]

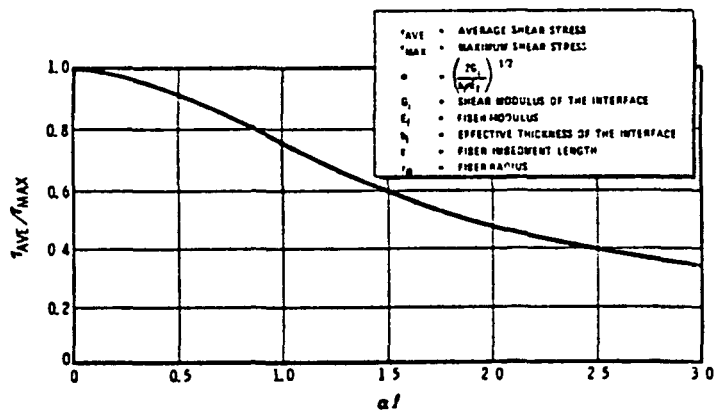


Fig.16. Shear stress ratio as a function of αl . [52]

$$\frac{T_{max}}{T_{ave}} = \alpha l \coth \alpha l$$

As $\alpha l \rightarrow 0$, $T_{max}/T_{ave} \rightarrow 1$; in other words, $T_{max} \rightarrow T_{ave}$. This condition can be used in determining the shear strength of the interface. Since, for a given matrix and filament, α will remain constant, $\frac{T_{max}}{T_{ave}}$ will be a function of imbedded length, l , only. By conducting the pullout tests on fiber that are imbedded in matrix to various lengths, the shear strength, T_{max} , of the interface can be estimated by plotting a curve T_{ave} versus l , and extrapolating T_{ave} at $l=0$.

The shear modulus of the interface can be evaluated as follows. For any given fiber imbedment length, the ratio T_{ave} / T_{max} can be calculated. Next, a value of αl that corresponds to the calculated T_{ave}/T_{max} ratio can be obtained from Figure 16. Finally, G_i can be calculated from Equation (11) if the effective thickness of the interface, b_i , is known.

3.5.2 Load to Pull-out when considering the Friction between Fiber and Matrix. [53]

For an embedded fiber loaded to P the shear stress at the point where the fiber enters the matrix is given by Equation (14),

$$T_{max} = \frac{KP}{R\sqrt{a}} \coth \sqrt{a} l \quad (14)$$

Consider an embedded fiber of length ℓ , debonded from the free end up to a length $(\ell - x)$ into the matrix, see Figure 17, under the load P . At the bonded/debonded interface the load in the fiber P' is given by

$$P' = P - \tau_i C (\ell - x) \quad (15)$$

where τ_i , interfacial shear strength due to friction, is assumed to be constant over the debonded region and C is the circumference of the fiber. The shear stress at this point is given by

$$\tau = \frac{KP'}{R\sqrt{a}} \coth \sqrt{a}x \quad (16)$$

If as the debonded length increases (i.e. x decreases) this expression is always equal to τ_s (the shear strength of the interface), the fiber will continue to debond. This will occur if the decrease in the term P' is compensated by the increase in the term $\coth \sqrt{a}x$ as x decreases. Thus from Equation (16),

$$\tau_s = \frac{KP'}{R\sqrt{a}} \coth \sqrt{a}x$$

Solving for P'

$$P' = \tau_s \frac{R\sqrt{a}}{K} \tanh \sqrt{a}x$$

Combining with Equation (15)

$$\begin{aligned} P &= P' + \tau_i C (\ell - x) \\ &= \tau_s \frac{R\sqrt{a}}{K} \tanh \sqrt{a}x + \tau_i C (\ell - x) \end{aligned}$$

Differentiating gives

$$\frac{dP}{dx} = \frac{\tau_s R a}{K} \operatorname{sech}^2 \sqrt{a} x - \tau_i c$$

The maximum value of P occurs when $dP/dx=0$

$$x = x_{\max} = \frac{1}{\sqrt{a}} \cosh^{-1} \sqrt{\frac{\tau_s}{\tau_i}}$$

At this point debonding continues without any further increase in P and the failure of bond is catastrophic. Clearly the stage at which debonding becomes catastrophic is dependent on the ratio τ_s/τ_i . When $\tau_s/\tau_i \geq \cosh^2 \sqrt{a} l$ then $x_{\max} = l$ and the debonding process is catastrophic immediately it commences. The maximum load on the fiber required to achieve complete debonding and pull-out is given by

$$P_{\max} = \frac{\tau_s R \sqrt{a}}{K} \tanh \sqrt{a} l, \quad l \leq x_{\max}$$

$$P_{\max} = \frac{\tau_s R \sqrt{a}}{K} \tanh \sqrt{a} x_{\max} + \tau_i c (l - x_{\max}), \quad l > x_{\max}$$

or alternatively

$$P_{\max} = P^{\infty} \tanh \sqrt{a} l$$

$$P_{\max} = P^{\infty} \left[\tanh \sqrt{a} x_{\max} + \frac{\tau_i}{\tau_s} \sqrt{a} (l - x_{\max}) \right] \quad \left. \vphantom{P_{\max}} \right\} (1)$$

where P^{∞} , the load required to debond an infinitely long fiber with no frictional forces present, is given by

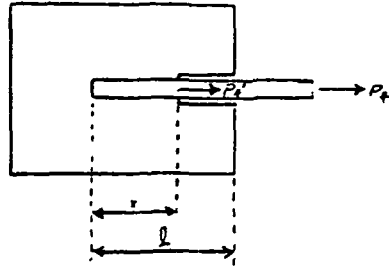


Fig.17. Debonded fiber configuration.[53]

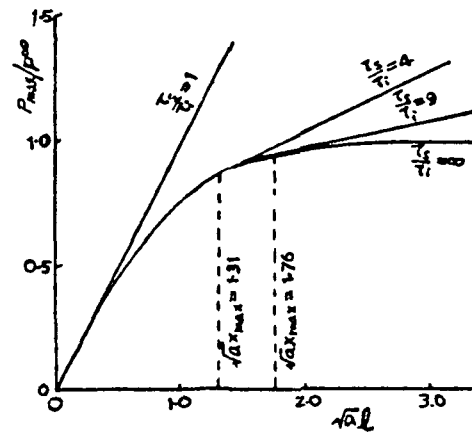


Fig.18. Variation of maximum fiber load with embedded fiber length factor for various friction conditions.[53]

$$p^{\infty} = \frac{\tau_s R \sqrt{a}}{K}$$

The variation in the load required to achieve complete debonding with the embedded fiber length factor $\sqrt{a} \ell$ is shown in Figure 18 (by plotting the ratio P_{max} / p^{∞} for various ratios of τ_s / τ_i). It is assumed that P_{max} is less than the breaking load of the fiber and pull-out, not fiber fracture, occurs. Once debonding has been completed and pull-out has commenced the load necessary to continue pull-out will fall to a value $\tau_i C \ell$ and continue to fall as the fiber is withdrawn from the matrix.

As described in Sec.3.4.1, Greszczuk[52] considered only the immediate catastrophic failure of the interfacial bond and assumed that all the fiber load is transferred to the matrix by shear forces with no frictional forces present. This requires that $\tau_i = 0$, so that from Equation(17) the maximum load to pull-out is given by the expression

$$P_{max} = p^{\infty} \tanh \sqrt{a} \ell$$

This is identical with the $\tau_s / \tau_i = \infty$ plot in Figure 18 (i.e. $\tau_i = 0$) and is a particular case of the more general equation, for P_{max} when $\ell \leq x_{max}$ and catastrophic failure always occurs.

3.5.3 Shear Stress Distribution along the Interface[55]

The geometry of a double-notched specimen is schematically shown in Figure 19. The condition for equilibrium of internal forces provides

$$dP + q = 0 \quad (18)$$

The fiber tensile stress σ at $L=0$ is

$$\sigma = P/\pi r_0^2 \quad (19)$$

where r_0 is radius of fiber. Differentiation and rearrangement of Equation(19) gives

$$dP = \pi r_0^2 d\sigma \quad (20)$$

The shear stress τ_r varies with radius r , where $r_0 \leq r \leq r_1$

$$\tau_r = -q/\pi r dx$$

The shear strain γ at position x and radius r is expressed in terms of shear displacement u_r as follows

$$\gamma_r = \frac{du_r}{dr}$$

where u_r is shear displacement. The matrix shear modulus G is defined as

$$G = \frac{\tau_r}{\gamma_r} = -\frac{q}{\pi r dx} \frac{dr}{du_r}$$

The total shear displacement u_x of matrix element of length dx from radius r_0 to r_1 is

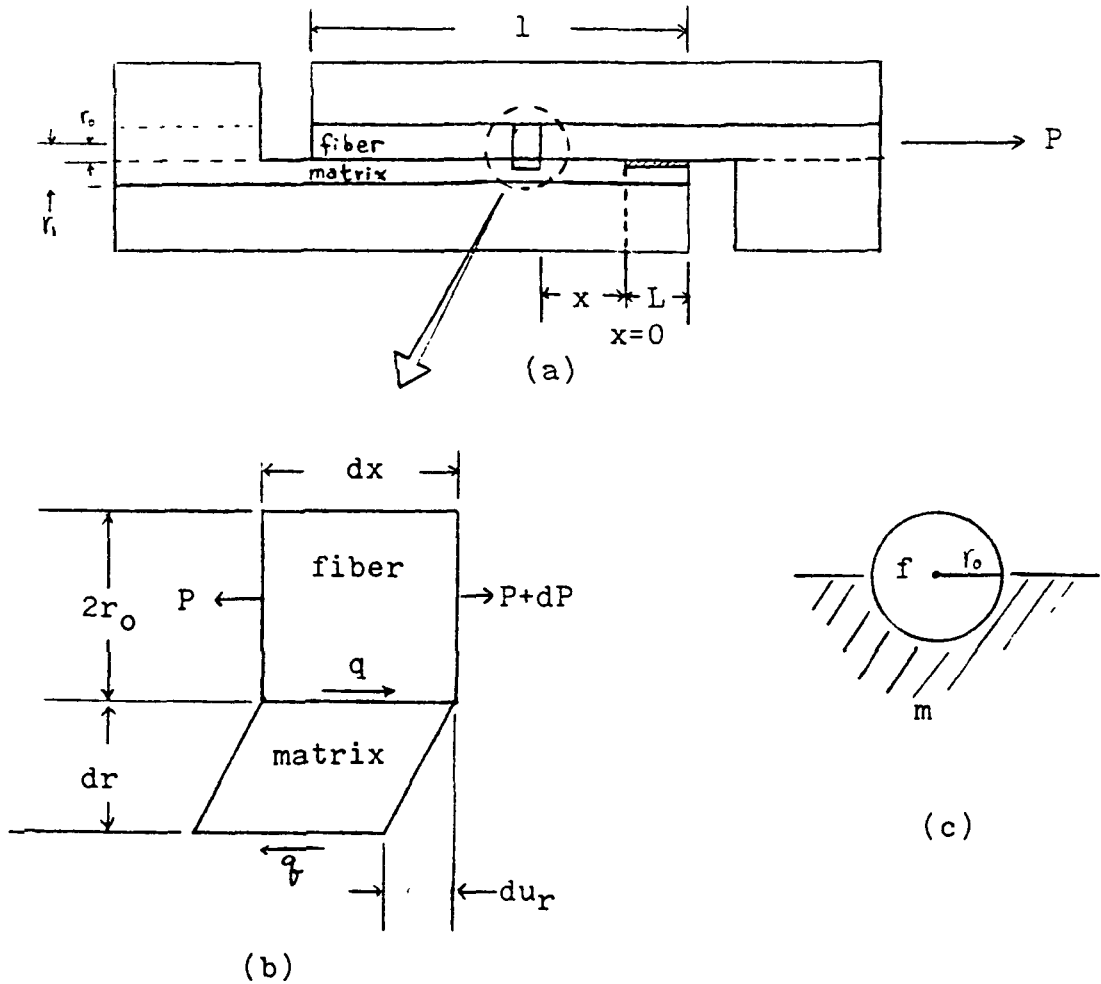


Fig.19. Schematic of forces and displacements about the fiber adjacent to the interface in a double-notched specimen. (a) cross section of the specimen where r_0 =fiber radius, $r_1 - r_0$ =thickness of matrix, l =distance between notches, L =length of debonded region where frictional force is applied, and P =uniformly distributed force. (b) balance of forces for an incremental length dx of fiber at some distance($-x$) where q =bonding shear force. (c) side view of interface.[55]

$$u_x = -\frac{q}{\pi G dx} \int_{r_0}^{r_1} \frac{dr}{r} = \frac{-q}{\pi G dx} \ln \frac{r_1}{r_0}$$

Rearrangement in terms of q provides

$$q = -\frac{\pi G u_x dx}{\ln \frac{r_1}{r_0}} \quad (21)$$

Substituting Equation (20) and (21) into Equation (18) provides

$$\pi r_0^2 d\sigma - \frac{\pi G u_x dx}{\ln \frac{r_1}{r_0}} = 0$$

$$\frac{d\sigma}{dx} = \frac{G u_x}{r_0^2 \ln \frac{r_1}{r_0}} \quad (22)$$

Since the total fiber deformation at x equals the matrix shear deformation u_x , the tensile strain in increment dx is

$$\frac{du_x}{dx} = \frac{\sigma}{E} \quad (23)$$

Differentiating Equation (22) gives

$$\frac{d^2\sigma}{dx^2} = \frac{G \frac{du_x}{dx}}{r_0^2 \ln \frac{r_1}{r_0}}$$

Substituting the above equation into Equation (23) gives

$$\frac{d^2\sigma}{dx^2} = \frac{G \frac{\sigma}{E}}{r_0^2 \ln \frac{r_1}{r_0}}$$

or,

$$\frac{d^2\sigma}{dx^2} - \frac{G/E}{r_0^2 \ln \frac{r_1}{r_0}} \sigma = 0 \quad (24)$$

Let

$$\alpha^2 = \frac{G/E}{r_0^2 \ln \frac{r_1}{r_0}} \quad (25)$$

Then Equation(24) becomes

$$\frac{d^2\sigma}{dx^2} - \alpha^2 \sigma = 0 \quad (26)$$

Solving Equation(26) gives

$$\sigma = C_1 e^{-\alpha x} + C_2 e^{\alpha x} \quad (27)$$

With boundary conditions $\sigma = P/\pi r_0^2$ at $x=0$ and $\sigma=0$ at $x=-\infty$, two constants C_1 and C_2 becomes

$$C_1 = 0, \quad C_2 = \frac{P}{\pi r_0^2}$$

Equation(27) becomes

$$\sigma = \frac{P}{\pi r_0^2} e^{\alpha x} \quad (28)$$

The shear stress at fiber/matrix interface is given as

$$\tau_{r_0} = \frac{-q}{\pi r_0 dx} \quad (29)$$

From Equation(18) and (20), $-q = dP = \pi r_0^2 d\sigma$. Substituting this equation into Equation(29) gives

$$\tau_{r_0} = r_0 \frac{d\sigma}{dx}$$

Differentiating Equation(28) and substituting into the above

equation provides

$$\tau_{r_0} = \frac{\alpha P}{\pi r_0} e^{\alpha x}$$

Let $\tau_{r_0} = \tau_0$ when $x=0$, then

$$\tau_0 = \alpha P / \pi r_0 \quad (30)$$

The shear stress at interface along the fiber length in terms of critical boundary stress (τ_0) becomes

$$\tau_{r_0} = \tau_0 e^{\alpha x}$$

This function can be easily proven to increase monotonously with x and drawn roughly as in Figure 20.

At this point it is very important to consider the physical meaning of α expressed in Equation(25). The stress decay factor (α) has demensions of reciprocal length and represents a measure of shear stress concentration. If the load P is applied such that $\tau_0 = \tau_s$, the shear strength of the interface, then the fiber will debond from the matrix at the point $x=0$. If we assume that the fiber continues to debond at the constant load P , i.e, if the fracture is catastrophic, then the load P to failure is, from Equation(30), $P = \pi r_0 \tau_s / \alpha$. If we assume that τ_s (interfacial bond strength) is constant, then P is a function of α only. Again α is a function of the shear modulus of matrix (G) and Young's modulus of the fiber (E) as seen in Equation(25). If we can assign G and E as a

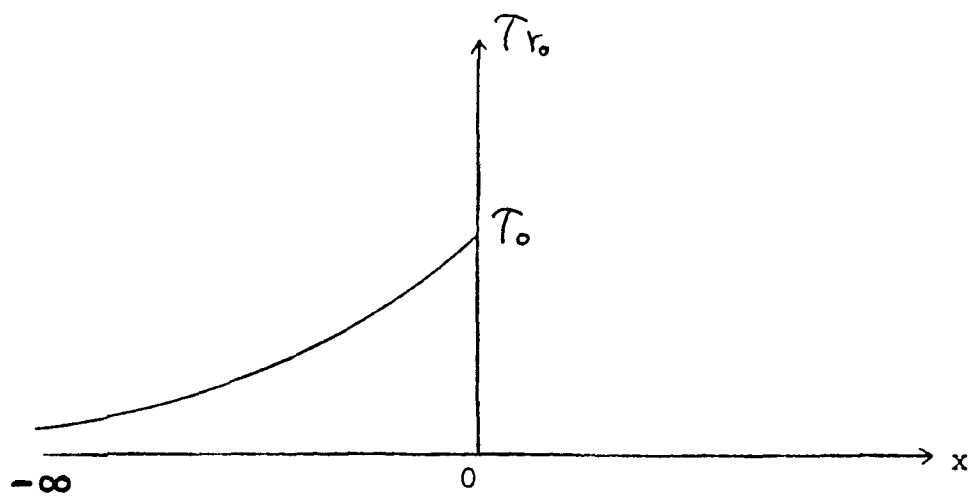


Fig.20. Shear stress distribution along the interface.

function of radiation dose, the breaking load P can be evaluated as a function of dose.

3.5.4 Work of Interfacial Fracture [55]

From Equation (30)

$$p = \frac{\pi r_0 \tau_0}{\alpha} = p_s$$

where p_s is the force required to generate a critical boundary stress (τ_0) for interfacial debonding. The work of propagating failure a distance L into the matrix is

$$W_s = p_s L = \pi r_0 \tau_0 L / \alpha$$

When a constant frictional stress $\lambda_f = f / \pi r_0$ exists between the fiber and matrix in the debonded region L the frictional force summation $\sum f$ is described as

$$f = \pi r_0 \lambda_f dx$$

$$\sum f = \pi r_0 \lambda_f \int_{x=0}^{x=L} dx = \pi r_0 \lambda_f L = p_f$$

When a debonded fiber breaks a distance L_f inside the matrix the frictional work is given by

$$W_f = \int_0^{L_f} p_f dL = \frac{1}{2} \pi r_0 \lambda_f L_f^2$$

An additional contribution to the work of interfacial fracture involves the work of tensile deformation W_D in the fiber length L which is lost at the instant of fracture. Outwater and Murphy[59] considered the case for constant frictional stress $\lambda_f = f / 2\pi r_0$ to show that

$$W_D = \frac{\pi r_0^2}{2} \int_0^L \left(\sigma - \frac{2 \lambda_f L}{r} \right)^2 dL$$

where σ is the tensile stress in the unconstrained fiber. Evaluating the above integral and substituting the relation $L = r_0 \sigma / 2 \lambda_F$ provides the following relation

$$W_D = \frac{\pi r_0^2 \sigma^2 L}{6 E}$$

for the fiber deformational work.

The above relations identify two contributions to the total pulling force P as

$$P = P_S + P_F$$

and three contributions to the work of fracture as

$$W = W_S + W_F + W_D$$

Recently, Kaelble[56] added another contribution of coating deformation (W_P) to this work of fracture.

4. REFERENCES

1. McGarry, F.J., "Properties of Glass Fiber Reinforced Plastics", Composite Materials and Composite Structures, 6th Sagamore Ordnance Materials Research Conference, Raquette Lake, N.Y. (1959)
2. Laird, J.A., and Nelson, F.W., "Glass surface Chemistry relating to the glass-finish-resin interface", Proc. 19th Ann. meeting of the Reinforced Plastics Div. of SPI, Chicago Ill. (1964) Sec. 11-C
3. Petker, I., "The Influence of Resin Strength and Defects on the Interlaminar Shear Strength of filament-wound Composites", SPE Transaction, 5 (1965), 49-58
4. Zisman, W.A., "Constitutional Effects on Adhesion and Abhesion", Adhesion and Cohesion (P. Weiss, ed.) Elsevier, Amsterdam (1962)
5. Zisman, W.A., "Influence of Constitution on Adhesion", Ind. Eng. Chem. 55 (1963), 19-38
6. Zisman, W.A., "Relation of the Equilibrium Contact Angle to Liquid and Solid Constitution", Advan. Chem. Ser., 43 (1964), 1-51
7. Good, R.J., and Girifalco, L.A., "A Theory for Estimation of Surface and Interfacial Energies", J. Phys. Chem., 64 (1960), 561-565
8. Good, R.J., "Theory for the Estimation of Surface and Interfacial Energies", Advan. Chem. Ser., 43 (1964),

74-87

9. Powkes, F.M., "Additivity of intermolecular Forces at Interfaces", J. Phys. Chem., 67 (1963), 2538-2541
10. Powkes, F.M., "Dispersion Force Contributions to Surface and Interfacial Tensions, Contact Angles, and Heats of Immersion", Advan. Chem. Ser., 43 (1964), 99-111
11. Johnson, R.E., Jr., and Dettre, R.H., "Contact Angle Hysteresis, part 1", Advan. Chem. Ser., 43 (1964), 112-135
12. Dettre, R.H., and Johnson, R.E., "Contact Angle Hysteresis, part 2", Advan. Chem. Ser., 43 (1964), 136-144
13. Powkes, F.M., "Donor-Acceptor Interactions at Interfaces", Recent Advances in Adhesion (L.H. Lee, ed.) Gordon and Breach, New York (1973), p39
14. Di Benedetto, A.T. and Nicolais, L., "Interfaces in Composites", Advances in Composite Materials (G. Piatti, ed.), Applied Science Publishers, London (1978), p153
15. Wake, W.C., Adhesion and the Formulation of Adesives, second ed., Applied Science Publishers, London (1982)
16. Levine, M., Ilkka, G.A., and Weiss, P., "Relation of the Critical Surface Tension of Polymers to Adhesion", J. Polymer Sci., Part B, 2 (1964), 915-919
17. Weaver, C., "Adhesion to High Energy Surfaces", Adhesion-Fundamentals and Practice (U.K Ministry of Tech. ed.), Gordon and Breach, New York (1969), p46
18. Derjaguin, B.V., and Smilga, V.P., "Electronic Theory of

Adhesion", Adhesion-Fundamentals and Practice (U.K. Ministry of Tech. ed.), Gordon and Breach, New York (1969), p352

19. Bikerman, J.J., The Science of Adhesive Joints, 2nd ed., Academic Press, New York (1968), p137-149
20. Huntsberger, J.R., "The Locus of Adhesive Failure", J. polymer Sci., Part A, 1 (1963), 1339-1344
21. Good, R.J., Treatise on Adhesion (R.L. Patrick ed.), Marcel Dekker, Inc. (1967), vol. 1, Chap. 2
22. Hildebrand, J.H., and Scott, R.L., Solubility of Non-electrolytes, 3rd ed., Reinhold, New York (1950), Chap. 4 and 7
23. Good, R.J., "Thermal Effects in the Peeling Separation of an Adhesive System", Aspects of Adhesion (D.J. Alner ed.), vol. 6 (1971), Univ. of London Press, p24-42
24. Narcus, H., "The electroplating of plastics; its present status", Trans. J. Plastics Inst., 35 (1967), 529-533
25. Perrins, L.E., and Pettett, K., "Mechanism for the Adhesion of electroplated copper to polypropylene", Plastics and Polymers, 39 (1971), 391
26. Andrews, E.H., and Kinloch, A.J., "Mechanics of adhesive failure", Proc. Roy. Soc., 332A (1973) 385-399
27. von Harrach, H. and Chapman, B.N., "Charge effects in Thin Film Adhesion", Thin Solid Films, 13 (1972), 157-161
28. Scola, D.A. and Brooks, C.C., "Surface Aspects of New Fibers, Boron, Silicon Carbide, and Graphite", J. Adhesion, 2 (1970), 213-237

29. Broutnan, L.J., "Measurement of the Fiber-Polymer Matrix Interfacial Strength" Interfaces in Composites, ASTM STP 452, 1969, p27-41
30. ASTM Bulletin, 1958(D 907-55), p706
31. Kwei, T.K., "Polymer-Filler Interaction", J. Polymer Sci. Part A, 3(1965), 3229-3240
32. Sharpe, L.H., "Interphase in Adhesion", J. Adhesion, 4(1972), 51
33. Patrick, R.L., Adhesion and Adhesives, vol.2, Marcel Dekker, New York (1969), p366
34. Lee, L.H., "Wettability of Organosilanes", 23rd Annual Technical Conference (1968), The Society of Plastic Industry, sec.9-D
35. Wake, W.C., "Surface Chemistry and Adhesion of Polymers", Trans. Inst. Rubber Ind., 35(1959), 145-165
36. Donnet, J.B., Papirer, E. and Dauksch, H., "Surface Modification of Carbon Fibers and their Adhesion to Epoxy Resins", Proc. 2nd Carbon Fiber Conference London, The Plastic Inst., 1974, p58-64
37. Griffith, A.A., "The phenomena of Rupture and Flow in Solids", Phil. Trans. Roy. Soc. London, 221A(1920), 163
38. Lipatov, Y.S., Fabulyak, F.G., Popova, N.G., and Nosalevich, I.M., "Molecular Mobility in Epoxy Polymers at different stages of curing in bulk and at the interface", Vysokomol. Soyed (Polymer Science U.S.S.R) A13(1971), 2601-2606
39. Erickson, P.W., "Historical Background of the Interface",

- J. Adhesion, 2(1970), 131-146
40. Patrick, R.L., and Brown, J.A., "Epoxide Resin Interacting with Tooth Surface", J. Colloid and Interface Sci., 35(1971), 179-130
 41. Patrick, R.L., Structural Adhesives, Marcel Dekker, New York (1976), p85
 42. Fitchmun, D.R. and Newman, S., "Surface Crystallization of Polypropylene", J. Polymer Sci. Part A-2, 8(1970), 1545
 43. Bascom, W.D., "Structure of Silane Adhesion Promoter Films on Glass and Metal Surfaces", Macromolecules, 5(1972), 792-798
 44. Baier, R.E., Shafrin, E.G. and Zisman, W.A., "Adhesion: Mechanisms that assist or impede it", Science, 162(1968), 1360-1368
 45. Wong, R., "Mechanism of Coupling by Silanes of Epoxies to Glass Fibers", Fundamental Aspects of Fiber Reinforced Plastic Composites (R.T. Schwartz ed.) Interscience Publishers, New York (1968), p237-243
 46. Goan, J.C. and Prosen, S.P., "Interfacial Bonding in Graphite Fiber-Resin composites", Interfaces in composites, ASTM STP452(1969), p3-26
 47. Wenzel, R.N., "Resistance of Solid Surfaces to Wetting by Water", Ind. Eng. Chem., 28(1936), 988-994
 48. Lee-L.H., "Adhesion of High Polymers. I. Influence of Diffusion, Adsorption, and Physical State on Polymer-Adhesion", J. Polymer Sci. Part A-2, 5(1967), 751-760
 49. Good, R.J., "Intermolecular and Interatomic Forces",

- Treatise on Adhesion and Adhesives (R.L.Patrick, ed.)
Marcel dekker, New York(1966), vol.1, p15
50. Vasenin,R.M., "Adhesion of High Polymers. Part 1: The Phenomenon of Adhesion", Adhesive Age, 8(1965), No.5, p18-25
51. Trivisssonno,N.M., Lee,L.H., and Skinner,S.M., "Adhesion of Polyester Resin to Treated Glass Surface", Ind. Eng. Chem., 50(1958), 912-917
52. Greszczuk,L.B., "Theoretical Studies of the Mechanics of the fiber-matrix Interface in Composites", Interfaces in Composites, ASTM STP452(1969), p42-58
53. Lawrence,P., "Some Theoretical Considerations of Fiber Pull-out from an Elastic Matrix", J. Materials Sci., 7(1972), 1-6
54. Kaelble,D.H., "Analysis of Interfacial Bonding Criteria for Fiber Composite Fracture Energy"' 16th National SAMPE Technical Conference(1984), p340
55. Kaelble,D.H., "Theory and Analysis of Fracture Energy in Fiber Reinforced Composites", J. Adhesion, 5(1973), 245-264
56. Plueddemann,E.P., Proc. 20th Ann. Tech. Conf. Reinforced Plastics Div. SPI.(1965) Sec.19-A
57. Throckmorton,P.E., and Browne,M.F., Proc. 20th Ann. Tech. Conf. Reinforced Plastics Div. SPI.(1965) Sec.15-A
58. Zisman,W.A., "Improving the Performance of Reinforced Plastics", Ind. Eng. Chem., 57(1965), 26-34
59. Outwater,J.O. and Murphy,J.C., "On the Fracture Energy

- of Uni-directional Laminates", Proc. 24th Ann. Tech. conf. Reinforced Plastics div. SPI(1969), Sec.11-C
60. Mixer,R.Y., and Parkinson,D.B., "Nuclear Radiation Effects on Structural Plastics and Adhesives, Part 3; Experimental Research", Stanford Research Inst., WADC TR56-534, Part 3, AF33(616)-3632, (1959)
61. Dauksys,R.J., and Ray,J.D., "Properties of Graphite Fiber Nonmetallic matrix composites", J. comp. Mat. 3(1969), 684-698
62. Butler,B.L. and Diefendorf,R.J., "Graphite filament Structure", 10th Ann. Symp. of Carbon composite Tech.(1970),New Mexico, p107-124
63. Allen,S., Cooper,G.A., and Mayer,R.M., "Carbon Fibers of High Young's Modulus", Nature, 224(1969), 684
64. Allen,S., Cooper,G.A., Johnson,D.J., and Mayer,R.H., "Carbon fibers of High modulus" 3rd Conf. on industrial Carbons and Graphite, Soc. of Chemical Ind. London(1970), 456-462
65. Cooper,G.A., and Mayer,R.M., J. Materials Sci., 6(1971), 60
66. Jones,R.F., Tenth Biennial Conf. on Carbon, Bethlehem, Pennsylvania, Summary of Papers(1971), 190
67. Bullock,R.E., "The Effects of Fast-neutron Irradiation on Tensile Strength of Carbon Fibers", Radiation Effects, 11(1971), 107-112
68. Thomas,J.M., Chemistry and Physics of Carbon (P.L.Walker, ed.), vol.1, Marcel Dekker, Inc., New York(1965), 121

69. McKague, E.L., Jr., Bullock, R.E., and Head, J.W., "Improved Mechanical Properties of Composites Reinforced with neutron irradiated Carbon Fibers", J. Comp. Mat., 7(1973), 288-297
70. Bullock, R.E., "The Effects of Fast-Neutron Irradiation on Elastic moduli of Carbon Fibers", Radiation Effects, 14(1972), 263
71. Jones, B.F., and Peggs, I.D., "Strengthening of Carbon Fibers by Fast-Neutron Irradiation", Nature, 239(1972), 95
72. Tuinstra, F., and Koenig, J.L., "Characterization of Graphite Fiber Surfaces with Raman Spectroscopy", J. comp. Mat., 4(1970), 492
73. Bullock, R.E., and McKague, E.L. Jr., "Radiation Effects on Mechanical Properties of Carbon/Carbon Composites", Carbon, 11(1973), 547-553
74. Raff, R.A.V., and Subramanian, R.V., "Effect of Gamma Radiation on the Adhesion of Metals to Epoxy Resin", J. Applied Polymer Sci., 15(1971), 1535-1537
75. Leung, C.L., "Space Environmental Effects on Graphite/Epoxy Composites", Composites for Extreme Environments, ASTM STP768(N.R. Adsit, ed.) (1982), p110-117
76. Kircher, J.F. and Bowan, R.W., Effects of Radiation on Materials and components, Rheinhold, New York(1964), Chap.6

77. Morgan, J.T., and Stapleton, G.B., "Post Irradiation Mechanical Properties of Radiation Resistance Cast Epoxy Resin Systems", Report RL-75-136, Science Research Council, Chilton, England (1975)
78. Bullock, R.E., General Dynamics Report ERR-FW-1026 (1970)
79. Wolf, K.W., "Effect of Ionizing Radiation on the Mechanical and Structural Properties of Graphite Fiber Reinforced Composites", Ph.D. dissertation, North Carolina State University (1982)
80. Riess, G., Bourdeaux, M., Brie, M., and Jouquet, G., "Surface Treatment of Carbon Fiber with Alternating and Block Copolymer", Proceedings of the International Conference on Carbon Fibers, The Plastic Institute, London (1974), Paper No. 8
81. Hancox, N.L., and Wells, H., "A Comparison of Three Methods of Measuring the Interlaminar Shear Strength of Unidirectional CFRP", Proceedings of the 10th Annual Symposium of the New Mexico section of ASME (1970), p35-53